Environmental Remediation Applications of Chemically Activated Tropical Hardwood Waste

A Thesis submitted to the Committee on Graduate Studies in Partial Fulfillment of the Requirements for the Degree of Doctor of Philosophy in the Faculty of Arts and Science

TRENT UNIVERSITY
Peterborough, Ontario, Canada

Environmental & Life Sciences PhD Graduate Program
September 2025

Abstract

Environmental Remediation Applications of Chemically Activated Tropical Hardwood Waste

Hamant E. France

Innovative strategies to manage copious waste streams by upcycling feedstocks to valorized products which are then used in environmental remediation applications is an attractive circular economy model. This thesis explores this approach using waste wood generated from the milling of *Chlorocardium rodiei* (greenheart), a tropical hardwood species abundant in Guyana. We evaluate the thermochemical conversion of this feedstock, using phosphoric acid as the activant, to super activated carbons with surface areas of more than 2200 m^2/g. Owing to the presence of surface heteroatoms, these adsorbents are amenable to further surface modifications including base-treatment, O-functionalization and N-functionalization. Using a facile oxidation procedure and shrimp waste-based dopants, we increase oxygen and nitrogen content by 8-fold and 5-fold respectively. These increases are realized without catastrophic loss of surface area and porosity as generally occurs with many reported functionalization approaches. Functionalized materials demonstrated efficient removal of both metal ions and the chlorinated herbicides 2,4-dichlorophenoxy acetic acid and paraquat. Pristine and base-washed ACs removed more than 90% of iron, aluminum and manganese from natural pit-lake waters. O-functionalized adsorbents also showed excellent removal efficiencies for

aluminum and lead but only removed moderate amounts of manganese. Nitrogen-enriched composites fabricated with the addition of commercial chitosan removed 67% 2,4-D and 89% paraquat from model solutions at environmentally relevant concentrations of 4 ppm and 40 ppm respectively. Their versatility is further demonstrated in their ability to remove both herbicides from binary mixtures albeit to different extents. Shrimp chitin-based composites were most effective at removing 2,4-D from model solutions with a maximum adsorption capacity of 101 mg/g. Both surface area and surface nitrogen had strong influences on the adsorption capacity of adsorbents. Mechanistically, physisorption interactions predominate the synergistic or antagonistic interaction between N-functionalized composites and herbicide species. These green adsorbent materials, fabricated from sustainable biopolymers, are promising candidates for diverse environmental remediation applications.

Keywords: *Environmental remediation, chemical activation, waste valorization, activated carbon, tropical hardwood waste, greenheart, N-functionalization, O-functionalization, greener fabrication, green chemistry, pit-lake, 2,4-D, paraquat, metal adsorption, organic herbicides, isotherm modelling, thermodynamic evaluation*

Preface

This thesis is presented in manuscript format. Chapters 1 and 2 present content that has not been published. Chapter 3, which presents the first experimental chapter and chapter 5, have been published. Chapters 4 and 6 are currently engaging the attention of peer reviewers and editors respectively. Co-authors and their contributions are included in the preface of each chapter. Only open-sourced journals have been and will be considered for all manuscripts.

Acknowledgments

Accomplishments are always the synergistic output of multiple individuals and entities. In this work, the assistance of the following is acknowledged: Andrea Barnes-France, Prof Andrew Vreugdenhil, Prof Suresh Narine and the Sustainable Guyana Program CGX, Frontera Energy, Phillip and Sheila France, IMRL Lab, University of Guyana, Elim Pentecostal and Calvary Pentecostal Churches, My Lord Jesus.

Table of Contents

List of Figures

List of Tables

List of Equations

List of Abbreviations and Symbols

AC	Activated Carbon
ANZECC	Australian and New Zealand Environment and Conservation Council
ARMCANZ	Agriculture and Resource Management Council of Australia and New Zealand
BET	Brunauer Emmet and Teller
Ch	Chitosan
2,4-D	2,4-dichlorophenoxyacetic acid
DFT	Density Function Theory
DI	deionized water
DTG	Differential of Thermogravimetric Plot
GH	Greenheart
GH-Ch-AC	Greenheart Chitosan Activated Carbon
GH-PAC-BW	Greenheart Phosphoric Acid Activated and Base Washed
GH-PAC-DIW	Greenheart Phosphoric Acid Activated and Deionized Water Washed Activated Carbon
GH-SC-AC	Greenheart Shrimp Chitin Activated Carbon
GH-SH-AC	Greenheart Shrimp Hydrochar Activated Carbon
GH-SS-AC	Greenheart Shrimp Shell Activated Carbon
GH-SW-AC	Greenheart Shrimp Waste Activated Carbon
GV	Guideline Values

I_D/ I_G	Ratio of Disordered Band Intensity to Graphitic Band Intensity
IMRL	Inorganic Materials Research Lab
IR	Interaction Ratio
K_F	Freundlich Model Constant
K_L	Langmuir Model Constant
K_s	Sips Model Constant
MI	Mixed Ions
MP-AES	Microwave Plasma Atomic Emission Spectroscopy
NDIR	Non-dispersive infrared
OFG	Oxygen Containing Functional Group
PAC	Phosphoric Acid Activated Carbon
pzc	Point of Zero Charge
Q_0	Monolayer Capacity
RWF	Rapid Wire Chamber Furnace
S_{BET}	BET Specific Surface
TGA	Thermogravimetric Analysis
TOC	Total Organic Carbon
V_{mic}	Micropore volume
V_{mes}	Mesopore volume
V_t	Total Pore Volume
WHO	World Health Organization
XPS	X-Ray Photoelectron Spectroscopy

1.1 Introduction

1.1.1 Waste Valorization

Circular economy strategies, involving the reuse of waste materials by their conversion to high value products continues to engage the attention of researchers (Bergna et al., 2020; Kirchherr et al., 2023; Ligero et al., 2024). Biomass wastes, such as waste wood and the shells of crustaceans are particularly useful given their availability and the wide array of valorized products that may be derived from them. For instance, waste wood has been successfully converted to biofuels and adsorbents (Fan et al., 2024; Radenković et al., 2024; Rahmana Putra et al., 2024), while crustacean waste like shrimp shells is a rich source of the polysaccharide chitosan (Wang and Zhuang, 2022). Globally, both wood and shrimp wastes are being produced in increasingly larger quantities (Gillett, 2008; Zimmer et al., 2018). This reality simultaneously poses environmental, and waste management challenges and provides copious amounts of biomass feedstocks which are amenable to upcycling. In this work, we demonstrate that the potential of these two feedstocks can be leveraged to produce efficient carbonaceous environmental remediation materials.

1.1.2 Carbon adsorbents: historical view

The exceptional adsorptive properties of carbon adsorbents are well documented and arise because of their porous structure and high surface area (Hynes et al., 2020). Additionally, the surface functionality of some forms of carbon give them excellent adsorption properties (Ania et al., 2002; Haydar et al., 2003). In antiquity (3750 BC) Egyptian and Sumerian civilizations used carbon in

the form of charcoal for metallurgical and medicinal purposes. Furthermore, the Phoenicians discovered that the freshness of their drinking water was maintained when it was stored in charred wooden barrels (Cecen, 2011). Later, discoveries by Scheele (1773), and later Lowitz (1786), showed the excellent adsorbent abilities of charcoal in removing molecules from gas and liquid phases(Cecen, 2011). Lowitz's work pioneered the removal of dyes from water using charcoal. In a most dramatic display, the adsorbent properties of charcoal were highlighted by the French chemist Michel Bertrand in 1811 when he ingested 5 g of arsenic along with charcoal and lived (Juurlink, 2016). A more recent derivative of charcoal that displays similar heightened adsorptive properties is activated carbon (AC).

1.1.3 Activated carbons: physical description and morphology

Activated carbons are materials which have extensive specific surface areas and well-developed porosities. Pores in AC are classified as micropores (< 2 nm), mesopores (2–50 nm) or macropores (> 50 nm) **Figure 0.1** These characteristics are achieved by exposing a precursor, a material with a high proportion of carbon, to a set of physicochemical conditions. From a macromolecular structural perspective, ACs are composed of layers of hexagonally bonded carbon atoms: graphene. Graphene layers in AC are disorderly arranged (Marsh and Rodríguez-Reinoso, 2006a). It is this disorder in the graphene network which generates porosity on the AC surface. Furthermore, it greatly increases the surface area. The surface area created by these pores in a 1 g sample of AC can be as large as 4000 m^2 (Sircar et al., 1996). Large surface areas are desirable in adsorption applications as they provide more sites for the interaction between target molecules or ions and AC. In addition to the physicochemical parameters used to produce AC, the type of starting material used, also called feedstock or precursor, is of primary import.

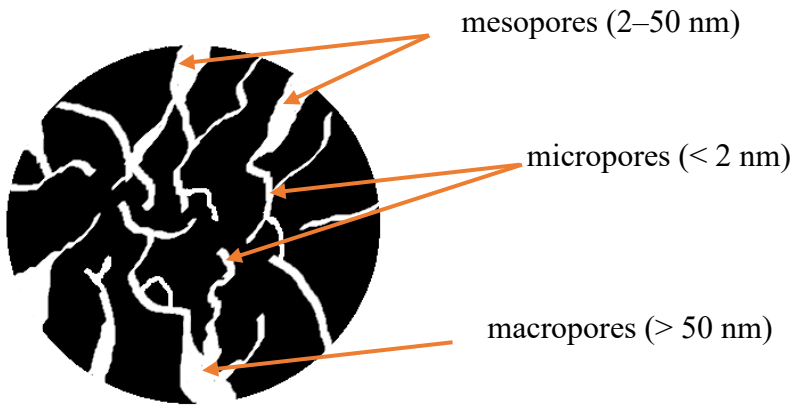

Figure 0.1 Porosity of activated carbon particle

1.1.4 Source material for activated carbons

A wide range of precursors such as petroleum coke, cherry stones, coconut shells and hemp stems have been successfully converted to ACs (Lim et al., 2010; Lupul et al., 2015; Olivares-Marín et al., 2006; Roy et al., 2025). Furthermore, great interest has been shown in the use of waste wood in general and waste wood derived from the milling of forest products. This is because this feedstock typically has fewer other value-added uses, is cheap and produced in large quantities. In fact, the global waste wood output is projected to exceed 7 billion metric tons by 2065 (Zimmer et al., 2018).

It has been reported that homogenous waste wood samples from chestnut, walnut, and cedar (Gómez-Serrano et al., 2005) have been used to make ACs. Furthermore, heterogenous wood samples have also been used. ACs produced from a mixture of hardwoods, predominantly composed of sweet and black gum, oak, and maple, yielded surface areas of more than 2000 m^2/g (Yagmur et al., 2013). While ACs with excellent texture have been produced from these temperate hardwoods, little has been reported on the suitability of tropical hardwoods to produce high surface area ACs utilizing existing activation protocols. In this work we use waste wood from the milling

of *Chlorocardium rodiei* (greenheart), a wood species that is abundant and widely harvested in Guyana. Greenheart waste wood is traditionally only used to make brickettes for fuel and a large quantity is used as a landfill material. In 2022 approximately 44,000 m^3 of this feedstock was produced. Homogeneous greenheart samples, a lignocellulosic feedstock, is used throughout this work to make activated carbons.

1.1.5 Lignocellulosic precursors: chemical composition

Three macromolecules (**Figure 0.2**) are present in varying ratios in lignocellulosic precursors: lignin, cellulose, and hemicellulose (Kazmi et al., 2019). Typically, hardwood stems contain 40–45% cellulose, 24–40% hemicellulose and 18–25% lignin (Menon and Rao, 2012; Rutherford et al., 2012). The elemental composition of C, H and O in these materials is approximately 48 wt%, 6 wt% and 45 wt% (Marsh and Rodríguez-Reinoso, 2006a). The relative amount of these biopolymers influences the texture (specific surface area, pore volume and pore size distribution) of ACs. Higher lignin content favours the formation of micropores. On the other hand, higher cellulose content favours the formation of mesopores (O. K. Strong et al., 2023). High proportions of carbon make lignocellulosic precursors suitable for chemical activation.

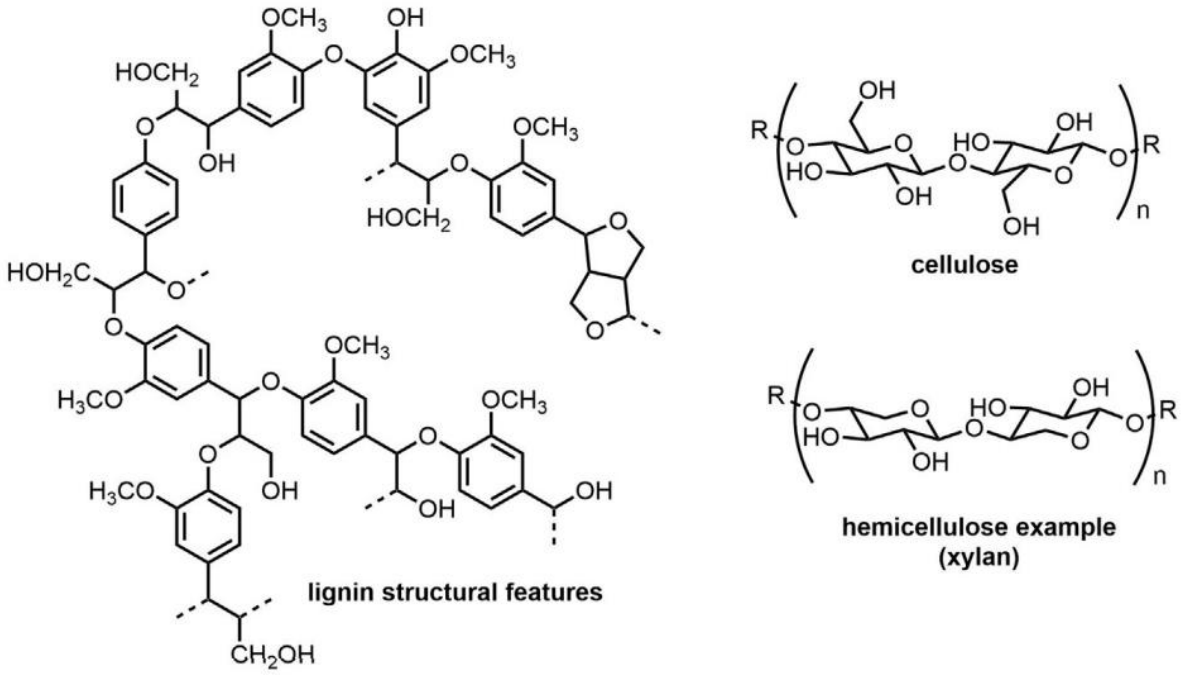

Figure 0.2 Types of macromolecules in lignocellulosic feedstock.

1.1.6 Activation methods and agents

Two general sets of protocols are used for AC production. Physical methods involve gasification reactions typically carried out at temperatures above 1000 ^{o}C in an inert atmosphere (N_2), steam or carbon dioxide (Marsh and Rodríguez-Reinoso, 2006a). Notably, when steam and carbon dioxide are used as activating agents, they create indentations on the precursor surface thereby increasing porosity. On the other hand, chemical activation can use lower temperatures (400–900 ^{o}C) (Marsh and Rodríguez-Reinoso, 2006b) in conjunction with chemical agents such as zinc chloride, potassium hydroxide or phosphoric acid. When phosphoric acid is used, it acts as a templating agent that occupies spaces within the precursor. With the application of heat under an inert atmosphere the carbon structure rearranges around the phosphoric acid which upon cooling (Marsh and Rodríguez-Reinoso, 2006b) is removed by washing, leaving the newly formed porosity behind. In addition, phosphoric acid has a comparatively benign environmental impact and

produces higher yields of AC (35–45%). Furthermore, up to 97% of the acid can be recovered for reuse (Strong, 2023). In comparison potassium hydroxide activation of lignocellulosic precursors has yielded ACs with surface areas of more than 3000 m^2/g (Li et al., 2017). The yield from KOH activation of lignocellulosic material is typically much lower than yields from H_3PO_4 activations. This is partially because of the higher activating temperatures of 800–1000 ^oC and the corresponding increase in burn-off. Generating these higher temperatures requires significantly higher energy inputs making it a more expensive process. However, precursor effects may result in deviations from this trend. Activation of tamarind seed, for instance, produced ACs with yields ranging from 50–80% (Mopoung et al., 2015). In this work, activation conditions were selected to minimize energy and chemical inputs while realizing high yields of adsorbent with optimized features. With this in mind, the activating agent selected for this work was phosphoric acid because of its comparative benign environmental character and the typically higher yields generated using this method.

1.1.7 Functionalized Adsorbents

Functionalization of activated carbons is known to enhance their adsorbent properties. Functionalization is done to enhance the heteroatom content (N, S, O) on the AC surface. O-functionalization, is typically used to enhance metal ion uptake, and is achieved by protracted exposure of the material to oxidants such as hydrogen peroxide, ozone, ammonium persulfate or nitric acid (Daud and Houshamnd, 2010; Haydar et al., 2003; Moreno-Castilla et al., 2000). Exposure to such harsh oxidizing conditions has been reported to cause catastrophic surface area loss and this has been a persistent worry in material oxidation applications (Somyanonthanakun et al., 2023). In this work we use nitric acid oxidations because of the large increases in surface oxygen generally produced by this method. We, however, evaluate a little explored flash oxidation procedure where ACs are exposed to strong nitric acid for minimal times at ambient

temperature. We hypothesize that these conditions are sufficient to produce strong increases in surface oxygen without catastrophic pore collapse and excessive loss of surface area.

N-functionalization, by the inclusion of amide, amine, and imine groups, is known to enhance the removal of organic contaminants in adsorption applications (Pellenz et al., 2022). Of the techniques used to increase N-heteroatoms in adsorbent materials, *in situ* polymerization and direct addition (composite formation) are widely used (Pellenz et al., 2022). The composite formation method was selected for this work given its comparative ease of application and for the incorporation of sustainably sourced nitrogenous wastes as dopants. Here, we use shrimp shells, shrimp chitin, shrimp hydrochar and commercially available shrimp chitosan to increase N-heteroatoms in ACs.

1.1.8 Activated carbons in environmental aquatic remediation

ACs have been produced, tailored, and used to remove contaminants such as melamine, ciprofloxacin (an antibiotic), selenite, selenate, and copper ions from aqueous solutions (de Celis et al., 2009; Hynes et al., 2020; O. K. Strong et al., 2023; Sun et al., 2012). It has been reported that Al, Mn, and Fe are among the cations most often found in elevated levels in bauxite mining pit lakes (Williams et al., 2020a). These metals were found to be in elevated levels in a frequently used recreational lake at Kara Kara in Linden, Guyana. There the Al ion concentration was 45 times above the recreational water quality safe limits of 0.2 ppm (Williams et al., 2020b). While the concentrations of Fe and Mn were lower, they still pose a health risk to the patrons frequenting the lake. The waters of this lake also contained Pb within safe limits (Williams et al., 2020b). While the threat of toxicity presented by this ion is not immediate, it was deemed prudent to assess the ability of the ACs to also remove it from solution.

Guyana's agricultural sector also uses large quantities of organic herbicides to combat plant species which compete with agricultural crops. While limited data is available on the use of herbicides in Guyana, it is known that 2,4-dichlorophenoxyacetic acid (2,4-D) and paraquat (Gramoxone) are in use. 2,4-D is a selective, systemic growth inhibitor while paraquat is a broad spectrum contact herbicide. Both herbicides are known to be toxic with 2,4-D being associated with the neurodegenerative disease Parkinson and with autism (Zuanazzi et al., 2020). In this work we evaluate the adsorption performance of both pristine and functionalized greenheart ACs in the removal of 2,4-D and paraquat. We study the impact of solution pH on the adsorption of these herbicides and proffer a basic mechanism by which they interact with N-functionalized adsorbents.

1.2 Thesis Objectives

The objectives of this research are:

1. To investigate the thermochemical transformation of greenheart feedstock to high surface activated carbons.
2. To functionalize pristine greenheart activated carbons by facile base washing, oxidative and nitrogenating procedures.
3. To characterize pristine and functionalized greenheart adsorbents.
4. To evaluate the adsorption performance of pristine, O- and N-functionalized greenheart AC in metal ion and herbicide adsorption.

Chapter 2

2.1 Key Instrumental Techniques

2.1.1 BET Surface Area Analysis (BET)

The BET technique, named after its inventors Stephen Brunauer, Paul Emmett and Edward Teller, is a widely used surface area analysis technique. A typical BET analysis initially involves sample preparation by degassing. Here, an accurately weighed mass of sample is introduced to a BET tube and subjected to elevated temperatures under vacuum for times of up to 6 h. This removes adsorbed volatiles and water from the material surface. Degassed samples are then transferred to the analysis unit where an adsorptive, typically nitrogen, argon or carbon dioxide, is introduced to the tube at various relative pressures ($\frac{p}{p^o}$) where "p" is the absolute pressure and "p^o" is the saturation vapor pressure of the adsorptive. In the case of nitrogen, analysis is done at, 77 K. The adsorptive interacts with the material surface forming a monolayer and, subsequently, multilayers as described by the BET non-linear equation (**EQ. 1**). Adsorption data are then fitted to the linearized BET equation (**EQ. 2**) forming the BET transformation plot. The slope and intercept of the transform plot are then used to calculate the statistical monolayer capacity (V_m) and the BET C value; an empirical constant relating to the enthalpy of adsorption. The monolayer adsorption capacity is used in conjunction with **EQ. 3** to calculate the specific surface area, where n_m, N_A, σ and m are the number of moles of adsorptive, Avogadro's number, cross sectional area of adsorptive and sample mass respectively.

EQ 1 Non-linear BET Equation $V_a = \frac{V_m C \frac{p}{p^o}}{\left(1-\frac{p}{p^o}\right)\left(1+(C-1)\frac{p}{p^o}\right)}$

EQ 2 Linearized BET Equation $\frac{\frac{p}{p^o}}{V_a(1-\frac{p}{p^o})} = \frac{1}{(V_m C)} + \frac{\frac{p}{p^o}(C-1)}{(V_m C)}$

EQ 3 Specific surface area $S_{BET} = \frac{n_m \, x \, N_A \, x \, \sigma}{m}$

Surface area measurements were typically taken in the traditional BET range of 0.05 – 0.3 relative pressure. In addition, the selected BET ranges of relative pressure was optimized by ensuring:-

- A positive BET C value
- Excellent linearity of EQ 2
- Increasing N_2 adsorbed with increases in relative pressure on the Rouquerol plot; a plot used to optimize selection of data points.

2.1.1.1 BET Analysis Parameters

Specific surface area, total and micropore volumes and pore size distribution were determined by nitrogen gas adsorption and desorption experiments. A Micromeritics Tristar II+ analyzer equipped with Density Functional Theory (DFT) capabilities was used to gather this data. The samples (~0.1000 g) were degassed for 6 h with vacuum of 1.33 x 10^{-2} mb. BET surface area measurements were made within the standard BET range of 0.05–0.3 relative pressure. Micropore volume was determined by the t-plot method. Mesopore volume was determined by the difference between total volume and micropore volume. Adsorption isotherms, measured at 77 K, were collected, and used to confirm the predominant pore size distribution of ACs.

2.1.2 X-Ray Photoelectron Spectroscopy (XPS)

X-ray photoelectron spectroscopy is a surface characterization technique which is used to obtain information about the elemental composition and chemical state of groups on material surfaces. In XPS the material is irradiated with soft x-rays typically from an aluminum or copper source. Soft x-rays eject core electrons from atoms in the top ~ 10 nm of the material surface. The kinetic energies of the ejected electrons are measured, and their binding energies are determined using **EQ. 4**. Omega (ϕ) is the instrument work function which relates to the minimum energy required to remove an electron from the materials surface under a vacuum.

EQ 4 Binding Energy $\boldsymbol{E_{binding} = E_{photon} - E_{kinetic} + \phi}$

2.1.2.1 XPS Analysis Parameters

Insights into the surface chemical composition and chemical states of the elements on ACs surfaces were obtained by XPS. A Thermofisher Scientific K(alpha) spectrometer using a monochromatic Al K(alpha) source (15mA, 15kV) with a pass energy of 50 eV was used. Absolute linearity of the binding energy scale was obtained by using sputter cleaned Au, Ag and Cu to calibrate the instrument work function. Values of 83.96 eV for the Au 4f7/2 line for metallic gold, 368.21 eV for Ag 3d5/2, and 932.62 eV for the Cu 2p3/2 line of metallic copper were returned. Conditions of 200 eV pass energy and a 1 eV/step were used for survey scans while x-ray spot size was 400 μm - a 2:1 ellipse with the noted spot size corresponding to the major axis. High resolution scans with an analysis area of 300 x 700 microns and 20 eV pass energy were conducted. Data analysis was done using CasaXPS (version 2.3.1). Spectra were corrected to the main line of the carbon 1s peak observed at 284.85 eV.

2.1.3 Microwave Plasma Atomic Emission Spectroscopy (MP-AES)

MP-AES is a spectroscopic technique used to identify and quantify metallic species in aqueous media. Aqueous ion-bearing samples are aspirated by a nebulizer and passed into a microwave energy, nitrogen-fueled plasma. Electrons in the sample particles are excited and after subsequent relaxation, photons, with characteristic energies are emitted. These are monochromated and detected.

2.1.3.1 MP-AES Analysis Parameters

The initial concentrations of ions in the lake water samples as well as the ion concentrations in the filtrates from batch experiments were determined by the Agilent MP-AES 4200. A pump speed of 15 rpm and stabilization time of 25 s was used. Nebulizer flow rates for analysis of Al, Mn and Fe were 0.95 L/min, 0.90 L/min and 0.65 L/min with Pb at 0.75 L/min. Calibration curves were plotted from 6 multi-ion standards of $Al(NO_3)_3$, $Mn(NO_3)_2$, $Fe(NO_3)_3$ and $Pb(NO_3)_2$ using concentrations 1 ppm, 5 ppm, 10 ppm, 25 ppm, 50 ppm and 100 ppm. A 5 % HNO_3 aqueous solution was used as the blank.

2.1.4 Total Organic Carbon (TOC)

TOC measurements involve the determination of non-volatile organic carbon in an aqueous sample by the conversion of organic carbon to carbon dioxide. Two modes are possible for TOC determination. In the difference method, the total carbon content of the same and the inorganic carbon content are determined. The difference between the two is the total organic carbon content. In the direct method, the sample is acidified causing the conversion of inorganic carbonates and bicarbonates to carbon dioxide. Carbon dioxide is then removed leaving organic

carbon only in the sample. The aqueous phase containing organic carbon is then injected into a furnace heated to 680-720 ℃ onto a platinum-containing column. Here, the catalytic oxidation of organic carbon to carbon dioxide occurs. The gas is then detected by an NDIR detector and quantified.

2.1.5 Point of Zero Charge (pH_{pzc}) Determination

The pH drift method was used to determine the point of zero charge of ACs. 1000 mL of 0.01 M NaCl solution were made up and bubbled with nitrogen at room temperature for 30 min to expel CO_2. Solutions of NaOH and HCl of concentrations of 0.1 M were then used to adjust the pH of 50 mL aliquots of NaCl to a pH in the range of 2–10. 150 mg of AC were then added to the pH adjusted NaCl solutions and the mixtures stirred for 24 h in sealed plastic cups at 200 rpm at 20 ℃. The final pH of mixtures was then determined, and plots of initial vs final pH of aliquots produced. The point of zero charge was estimated to be the pH at which the plot of initial pH vs final pH intersected the line of initial pH equal to final pH.

2.1.6 Thermogravimetric Analysis (TGA)

A TGA Q500 (TA Instruments, Newcastle, DE, USA) was used to analyze changes in the greenheart sawdust sample with changes in temperature. This allowed for moisture content determination of the precursor as well as the determination of the temperature ranges in which key degradation events occurred. A 10–15 mg sample was heated on a platinum pan from 25 ℃ to 600 ℃ at 10 ℃/min under nitrogen flowing at 60.0 mL/min. The temperature at which the maximum rate of degradation occurred (T_D) was obtained from the derivative of the TGA (DTG). Shrimp waste composites were analyzed by a Perkin-Elmer TGA 8000. The thermal stability of the

samples was explored by heating them from 30 °C to 1000 °C at a heating rate of 20.0 °C/min under argon gas passing through the cell at 50.0 mL/min rate.

2.2 Materials and Methods

2.2.1 Materials

Phosphoric Acid, 85 %, was obtained from Caledon Laboratory Chemicals, while 70 % nitric acid, all 1000 ppm standards of $Al(NO_3)_3$, $Mn(NO_3)_2$, $Fe(NO_3)_3$, NaCl, NaOH, HCl, paraquat, 2,4-D and low molecular weight chitosan were purchased from Sigma Aldrich. $Pb(NO_3)_2$ was obtained from Alfa Aesar Chemicals. Food-grade citric acid was obtained from Eastchem Inc Canada.

2.2.2 Sample collection and sizing of greenheart precursor

Greenheart sawdust was obtained from a local sawmill in Parika (Guyana) and sun-dried for 2 h. Samples were then placed into sealed sample bags and stored at room temperature. A 5 g sample of the precursor was sized using a manual Keck sieve shaker (Cole Parmer) fitted with OPN 40, 26, 20 and 9 sieves. Most of the particles ranged in size from 1–0.2 mm, with the major size fraction being 0.5 mm. Consequently, further size reduction of the precursor was unnecessary.

2.2.3 Fabrication of greenheart phosphoric acid activated carbon (GH-PAC-DIW) and base-washed activated carbon (GH-PAC-BW)

The method used for activation of greenheart (**Figure 2.1**) was a modified version of that developed by Strong et al. (2023). Key modifications included additional activations at 500 ℃ and 600 ℃ and digestion and carbonization for times ranging from 0.5–20 h at 110 ℃. In addition, base-modified ACs were prepared by washing GH-PAC-DIW with 0.1 or 0.4 M NaOH solutions with 1 or 2 h of stirring at 400 rpm.

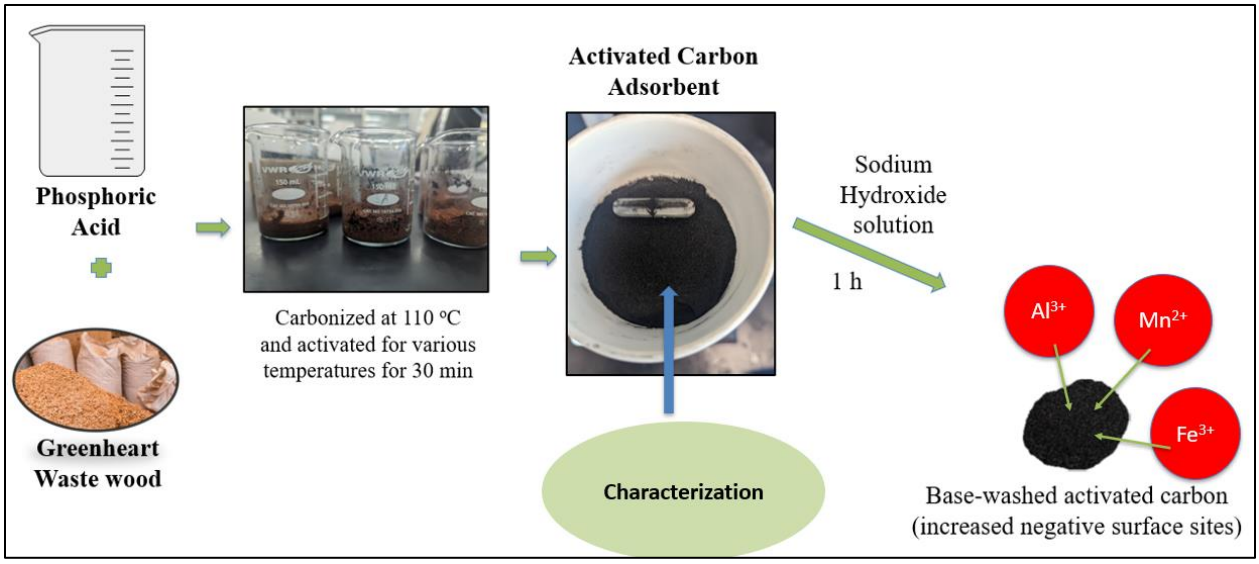

Figure 2.1 Schematic for fabrication of pristine and base-washed greenheart ACs and metal ion batch test.

2.2.4 O-functionalization of pristine greenheart AC by flash oxidation with HNO_3

Three hundred and fifty milligram samples of pristine (unoxidized) GH-PAC_{600} were weighed out into sealable plastic cups. To each sample, 15 mL of 5 M or 10 M nitric acid was added. Mixtures were agitated at room temperature (22 °C) on an orbital shaker table at 200 rpm for times ranging from 15–60 min. Oxidized ACs were subsequently washed 5 times with a total of 400 mL of room temperature DI water.

Samples were then dried at 110 °C overnight. Oxidized carbons were named based on the concentration of acid used to prepare them and the residence time. e.g., GH-OX5M15 was prepared from pristine GH-PAC_{600} using 5 M nitric acid with 15 min of oxidation.

2.2.5 Preparation of shrimp shell, shrimp hydrochar and shrimp chitin

Shrimp shell waste (*Pandalus borealis*), obtained from the Fisheries and Marine Institute of Memorial University, Newfoundland, were variously treated based on the methods reported by Pohling, (Pohling et al., 2022). Briefly, shrimp shells (SS) were ground to 1.4 mm, washed and dried at 40 ℃ for 80 min. Shrimp hydrochar (SH) was prepared by subjecting previously prepared SS to a hydrothermal carbonization (HTC) treatment at 250 ℃ and 42–43 bars pressure. Shrimp chitin was prepared by exposing SS to a 2-stage citric acid treatment followed by deproteination with an industrial protease and drying at 40 ℃.

2.2.6 Preparation of chitosan and shrimp waste augmented greenheart activated carbons (GH-Ch-AC)

Chitosan was added to 5 g of greenheart precursor to produce mixtures with compositions of 10–30 wt% chitosan. 12 ml of 25% H_3PO_4 was then added to each mixture while stirring. The method used for activation of chitosan augmented mixtures was a modified version of that developed by Strong et al (O. K. Strong et al., 2023). A key modification was carbonization for 20 h at 110 ℃ in air. ACs were named based on whether greenheart (GH) or chitosan (Ch) were used as precursors and the weight % of chitosan added. GH-$Ch_{20\%}$ therefore was made by activating a mixture of 80% greenheart and 20% chitosan at 400 ℃. Similarly, composites were made from a shrimp hydrochar, shrimp chitin and shrimp shells following the experimental scheme in **Figure 2.2**.

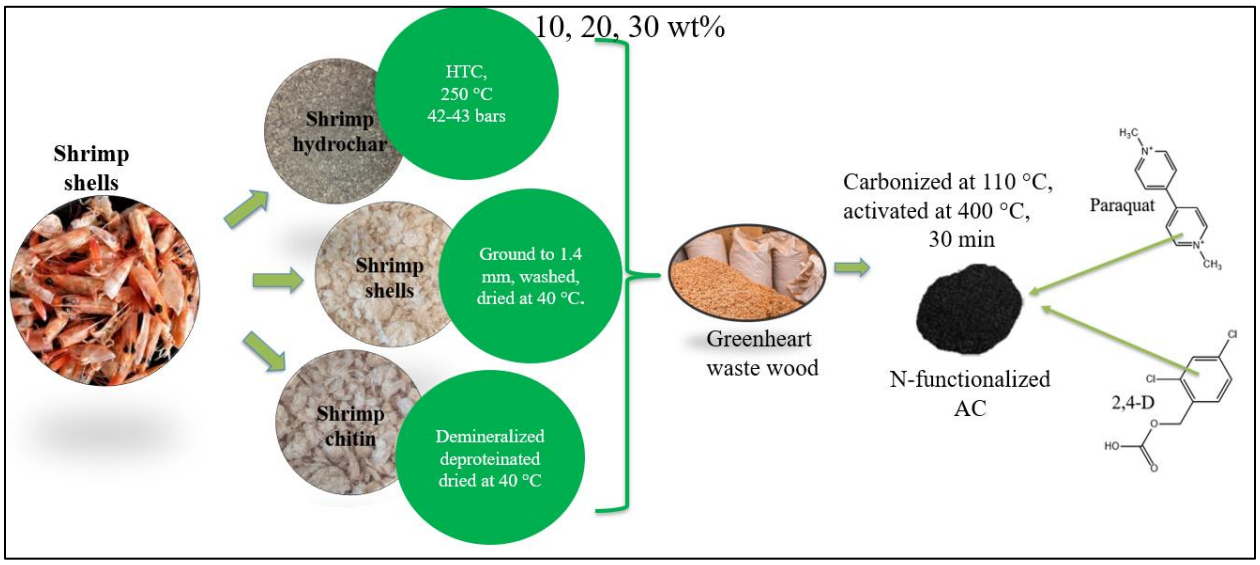

Figure 2.2 Schematic for the fabrication of chitosan and shrimp waste ACs and herbicide batch adsorption tests

2.2.7 Single, binary and ternary metal ion batch tests

Single ion standard solutions of 10 ppm $Al(NO_3)_3$, 2 ppm Mn $(NO_3)_2$, and 2 ppm $Fe(NO_3)_3$ were prepared from 1000 ppm stock solutions and buffered at pH 5. 25 mL of each solution was placed into separate 125 mL sealable plastic cups and 50 mg of AC added. Suspensions were shaken at 200 rpm for 24 h (digital orbital shaker table, Ultident) at 20 °C. Aliquots of the supernatant were removed and filtered with a 0.45 µm syringe filter and made up to 25 mL with 5 % HNO_3. The concentrations of ions in the samples were determined by the Agilent MP-AES 4200 at wavelengths of 372 nm, 293 nm 283 nm and 394 nm for Fe, Mn, Pb and Al. A pump speed of 15 rpm and stabilization time of 25 s was used. Nebulizer flow rates for analysis were 0.75 L/min. Calibration curves were plotted from 6 multi-ion standards of concentrations of 25–250 ppm with 5 % HNO_3 solution used as the blank. Binary and ternary ion batch tests were conducted similarly to single ion tests but with multi-ion solutions.

2.2.8 Lake water batch tests

25 mL of lake water samples were added to 50 mg of GH-PAC-DIW or GH-PAC-BW and then agitated at 200 rpm for 24 h. Suspensions were filtered with 0.45 µm membrane syringe filters and aliquots were made up to 25 mL with 5 % HNO_3. Analyte concentration was again determined by MP-AES. Experiments were conducted at the native pH of lake water; 3.10 at 20 °C. Solution pH was measured before and after the adsorption equilibrium studies.

2.2.9 2,4-D and paraquat batch tests and kinetics

2,4-D solutions (25 ml) with an initial concentration of 4 ppm were prepared and equilibrated with 50 mg of GH-$Ch_{20\%}$ AC for 24 h at pH 4–8. Solutions were filtered and 2,4-D equilibrium concentrations were measured using a TOC method developed by Roy et al (Roy et al., 2025). Isotherm data were collected by equilibrating 30 mg of AC with 25 ml of 2,4-D model solution with initial concentrations ranging from 20–500 ppm at 303 K, buffered with a phosphate buffer at pH 7. A similar procedure was used for paraquat adsorption studies with the exception that an adsorbent mass of 18 mg and an initial adsorbate concentration of 40 ppm and 20–250 ppm were used for the initial batch tests and isotherm modelling respectively. Kinetics data were obtained in the time range of 5–1440 min from model solutions at 303 K at pH 7.

2.2.10 Evaluation of the impact of changes in surface area and N-heteroatom content on 2,4-D and paraquat adsorption

In order to evaluate the impact of increased surface area and chitosan-furnished N-heteroatom content of functionalized ACs several experiments were conducted. The adsorption performance of Ch-AC and GH-AC were evaluated under similar conditions to GH-$Ch_{20\%}$. To evaluate the impact of increasing N-heteroatom content, isotherms for GH-$Ch_{10\%}$ and GH-$Ch_{30\%}$ were done under the same conditions as for GH-$Ch_{20\%}$. The Langmuir-derived maximum adsorption capacities were used to make conclusions about the impact of chitosan functionalities in promoting adsorption of 2,4-D and paraquat. The versatility of the adsorbent was evaluated using a binary mixture of 2,4-D and paraquat with the same initial concentration as other batch tests. A modified version of the HPLC method reported by Peixoto et al (Peixoto et al., 2008) was used to quantify the amounts of 2,4-D and paraquat remaining in the binary mixture after treatment with composite ACs. Paraquat was eluted with a 20% methanol-phosphate buffer mixture while 2,4-D was eluted with a 50% methanol-buffer mixture.

2.2.11 Isotherm modelling for metal adsorption

Many adsorption models have been developed to describe adsorption phenomena. These models are derived based on assumptions which may be applicable to the system under consideration. The Langmuir model (**EQ. 5**), one of the more ubiquitously applied models, assumes monolayer coverage of adsorbate on a homogeneous adsorbent. Further, it is assumed that there are no lateral interactions between adsorbed species.

EQ 5 Langmuir Adsorption Model $q_e = \frac{q_m K_L C_e}{1 + K_L C_e}$

The model parameters q_e and q_m are the amount of adsorbate adsorbed at equilibrium and the maximum monolayer adsorption capacity (mg/g) respectively. Equilibrium concentrations of adsorbate and the Langmuir constant are denoted by C_e (mg/l) and K_L (L/mg). The Freundlich Model (**EQ. 6**) is empirical in nature and assumes multilayer adsorption on a heterogeneous surface. Here, the Freundlich constants are K_F ((mg/g)/(mg/l)n) and n (Wang and Guo, 2020).

EQ 6 Freundlich Adsorption Model $\boldsymbol{q_e = K_F C_e^n}$

The Sips Model **(EQ. 7**) is a three-parameter model and a hybrid of the Langmuir and Freundlich Models. It assumes monolayer coverage of adsorbate on the adsorbent surface. Further, its hybrid nature allows for application to both homogeneous and heterogeneous surfaces. In this model, the Sips parameter denoting maximum adsorption capacity is q_{ms}, while K_S (L/mg^{ns}) and n_s are the Sips constant and heterogeneity factor respectively, with $0 \leq ns \geq 1$ (Wang and Guo, 2020). The Sips model reduces to the Langmuir model when $n_s = 1$ and to the Freundlich model at initial concentrations, C_0.

EQ 7 Sips Adsorption Model $\boldsymbol{q_e = \frac{q_{ms} K_S C_e^{ns}}{1 + K_S C_e^{ns}}}$

The Redlich-Peterson (R-P) isotherm model (**EQ. 8**) is described as an empirical hybrid of the Langmuir and Freundlich models (Wang and Guo, 2020). Like the Sips model, its hybrid nature allows it to be applied to both homogeneous and heterogeneous adsorption processes.

EQ 8 Redlich Peterson (R-P) Model $\boldsymbol{q_e = \frac{K_{RP} C_e}{1 + a_{RP} C_e^g}}$

The R-P constants are K_{RP} (L.g^{-1}) and a_{RP} (L^{g}.mg^{-g}). The exponent (g) assumes values from 0 = g ≤ 1. When g = 1, the R-P model reduces to the Langmuir model and when g approaches 0 it reduces to the linear Henry's Law.

2.2.12 Isotherm modelling and determination of standard state thermodynamic parameters for herbicide adsorption

Adsorption data were fitted to two 2-parameter models: Langmuir and Freundlich, and a 3-parameter: Sips. Standard state thermodynamic parameters were determined by the Van't Hoff equation (**EQ. 9**) and plots where the natural log of Langmuir derived equilibrium constant was plotted against the inverse of the temperature at which the adsorption was carried out. Standard enthalpy of adsorption (ΔH^o) and entropy (ΔS^o) were calculated using **EQ 9** while Gibbs energy of adsorption (ΔG^o) was calculated using **EQ. 10**.

EQ 9 Van't Hoff Equation

$$\boldsymbol{lnK_c = \frac{\Delta H^\circ}{R} * \frac{1}{T} + \frac{\Delta S^\circ}{R}}$$

EQ 100 Gibbs Free Energy ΔG° = ΔH° – TΔS°

2.2.13 2,4-D batch tests, isotherm modeling and kinetics for 2,4-D adsorption on GH-SW-ACs

Kinetics data were obtained by equilibrating 18 mg of adsorbent in 25 ml of 2,4-D model solution with an initial concentration of 50 ppm at 303 K at pH 7 in the time range 5–1440 min. Solutions were filtered, and 2,4-D equilibrium concentrations were measured using a TOC method developed by Roy et al (2025) (Roy et al., 2025). Isotherm data were collected by equilibrating 18 mg of each composite with 25 ml of 2,4-D model solution with initial concentrations ranging from 5–250 ppm at 303 K, buffered at pH 7. Equilibrium concentrations of 2,4-D were again measured by TOC. Adsorption data were fitted to the Langmuir, Freundlich and Sips adsorption isotherm models. Full descriptions of these models, including assumptions are given elsewhere (Roy et al., 2025; Tran et al., 2017).

2.2.14 Sample replicates and errors

Sample fabrication and batch testing was done in triplicate with the standard deviation of measurements being represented as the errors. Three replicates were also used for BET surface area measurements. The errors for fitted parameters for adsorption isotherm modelling was the standard error. Model fit was evaluated using the adjusted – R^2, and reduced- χ^2. The Akaike Information Criterion (AIC) also provide additional information on which of a pair of models fitted adsorption data better.

Chapter 3

Preface

Title: Pit-Lake Remediation by Chemically Activated Tropical Hardwood Waste: Simultaneous Metal Ion Removal from Acidic Waters

Authors: Hamant E. France, O.L.K. Strong, Kevin M. Scotland, Tyler M. Roy, Andrew J. Vreugdenhil,

Published in: Sustainable Chemistry for the Environment, Volume 6, 2024, 100103, ISSN 2949-8392, https://doi.org/10.1016/j.scenv.2024.100103.

Contributions H.E. France and A.J. Vreugdenhil proposed the concept. H.E. France performed the experiments and wrote the manuscript. Oliver K.L. Strong assisted with XPS data curation and analysis, K.M. Scotland assisted with Raman analysis and Tyler M. Roy assisted with modelling analysis. All authors contributed to manuscript generation and revision.

3.1 Graphical Abstract

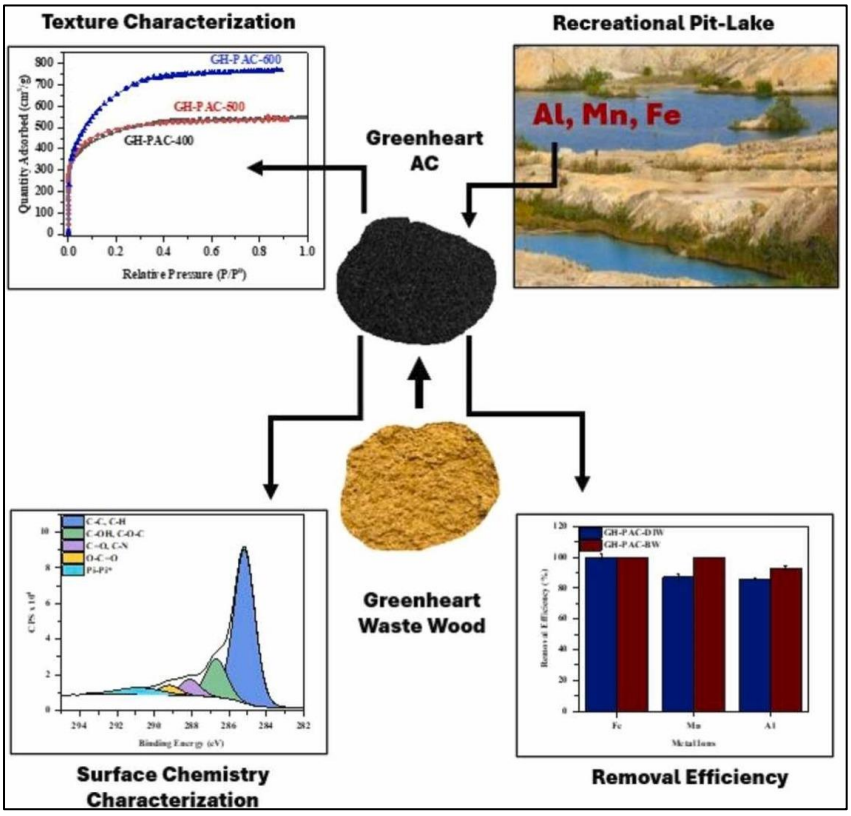

3.2 Abstract

The current study investigates the valorization of waste wood from a tropical hardwood found in Guyana (Greenheart – *Chlorocardium rodiei*) to high surface area activated carbons (AC). We subsequently deployed these adsorbents to sequester Mn^{2+}, Fe^{3+}, and Al^{3+} from the acidic waters of a recreational bauxite pit-lake. We studied the impact of activation parameters such as temperature, impregnation ratio and acid concentration on the texture and surface chemistry of ACs and demonstrate that optimized low pH at point-of-zero charge (pH_{pzc}) ACs are efficient adsorbents for the target ions. A mesoporous AC with specific surface area of 2208 m^2/g, 11 % surface oxygen and pH_{pzc} of 1.98 was produced under optimized conditions. ACs removed 93–100 % of target ions from pit-lake waters at a native pH of 3.1. Al^{3+} exerted an antagonistic effect on Mn^{2+} adsorption in synthetic binary ion systems, reducing adsorption by as much as 56 %. The Sips Model fitted the adsorption data best predicting maximum adsorption capacities for Mn^{2+}, Fe^{3+} and Al^{3+} of 17.8 mg/g, 23.7 mg/g, and 6.12 mg/g for these low pH_{pzc} optimized materials. These materials show great promise in removing heavy metals from acidic waters.

Keywords: chemically activated carbon, tropical waste wood, acidic lake, antagonistic interaction, greenheart

3.3 Introduction

Pit-lakes, an environmental legacy of open pit mining, are formed by the accumulation of ground and surface waters in abandoned pit-mines (Castendyk et al., 2015; Castro and Moore, 2000; Hinwood et al., 2012). These lakes are aesthetically pleasing and are an important recreational resource for some communities (Hinwood et al., 2012; McCullough et al., 2020). Bauxite pit-lakes in particular are known to have very low pH and contain elevated levels of metal ions, particularly Al^{3+}, Mn^{2+}, and Fe^{3+} (Núñez-Gómez et al., 2017a; Williams et al., 2020a). Elevated levels of these ions pose health risks to swimmers, particularly vulnerable swimmers such as children (Hinwood et al., 2012; Sharma et al., 2021). Levels of heavy metals in natural waters can be reduced by low-cost carbonaceous adsorbents (Anirudhan and Sreekumari, 2011; Wajima et al., 2009; Xu et al., 2017; Zeng et al., 2024). Low-cost adsorbents provide significant advantages in pollutant removal such as versatility, economically feasible fabrication, ease of application and potential for regeneration (Abdulhamid et al., 2023; Fadhil et al., 2021; Hussein and Fadhil, 2021).

Activated carbon is an adsorbent material with extensive specific surface area, well-developed pore structure and distinctive surface chemistry (Hynes et al., 2020). These properties of ACs make them well suited to removing pollutants from aquatic media and their versatility has been demonstrated in their use to remove both inorganic and organic species from aqueous systems (Carabineiro et al., 2011; Hwang et al., 2017; Hynes et al., 2020; Patawat et al., 2020). Marrakchi et al 2017 fabricated ACs from chitosan flakes and cross-linked chitosan/sepiolite and successfully applied them in methylene blue and reactive orange 16 removal (Marrakchi et al., 2017, 2016). Khalid et al 2023 used pinecone to produce activated carbons which were

subsequently used in dibenzothiophene from model gasoline-based adsorbates (Khalid and Fadhil, 2024)

Typical ACs may, however, be unsuitable to remove metal ions from waters with low pH. This is challenging since the point-of-zero charge of typical ACs at low pH is generally higher than solution pH (Ghasemi et al., 2023; Kostenko et al., 2019). This results in unfavorable electrostatic interactions and poor adsorption typically results below pH 4. This challenge can be overcome by fabricating adsorbents with low pH_{pzc}.

In this study, we produce high surface area, low pH_{pzc} ACs by a two-staged phosphoric acid activation of a novel precursor; waste wood from *Chlorocardium rodiei* (greenheart). The activant phosphoric acid was used because it typically produces ACs with yields approaching 50% and up to 96% of the acid is recyclable (O. K. L. Strong et al., 2023).

We used ACs to remove Al^{3+}, Mn^{2+} and Fe^{3+} from the waters of an acidic bauxite pit lake (pH 3.1) in Guyana widely used for recreational purposes. Other works have addressed the use of various adsorbents to remove these cations from water, however, these typically have been done using model solutions with pH >3 or typically report poor adsorption at low pH (A. Akl, 2013; Goher et al., 2015; Lobo-Recio et al., 2021; Siabi et al., 2021). Moreover, a ubiquitous approach in adsorption experiments involving metal ions is to optimize the pH at which adsorption occurs and conduct batch tests at this pH. This approach, however, has largely left metal ion adsorption from strongly acidic waters unexplored and hence materials which can efficiently function under such conditions undeveloped.

We characterized the texture and surface chemistry and investigated adsorption behaviors of ACs using gas adsorption, TGA, XPS, Raman, pH drift and batch adsorption experiments. To obtain estimates of their maximum adsorption capacities, we modelled the adsorption of ions onto ACs using Langmuir, Freundlich and Sips adsorption models.

3.4 Experimental (Please refer to Chapter 2 - *Sections: 2.1.1.1, 2.1.2, 2.1.2.1, 2.1.3, 2.1.5, 2.2.2, 2.2.3, 2.2.7, 2.2.8 and 2.2.11*)

3.5 Results and Discussion

3.5.1 BET surface area, pore volume and pore size distribution of ACs

AC production from greenheart was optimized at 600 ℃, 1:1 impregnation ratio with 20 h of digestion (**Figure 3.1**(a-c)). This AC was predominantly mesoporous and had a trimodal pore size distribution (**Figure 3.1**(a) - inset) with about 80% of the pore volume contribution being due to mesopores. Hysteresis, caused by the phenomenon of capillary condensation, is observed on the isotherm at 600 ℃ (**Figure 3.1**(a)) and provides strong evidence for mesoporosity (Thommes et al., 2015a). The extensive surface area and mesoporous texture of GH-PAC-DIW likely resulted from the dual effects of adequate heat energy to mediate bond rearrangement in the material and the presence of sufficient phosphoric acid molecules to act as templating agents. GH-PAC-DIW texture compared favorably with ACs produced from other wood-based feedstock under similar activation conditions including cedar, chestnut, cannabis, prosopis and mixed hardwood (**Figure 3.1**(d)) (de Celis et al., 2009; Díaz-Díez et al., 2004; Lupul et al., 2015). These results suggest the viability of greenheart waste wood as a suitable and sustainable feedstock for fabricating high surface area activated carbons with well-developed porosity.

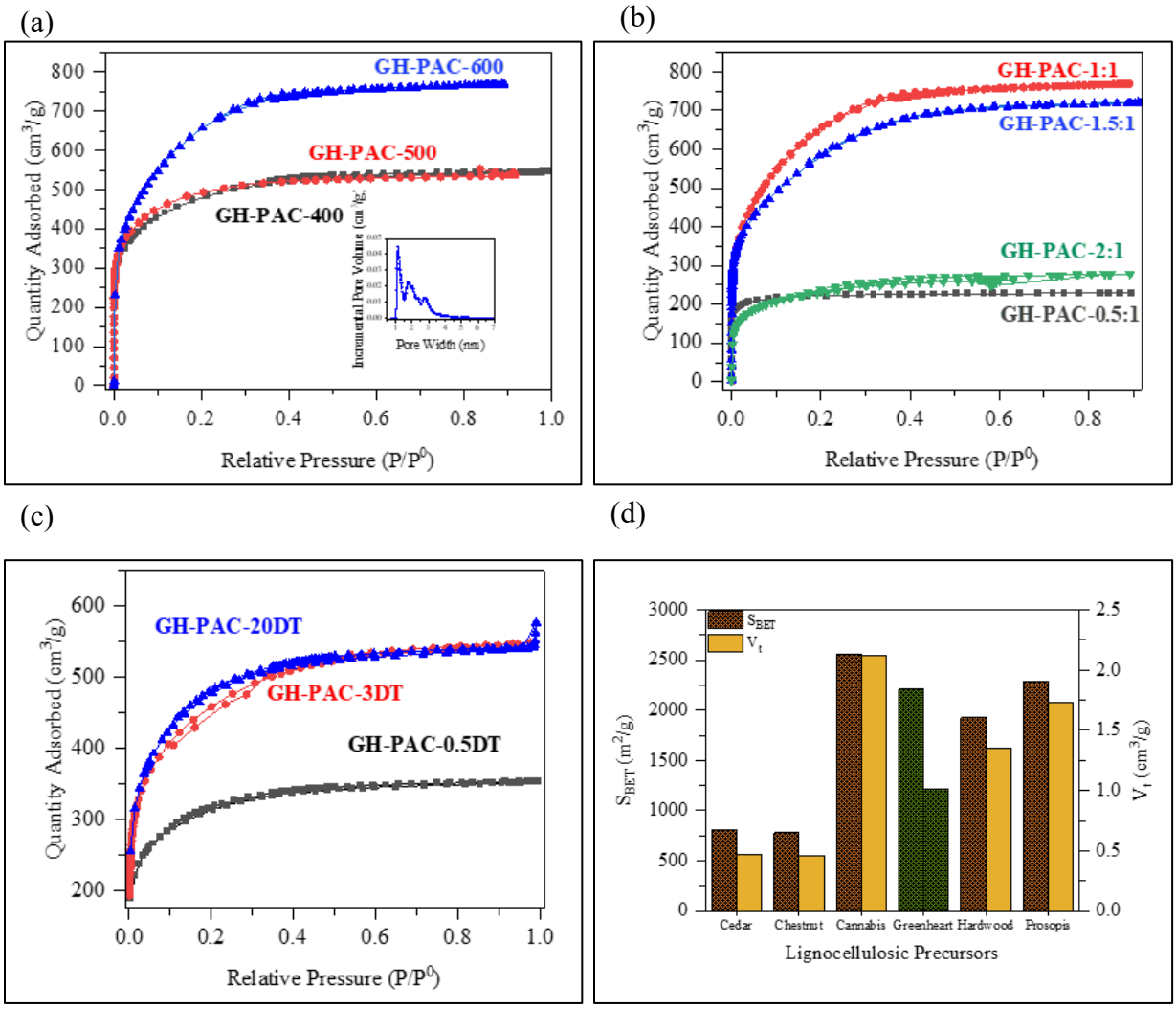

Figure 3.1 BET isotherm plots for ACs produced at 400–600 ℃, (b) 0.5–2 impregnation ratio (c) 0.5–20 h digestion, and (d) comparison of GH-PAC-DIW texture with other ACs.

3.5.2 Impact of activation parameters on material texture

Table 3.1 summarizes the impact of activation parameters on textural characteristics of AC for samples labelled C1-C13. Increases in impregnation ratio correlated with increases in specific surface area up to a critical maximum (**Figure 3.2**(a)); 1:1 ratio. Surface area decreased thereafter. When higher ratios of acid are used, pyrophosphates are more likely to form and

occupy more spaces in the material. Subsequent removal of pyrophosphates by washing engenders larger mesopores and macropores in AC (O. K. L. Strong et al., 2023). These larger pores may be unstable and consequently collapse leading to a decrease in surface area. Pore collapse is mitigated by using lower concentrations of acid and optimized impregnation ratios as this reduces the likelihood of the formation of polymeric acid species. Increases in digestion time allowed for improved permeation of the activant into the natural porosity of the precursor which resulted in better cleavage of aryl-ether and glycosidic bonds in lignin and cellulose respectively. Higher activation temperatures provided more energy for the elimination of volatiles and the reorganization of carbon centers. Since this reorganization leaves spaces on the order of nanometers in the material, a network of porosity and increased surface area result (Kumar and Jena, 2016; Marsh and Rodríguez-Reinoso, 2006a; Yorgun and Yildiz, 2015). These results show that moderate temperature and minimal chemicals can generate ACs with good texture from greenheart waste wood. They further suggest that this feedstock is a good candidate for efficient and economical valorization to ACs.

Table 3.1 Specific surface areas, micropore and total pore volumes of ACs produced under various conditions.

AC	Carbonization Time (h)	Activation Temperature (℃)	Acid Conc. (wt %)	Impregnation Ratio	S_{BET} (m^2/g)	V_t (cm^3/g)	V_{mic} (cm^3/g)
C1	0.5	400	25	1:1	1140 ± 35	0.54 ± 0.02	0.24 ± 0.00
C2	3.0	400	25	1:1	1201 ± 34	0.55 ± 0.03	0.22 ± 0.02
C3	20	400	25	1:1	1841 ± 52	0.84 ± 0.04	0.28 ± 0.03
C4	20	600	25	1:1	1986 ± 159	1.01 ± 0.07	0.19 ± 0.04
C5	20	400	50	1:1	1743 ± 111	0.84 ± 0.04	0.29 ± 0.09
C6	3.0	400	25	2:1	750.0 ± 67	0.34 ± 0.02	0.10 ± 0.02
C7	5.0	600	50	1:1	1814 ± 139	0.85 ± 0.07	0.34 ± 0.13
C8	20	500	50	1:1	1888 ± 37	0.83 ± 0.02	0.46 ± 0.01
C9	20	600	50	0.5:1	873.6 ± 59	0.36 ± 0.02	0.28 ± 0.01
C10	20	600	50	1:1	2208 ± 91	1.01 ± 0.03	0.20 ± 0.02
C11*	20	600	50	1:1	1740 ± 22	1.92 ± 0.38	0.48 ± 0.01
C12	20	600	50	1.5:1	2165 ± 143	1.11 ± 0.07	0.35 ± 0.04
C13	20	600	50	2:1	1065 ± 145	1.18 ± 0.11	0.17 ± 0.01

*Base Washed AC (GH-PAC-BW_0.1)

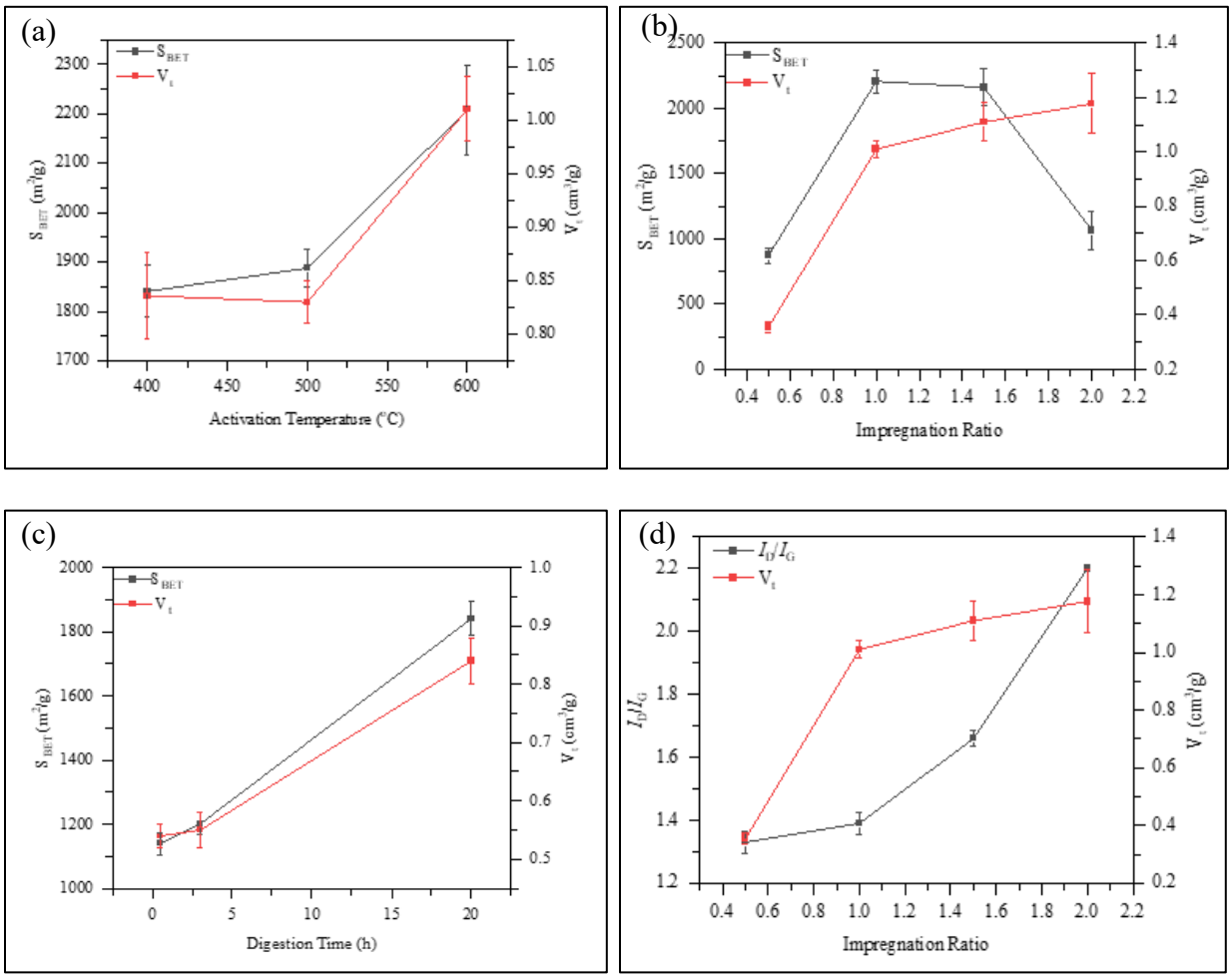

Figure 3.2 Impact of (a) impregnation ratio, (b) activation temperature with 1:1 impregnation ratio (c) digestion time with 1:1 impregnation ratio on acs texture and (d) relationship between I_D/I_G ratio and total pore volume with impregnation ratio for ACs produced with 50% H_3PO_4 at 600 ℃.

3.5.3 TGA and Raman analysis

The initial portion of the TGA scan under nitrogen of the raw greenheart precursor (**Figure 3.3**(a)) indicates a loss of mass of ~5% at an onset temperature of 57 ℃. This change is most likely due to loss of adsorbed moisture on the precursor surface. On the DTG curve, a clear peak at 354 ℃ with a subtle shoulder at ~260 ℃ is observable. These features most likely owe their

appearance to decomposition of the major macromolecular components of the wood precursor. As described previously in the literature, decomposition of the three macromolecular components of wood take place in narrow temperature ranges which overlap (Poletto et al., 2012; Sebio-Puñal et al., 2012). Hemicellulose and cellulose decompose within the temperature ranges 220–315 ℃ and 315–400 ℃, respectively (Yang et al., 2007)

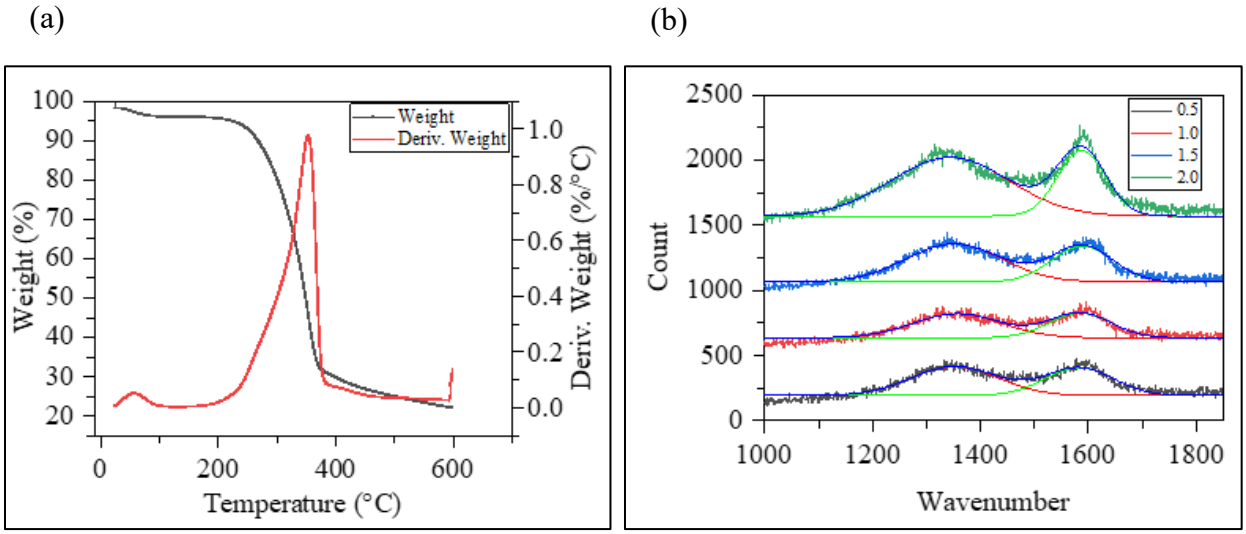

Figure 3.3 TGA and DTG scans of greenheart under N_2 (60 mL/min) at a scan rate of 10 ℃/min and (b) Raman spectra of ACs produced at impregnation ratios in the range 0.5–2.

TGA and DTG analysis confirms the suitability of the activation temperatures used in this work as they overlap with the major decomposition ranges of the major constituents of wood. The amorphous texture of the materials was confirmed by characteristic Raman D and G-bands (**Figure 3.3**(b)) at ~1350 cm^{-1} and ~1580 cm^{-1} respectively (Lota et al., 2016; Seo et al., 2009). The relative intensities of these bands yield the I_D/I_G ratio. This metric provides a measure of the degree of disorder in the sample. It was observed that the I_D/I_G ratio was proportional to the phosphoric acid impregnation ratio as well as total pore volume of the ACs (**Figure 3.3**(d)).

3.5.4 pH at point-of-zero of charge

GH-PAC-DIW had a low point of zero charge pH of 1.98; a consequence of the presence of protonated residual phosphoric acid species on the AC surface. Control of this parameter was critical to the adsorption of target ions [43]. Base-wash treatments produced GH-PAC-BW-0.1 and GH-PAC-BW-0.4 with increased pH_{pzc} of 2.95 and 7.08. These treatments deprotonated acidic functions on the material surface. Consequently, batch tests in this work were carried out using GH-PAC-DIW and GH-PAC-BW-0.1 at pH 3.10 (the native pH of lake water samples) and at pH 5 for buffered synthetic solutions. Base wash treatments therefore provide a means of tailoring the surface charge of ACs.

3.5.5 Surface chemistry of ACs and impact of base wash treatment

Greenheart precursor was predominantly composed of carbon and oxygen with modest amounts of silicon and nitrogen (**Figure 3.4**(a, d)) and **Table 3.2**. Activation simultaneously increased the percentages of C and decreased the percentages of heteroatoms (Marsh and Rodríguez-Reinoso, 2006a). The resultant adsorbents both contained ~97% carbon and oxygen. As expected, GH-PAC-BW contained sodium on its surface from the base washing process (**Figure 3.4**(d)). Interestingly, this AC also showed reduced specific surface areas. GH-PAC-BW had ~21% smaller surface area than GH-PAC-DIW (**Table** 3.1). This reduction in surface area may be largely due to pore widening, and pore collapse because of the etching effect of sodium hydroxide on the walls of pores; particularly micropore walls (Gao et al., 2013; Zhang et al., 2020). Sodium adsorption on AC surface may have also played a role in surface area loss. This may have occurred in two ways. Firstly, the additional mass of sodium would reduce the specific surface of AC without contributing to the surface area. Secondly, sodium salt precipitates may

have filled otherwise accessible pores. The need to moderate base washing so as to preserve material texture is made apparent from these results.

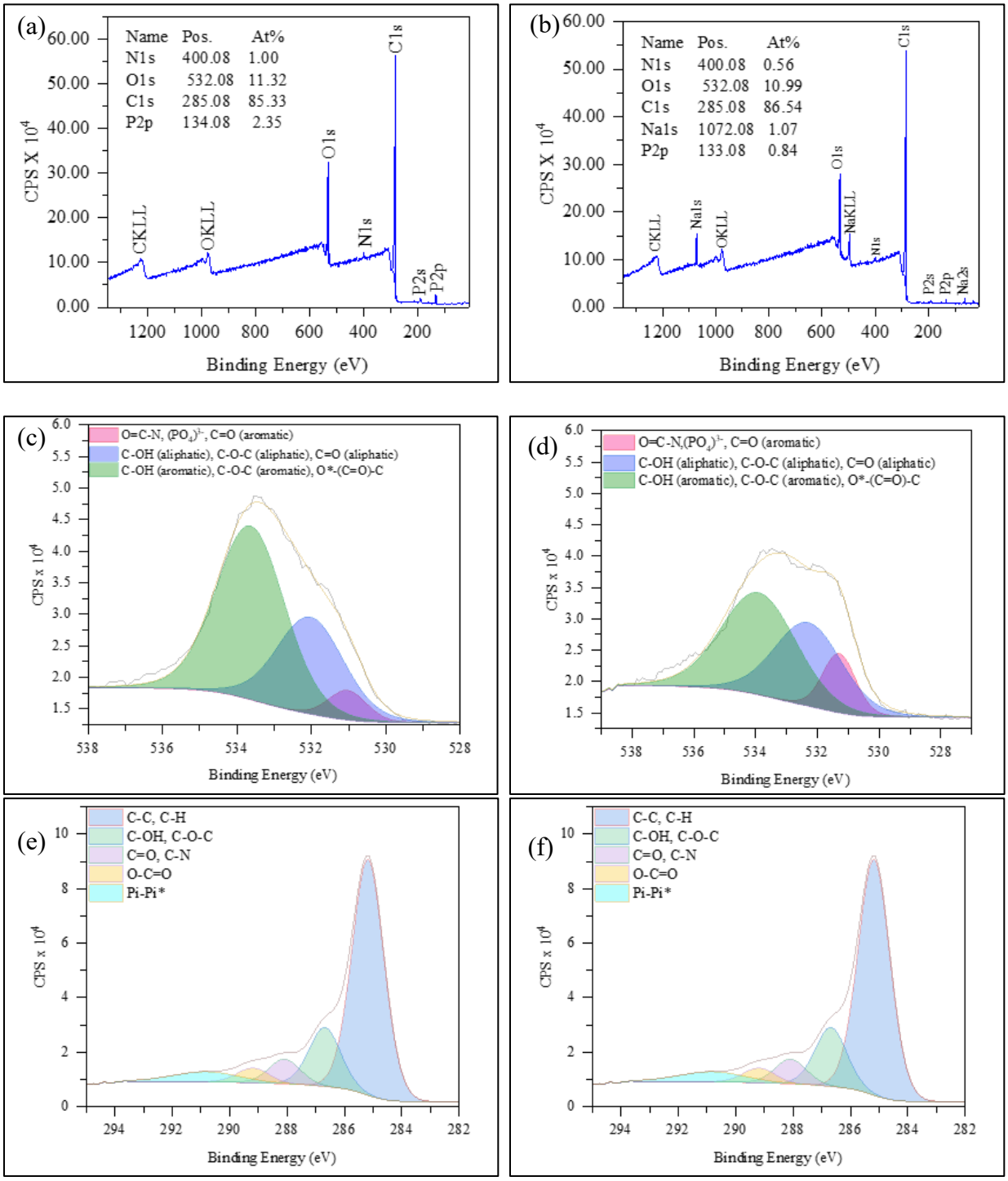

Figure 3.4 Typical XPS wide scans, O1s and C1s high resolution scan of (a-c) GH-PAC-DIW and (d-f) GH-PAC-BW.

Table 3.2 Average atomic percentages of elements from XPS survey scans of greenheart precursor and ACs.

	Atomic %		
Atomic Species	GH-Precursor	GH-PAC-DIW	GH-PAC-BW-0.1
C1s	69.81 ± 3.22	85.78 ± 0.32	86.04 ± 0.41
O1s	21.58 ± 1.53	11.34 ± 0.14	11.26 ± 0.33
N1s	2.65 ± 0.14	0.61 ± 0.29	0.67 ± 0.09
Si2s	5.96 ± 1.90	0	0
P2p	0	2.30 ± 0.09	0.78 ± 0.05
Na1s	0	0	1.24 ± 0.12

Residual phosphorous peaks (**Figure 3.4**(a)) were present at ~134 eV. Base wash treatment reduced the proportions of phosphorus in GH-PAC-BW (**Figure 3.4**(b)). While base wash treatment reduced the proportions of Lewis base functionalities, the impact of increasing negative surface charge was sufficient to enhance the adsorption behaviour of GH-PAC-BW to target ions in lake water (**Figure 3.5**(b)).

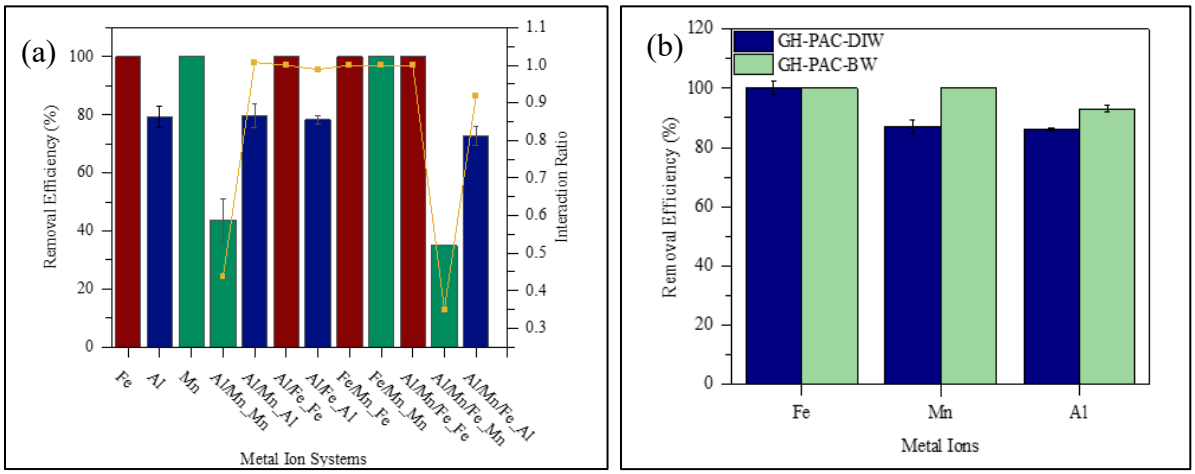

Figure 3.5 Removal efficiencies and interaction ratios of (a) acs with single, binary and ternary-ion synthetic systems and (b) lake water samples.

Deconvolution of the O1s peak (**Figure 3.4**(b) and **Figure 3.4**(e)) showed the presence of ethers and esters (~533 eV), phenolic groups (~532 eV) and amides and aromatic ketones (~531 eV), on ACs. C1s deconvoluted high resolution spectra provided complementary evidence for these functionalities (**Figure 3.4**(c) and **Figure 3.4**(f)). Oxygen containing functional groups (OFGs) were critical in facilitating removal of target cations. It is known that ACs with high proportions of OFGs show good cationic adsorption performance (Song et al., 2010). This is generally ascribed to increased columbic attractions between the resulting negatively charged AC surface and cationic species (Duan et al., 2020).

3.5.6 Lake water quality and batch adsorption tests analysis

3.5.6.1 Lake water quality and batch adsorption tests analysis

Target ion levels were respectively one (Mn^{2+} and Fe^{3+}) or two (Al^{3+}) orders of magnitude above the guideline values (GVs) for recreational water quality as outlined by the Australian and New Zealand Fresh and Marine Water Quality guidelines (ANZECC & ARMCANZ-2000) (Australian and New Zealand Environment and Conservation Council. and Agriculture and Resource Management Council of Australia and New Zealand., 2000) (**Table 3.3**). Comparison to drinking water reference guidelines may be justified when the possibility of frequent and protracted use of pit lakes for swimming is considered.

Table 3.3 Comparison of lake water chemistry with literature and water standards.

	Lake Water Ion Concentration (ppm)		Guideline Values for Recreational Water (ppm)		Guideline Values for Drinking Water (ppm)
	This Study	Williams 2020	ANZECC (2000)	WHO (2021)	WHO (2021)
pH	3.10 ± 0.01	3.4	5–9	-	6.5–9.5
Fe	1.47 ± 0.15	3.69	0.3	NA	NA
Mn	1.23 ± 0.12	2.40	0.1	8	0.4
Al	7.49 ± 0.75	9.02	0.2	18	0.9

3.5.6.2 Batch adsorption tests with lake and synthetic waters

The initial pH of lake water samples was 3.10 (**Table 3.3**) with no significant alteration in pH after batch experiments. Both GH-PAC-DIW and GH-PAC-BW demonstrated excellent removal efficiencies of Fe^{3+}, Mn^{2+} and Al^{3+} (**Figure 3.5**), with removal efficiencies >80%. Lobo-Recio et al. (Lobo-Recio et al., 2021) reported removal efficiencies for Fe^{3+}, Mn^{2+} and Al^{3+} at pH 4 of 15%, 43% and 54% on a zeolite. Enhanced removal of Al^{3+} and Mn^{2+} was observed in the lake water batch tests with GH-PAC-BW which had pH_{pzc} of 2.95. (**Figure 3.5**(b)). The complementary surface charge of greenheart ACs at the native pH of lake water and the presence of sufficient OFG adsorption sites most likely facilitated excellent performance of these tropical hardwood adsorbents.

In single ion batch tests, GH-PAC-DIW, completely removed Fe^{3+} and Mn^{2+}. Here too, extensive surface area and complementary charge facilitated adsorption. Additionally, the comparatively

low initial concentration of these two species (2 ppm) did not exhaust the available adsorption sites. Moreover, these two cations had comparatively large Sips K_s constants: 1.32 and 3.46 for Mn^{2+} and Fe^{3+} respectively (**Table 3.4**). Generally, the Langmuir affinity factor K_L is used to infer the strength of the interaction between adsorbate and adsorbent (Kocherbitov and Arnebrant, 2010). In our modelling analysis, the Sips constant (n_s) approaches unity for all adsorption systems (**Table 3.4**) implying that the Sips model reduces to the Langmuir model. Consequently, K_s can be used in place of K_L to infer the strength of adsorbate-adsorbent interaction (Kocherbitov and Arnebrant, 2010). The percentage removal for Al^{3+} was ~77.0 ± 3.21 % in all systems. Additionally, of the three cations, Al^{3+} had the smallest K_s constant (0.26) implying relatively weaker interaction with greeheart ACs. These results suggest that greenheart ACs are promising materials for remediating acidic waters containing heavy metals. Furthermore, since their fabrication involves the valorization of greenheart waste wood with minimal chemical input, they allow for a green approach to remediating polluted waters. Moreover, these materials may have value in assisting efforts to recover valuable metals from waters impacted by acidic mine drainage particularly where other methods are costly or inefficient.

Table 3.4 Model parameters and statistical evaluation of model fit for Langmuir, Freundlich and sips isotherms.

Metal Ions	Model Parameters			Model Fit
	Langmuir			Adj R^2
	Q_0 *(mg/g)*	K_L *(L/mg)*		
Mn	17.8 ± 3.05	3.46 ± 3.30		0.839
Fe	23.7 ± 1.76	1.32 ± 0.33		0.976
Al	6.01 ± 0.24	0.27 ± 0.04		0.991
	Freundlich			
	K_F *(L/mg)*	n		
Mn	13.7 ± 0.06	9.44 ± 0.19		0.772
Fe	11.3 ± 1.21	3.00 ± 0.55		0.955
Al	2.21 ± 0.20	3.74 ± 0.04		0.930
	Sips			
	Q_0 *(mg/g)*	K_s	n_s	
Mn	17.8 ± 1.31E-16	3.46 ± 1.94E-16	1.00 ± 5.73E-17	1.00
Fe	23.7 ± 3.60E-16	1.32 ± 5.08E-17	1.00 ± 4.10E-17	1.00
Al	6.12 ± 5.29 E-1	0.26 ± 7.11E-2	0.96 ± 1.61E-1	0.99

3.5.7 Metal ion interactions

In the binary and ternary systems, ion interaction appeared to influence the adsorption behaviour of ions. This gave rise to system dependent adsorption of Mn^{2+}. These effects were most clearly observed in the systems containing both Mn^{2+} and Al^{3+} (**Figure 3.5**(a)). Generally, the adsorption interactions of ions in multi-ion systems may be of three types. Firstly, interactions may be synergistic with interaction ratio (IR) > 1. Such interactions are characterized by increased adsorption of one or more species in the mixture when compared to single ion adsorption. Secondly, antagonistic interactions (IR < 1) may occur where decreased adsorption of one or more species results. And thirdly, there may be noninteractions (IR = 1) (Srivastava et al., 2008).

Antagonistic interactions may have occurred between Mn^{2+} and Al^{3+} in the binary and ternary ion systems where the IRs were 0.44 and 0.35 respectively (**Figure 3.5**(a)). These effects may be due to differences in ionic strengths of the aluminum-containing systems where Al^{3+} concentration was 10 ppm. It is known that increasing ionic strength reduces adsorption of some cations on adsorbents due to decreased activity coefficients. Lower activity coefficients result in retardation of species transfer to adsorbent sites (Rao et al., 2007). A greater retardation in Mn^{2+} removal was seen in the ternary system (35% removal) compared to the binary system (44% removal). This was likely due to increased competition for adsorption sites from the two trivalent cations.

3.5.8 Isotherm modelling analysis

To better understand the interactions between ACs and analyte systems, the adsorption data were fitted to the Langmuir, Freundlich and Sips Models (**Figure 3.6**(a–c).

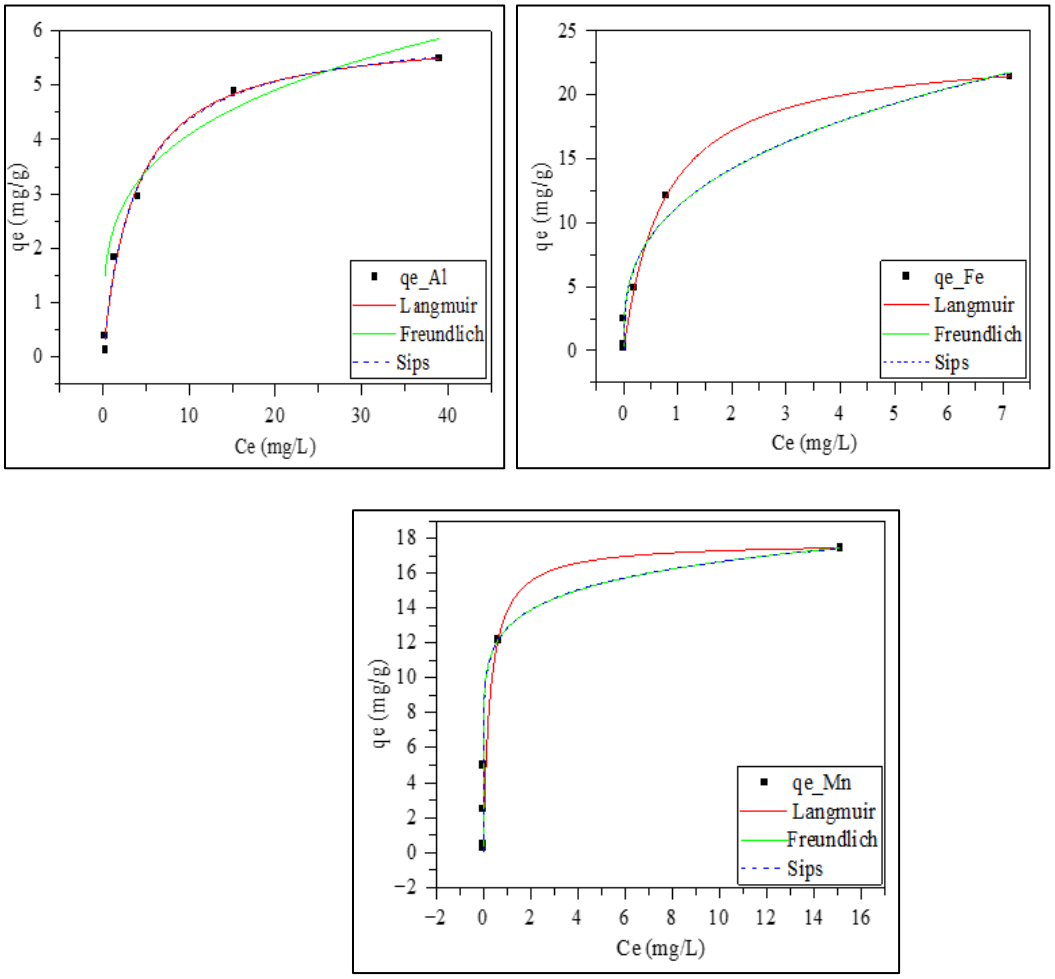

Figure 3.6 Langmuir, Freundlich and Sips Adsorption model isotherms for (6a) Al, (6b) Fe and (6c) Mn, in single ion systems.

Model parameters are shown in **Table 3.4**. The Sips Model fitted the adsorption data best. Maximum adsorption capacities (Q_{max}) of 17.8 mg/g, 23.7 mg/g, and 6.12 mg/g for Mn^{2+}, Fe^{3+} and Al^{3+} respectively were predicted (**Table 3.4**). Q_{max} for adsorption of Mn^{2+}, on greenheart AC was greater than that reported by Goher et al. (Goher et al., 2015) (0.176 mg/g) for adsorption on a commercial AC and Nunez-Gomez et al. (Núñez-Gómez et al., 2017b) (3.87 mg/g) for adsorption on shrimp shells. Adsorption on a zeolite at pH 4 was however greater (50.11 mg/g) (Lobo-Recio et al., 2021). GH-PAC adsorption capacity for Al^{3+} was lower than reported in the literature, with Lobo-Recio et al. (Lobo-Recio et al., 2021) reporting Q_{max} of 13.9 mg/g and Goher et al. (Goher et al., 2015), 106.5 mg/g. These experiments were however done in the pH range 4–7. Al-Muhtaseb et al. (Al-Muhtaseb et al., 2008) reported maximum adsorption of Al^{3+} of 0.676 mg/g on a date-pit AC at pH 3. The maximum adsorption capacities of Mn^{2+} and Fe^{3+} on GH-PAC was generally comparable with other adsorbents, but Al^{3+} Q_{max} was typically lower (Appendix i, **Table 0.1**).

Excellent model fit was seen for all ions as indicated by R^2 values approaching unity (**Table 3.4**). The extent of this correlation may have been improved by the inherent advantages of model fit due to the use of a three-parameter model. Furthermore, n_s values and the nearly identical K_L and K_s values show that the Sips model reduced to the Langmuir model for all systems considered.

Modelling analysis confirms that greenheart ACs perform well in acidic environments and therefore may be deployed as remediation materials for acidic pit-lakes and waters impacted by acid mine drainage. Further, these low pH_{pzc} materials may additionally be suitable candidates for isolating valuable metals from acidic waters.

3.6 Conclusions

This work demonstrates the valorization of a waste lignocellulosic feedstock produced by industry proximate to the metal contaminated pit lakes. The valorization is accomplished by conversion to low-pH-at-pzc activated carbons which remove environmentally relevant levels of important metal contaminants from low pH waters. Our results show that low pH_{pzc} ACs with surface areas of 2200 m^2/g are achievable with minimal chemical inputs, at low activation times and moderate temperatures. Since moderate temperatures and minimal chemical inputs were used to produce these high surface area materials, their fabrication is both economically feasible and sustainable. Fabrication of these ACs derive the dual benefits of diverting a copious local waste stream and converting it, via a largely environmentally friendly process, to efficient environmental remediation materials. Evaluation of the AC processing parameters demonstrated that S_{BET} and total pore volume increased with increasing impregnation ratio. Modelling analysis confirms that greenheart ACs perform well in acidic environments and therefore may be deployed as remediation materials for acidic pit-lakes and waters impacted by acid mine drainage. Further, these low pHpzc materials may additionally be suitable candidates for isolating valuable metals from acidic waters.

Chapter 4

Preface

Title: Fabrication and Ambient Temperature Flash O-Functionalization of Chlorocardium rodiei-based Carbon for Toxic Metal Adsorption

Authors: Hamant E. France, O.L.K Strong, Andrew J. Vreugdenhil

Reference: This chapter is currently under review. The published version of this manuscript will appear with minor modifications from the chapter presented here.

Contributions: H.E. France and A.J. Vreugdenhil proposed the concept. H.E. France performed the experiments and wrote the manuscript. Oliver K.L. Strong assisted with XPS data curation and analysis. All authors contributed to manuscript generation and revision.

4.1 Graphical Abstract

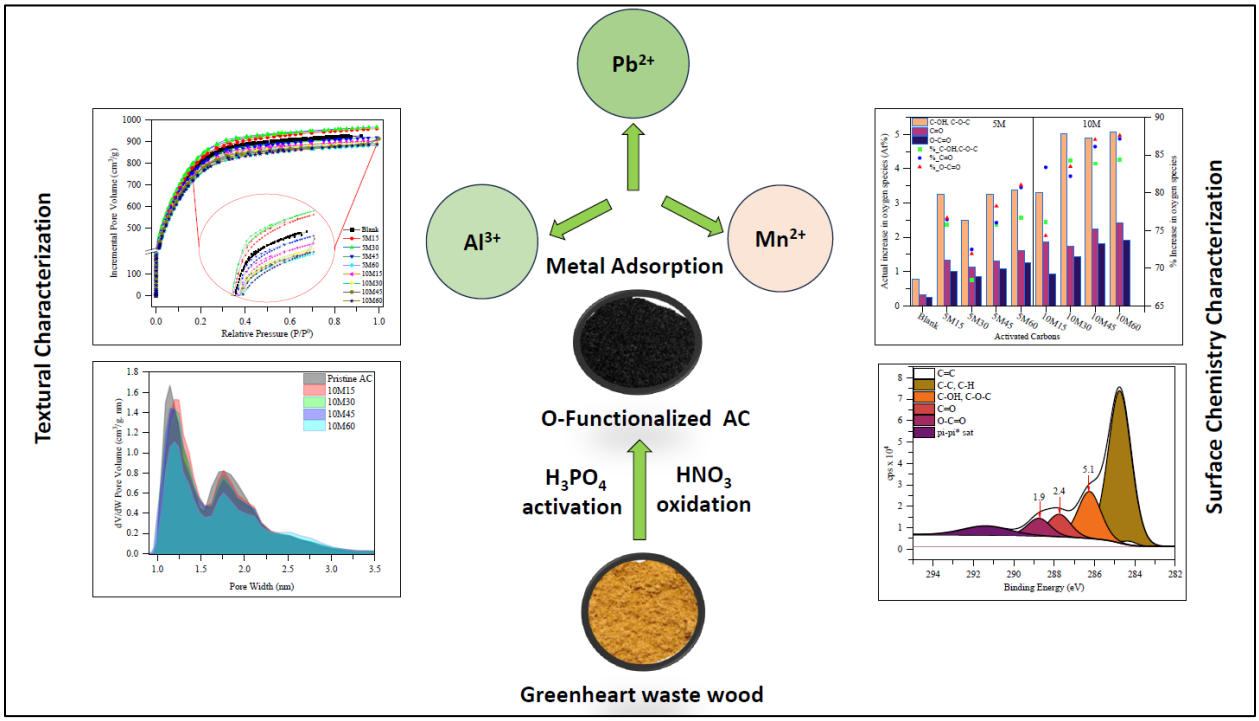

4.2 Abstract

Fabrication of activated carbons from lignocellulosic feedstock is a well-established means of waste valorization. Adsorbent functionalization by increasing oxygen heteroatom content is an important modification technique. Wet oxidation with concentrated nitric acid is among the most ubiquitous and productive strategies but current oxidation regimes utilize extended residence times and cause undesirable losses in specific surface area. Here, we fabricated activated carbons from *Chlorocardium rodiei* waste wood and evaluated the changes in physicochemical properties of this adsorbent when subjected to a little explored, ambient temperature, low-residence time oxidation procedure. We evaluated the types of oxygen speciation generated under various regimes and studied their impact on the removal efficiencies of Pb^{2+}, Al^{3+} and Mn^{2+} in model solutions at pH 3. Flash oxidation with 10 M nitric acid for 60 min resulted in only a 12 % loss in specific surface area and increased the total carbon-bound oxygen content by 8 atomic %. This enhanced adsorption of Al^{3+} and Pb^{2+} by 22% and 5% respectively. Al^{3+} and Pb^{2+} removal efficiencies were strongly correlated with the presence of carbonyl and alcohol functional groups while Mn^{2+} was poorly adsorbed and had a negative correlation with acidic groups. The adsorption of each metal was therefore predominantly mediated by different oxygen moieties on the material surface. These results demonstrate that flash oxidation can yield strong increases in oxygen while preserving surface area and is a viable addition to existing oxygen heteroatom functionalization strategies.

4.3 Introduction

Activated carbons (ACs) have long been successfully used in aquatic remediation due to their extensive surface area, well-developed pore structure and distinctive surface chemistry (Bhatnagar et al., 2013; Fashola et al., 2016). These adsorbents have been fabricated from a wide range of feedstocks, but lignocellulosic biomass like wood, nut shells and coconut shells are ubiquitously used (Zou et al., 2024). A wide range of cations and organics have been successfully removed from aqueous systems using lignocellulosic derived ACs. (Carneiro Brandão Pereira et al., 2020; Du et al., 2022). The efficacy of carbon adsorbents can be improved by functionalization with various heteroatoms. Functionalization techniques include N-doping to improve organic molecule adsorption, metal ion impregnation to improve oxyanion adsorption and various oxidations (Daud and Houshamnd, 2010; Haydar et al., 2003; Jaramillo et al., 2010; Mishra et al., 2021; O. K. L. Strong et al., 2023).

Oxidations are typically employed to enhance metal ion uptake (Qasem et al., 2021) or may be an initial procedure before initiator attachment in polymer grafting (Bégin et al., 2023). Oxidations may be classified as either wet or dry. Wet oxidations involve the use of aqueous solutions such as nitric acid or hydrogen peroxide. Dry oxidations are mediated by reagents such as ozone or oxygen. Nitric acid oxidations in particular are known to yield strong increases in oxygen containing functional groups (OFGs) (Jaramillo et al., 2010).

While the use of strong acids to increase OFGs is well established, most works utilize extensive residence times and elevated temperatures to derive desirable oxidation. This, however, is done at the expense of specific surface area as under these conditions pore collapse results. Protracted

oxidation can cause the loss of up to 50% of the surface area of an adsorbent (Radkevich et al., 2008). The need for techniques which simultaneously improve OFGs while preserving specific surface area therefore persists.

Here, we hypothesize that: -

1. The exposure of a pristine, tropical-hardwood-based AC to concentrated nitric acid for times of 60 min or less significantly improves OFGs.
2. Specific surface area is generally preserved by the procedure.
3. Enhanced adsorption of Pb^{2+}, Mn^{2+} and Al^{3+} at acidic pH accrues from the functionalized adsorbents.

We first fabricate activated carbons by two-staged phosphoric acid activation of a novel tropical hardwood sawdust precursor, *Chlorocardium rodiei* (greenheart), and then use a facile, ambient temperature, flash oxidation technique to improve oxygen heteroatom functionality. Here, flash oxidation is defined as post-activation treatment of AC with strong nitric acid for 60 min or less. We compared the adsorption performance of pristine and flash oxidized ACs in the removal of Al^{3+}, Mn^{2+} and Pb^{2+} from model solutions at pH 3. We probed the textural characteristics of the ACs by gas adsorption while XPS and batch adsorption experiments provided information on the chemical characteristics of AC surfaces and their adsorption behaviour. We further fitted adsorption data to non-linear Langmuir, Freundlich, Sips and Redlich-Peterson adsorption models to derive estimates of the maximum adsorption capacities of our materials. To the best of our knowledge, no study has been reported on the impact of flash oxidation on the texture, and surface chemistry of wood based activated carbons and the subsequent effects on adsorption performance of Pb^{2+} Mn^{2+} and Al^{3+}.

4.4 Experimental (Please refer to Chapter 2: *Sections - 2.1.1.1, 2.1.2, 2.1.2.1, 2.1.5, 2.2.4, 2.2.7, 2.2.11*)

4.5 Results and Discussion

4.5.1 BET Surface Area, Pore Volume and Pore Size Distribution Analysis

Table 4.1 shows the textural parameters of the pristine and flash-oxidized ACs. Pristine GH-PAC_{600} had a surface area of 2676 ± 3 m^2/g with total pore volumes and micropore volumes respectively of 1.18 ± 0.00 and 0.47 ± 0.02 cm^3/g. Oxidative treatment with 5 M nitric acid for 15 min lead to a subtle increase in the specific surface area to 2723 ± 32 m^2/g (**Figure 4.1**(a) and **Figure 4.11**(b)). Ang et al (2021) also reported increases in surface area due to oxidative treatment of activated carbons (Ang et al., 2021). This increase in surface area was accompanied by a slight increase in total pore volume. Surface area change was most likely due to the "cleaning action" of the concentrated oxidant which removed residual phosphates and simultaneously widened micropores. Phosphate removal was confirmed by XPS survey scans (**Figure 4.2**(b)) which showed an approximately 50% decrease in phosphorus between pristine GH-PAC_{600} and GH-OX_{5M15}.

With 5 M acid, longer residence times typically resulted in decreases in surface area, and total pore volumes affecting both the micropore and mesopore volumes. (**Table 4.1** and **Figure 4.1**(a-d)). Surface area loss started after 30 min of oxidation and progressed at an average rate of 1.4 m^2/min. Surface area loss is attributed to the collapse of larger unstable mesopores which were generated by the etching action of the acid over a longer duration. A marginal transformation of micropores to mesopores was seen (8 % increase) between GH-PAC_{600} and GH-OX_{5M30} (**Figure 4.1**(d)). At the higher acid concentration (10 M), surface area, total and micropore volumes also decreased with residence time. As expected, the largest loss in surface area occurred after 60 min of oxidation and was ~ 4 times faster (5.2 m^2/min) with the stronger oxidant. Mesoporosity of

oxidized ACs decreased relative to pristine AC but increased relative to microporosity (**Figure 4.1**(e)).

Notwithstanding the above changes in the textural features of the oxidized adsorbents, the materials' texture remained largely intact. In fact, surface area decreased by only 82 m^2/g (3%) and 312 m^2/g (12%) for oxidation with 5 M and 10 M acid respectively after 60 min of oxidation. Additionally, the total loss of porosity was no more than 3% and 8.5%. These findings demonstrate that flash oxidation largely preserved the texture of the adsorbents. They are significant given the fact that some current treatments have been widely shown to cause catastrophic textural losses (**Table 4.2**). Furthermore, the ease of application of this procedure, its brevity and the fact that it can be done at ambient temperature is promising in the context of greener fabrication efforts. Moreover, our findings imply that careful control of oxidation parameters is key to realizing the dual benefits of high oxygen content and preserved surface texture.

Table 4.1 Experimentally determined texture of GH-OX ACs oxidized with 5 M and 10 M HNO_3 for times ranging from 15–60 minutes at ambient temperature.

Greenheart ACs	S_{BET} (m^2/g)	V_t (cm^3/g)	V_{mic} (cm^3/g)	V_{me} (cm^3/g)
GH-PAC_{600}	2676 ± 3	1.18 ± 0.00	0.47 ± 0.02	0.72 ± 0.02
GH-OX_{5M15}	2723 ± 32	1.21 ± 0.04	0.48 ± 0.03	0.73 ± 0.01
GH-OX_{5M30}	2746 ± 21	1.23 ± 0.02	0.45 ± 0.00	0.78 ± 0.02
GH-OX_{5M45}	2672 ± 40	1.18 ± 0.01	0.47 ± 0.02	0.70 ± 0.03
GH-OX_{5M60}	2594 ± 112	1.15 ± 0.06	0.40 ± 0.03	0.75 ± 0.03
GH-OX_{10M15}	2556 ± 56	1.13 ± 0.02	0.39 ± 0.01	0.74 ± 0.01
GH-OX_{10M30}	2507 ± 106	1.13 ± 0.02	0.38 ± 0.04	0.75 ± 0.02
GH-OX_{10M45}	2532 ± 34	1.15 ± 0.02	0.38 ± 0.06	0.77 ± 0.04
GH-OX_{10M60}	2364 ± 51	1.08 ± 0.15	0.34 ± 0.01	0.62 ± 0.16

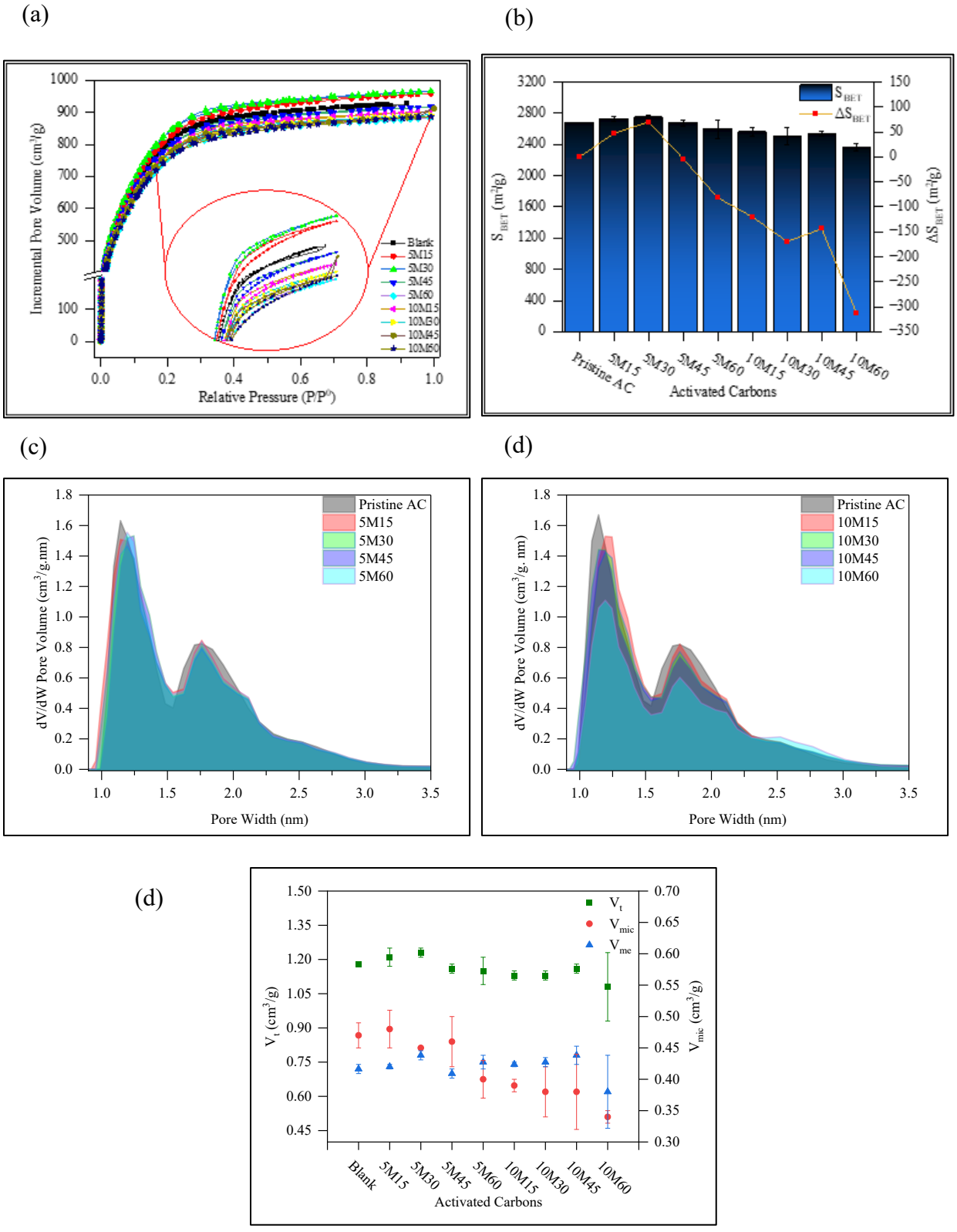

Figure 4.1 a – BET isotherms for GH-OX ACs, b – comparison of total surface area with loss of surface area for oxidized ACs and pore size distributions of c – 5 M and d – 10 M oxidized ACs

Table 4.2 Comparison of production parameters and atomic % oxygen of flash-oxidized AC in this work and selected ACs from other HNO_3 treatments.

Precursor	Treatment/Conditions	Surface Area Change		Oxygen At wt% Increase	Reference
		m^2/g	%		
Stone-fruit	5 M HCl, 30% HNO_3, 2 h, 373 K.	- 470	49	14.6	(Radkevich et al., 2008)
Cherry Stones	5 M, 363–368 K, 10 h	-205	34	-	(Jaramillo et al., 2010)
Coal	6 M, 3 h	-063	7	16.1	(Ryczkowski et al., 2004)
Olive stones	13.9 M, until dryness, 353 K	-190	20	7.4	(Moreno-Castilla et al., 2000)
Almond shells	13.9 M, until dryness, 353 K	-780	49	-	(Moreno-Castilla et al., 1995)
Sugarcane bagasse	4 M, 4 h, 353 K	-231	30	22.5	(Somyanonthanakun et al., 2023)
Sugarcane bagasse	10 M, 4 h, 353 K	-349	45	28.4	(Somyanonthanakun et al., 2023)
Wood	40%, 2 h, 341–343	+43	6	5.72	(Valentín-Reyes et al., 2019)
Greenheart Sawdust	**5 M, 1 h, 295 K,**	**-82**	**3**	**6.25**	**This study**
Greenheart Sawdust	**10 M, 1 h, 295 K**	**-312**	**12**	**9.41**	**This study**

4.5.2 Surface Chemistry of GH-OX ACs

Initial perusal of XPS data (**Figure 4.2**(a)) suggests that oxidative treatments did not increase oxygen functionality substantially. However, this apparent result only contemplates the total oxygen atomic % of ACs. The total oxygen content of pristine GH-PAC600 was inflated by contributions from SiO_2 and residual phosphate species. When these additional oxygen sources are accounted for, the true carbon-bound oxygen amount of 1.34 atomic % is seen (**Figure 4.2**(b)). Further consideration of the types of C-bonded oxygen species indicates that as much as an 8 atomic % increase was attained (**Figure** 4.2(b)). When compared with other nitric acid oxidations of lignocellulosic ACs (**Table 4.2**), it is readily observable that facile flash oxidation yields comparable increases in oxygen content and has the added benefit of removing unwanted impurities from the activated carbon.

Surface carbon-bound oxygen functionalities were predominantly hydroxyl, carbonyl and carboxylic acids (**Figure 4.2**(c) and **Figure 4.2**(d)). **Figure 4.2**(e) shows the increases in atomic % for each of these oxygen species under various treatment conditions. For each treatment regime, increases in oxygen species typically followed the order -OH > C=O > O-C=O. This trend is most likely informed by the relative ease of formation of these functional groups and is consistent with the well-established fact that increasingly harsh oxidation conditions progressively convert alcohols to carbonyls and carbonyls to organic acids ((Jaramillo et al., 2010; Clayden et al., 2012). In addition to this trend, the largest percentage increases, relative to pristine GH-PAC_{600}, were seen for carboxylic acid functions (**Figure 4.2**(e)). This observation can be explained in terms of the comparatively low initial proportions of acidic functions (0.24 atomic %) in the pristine material. These results are consistent with what has been reported

elsewhere (Jaramillo et al., 2010). These results demonstrate that protracted and extreme oxidation conditions may not be necessary to yield good increases in surface oxygen. Moreover, flash-oxidation offers a greener and more sustainable approach to oxygen heteroatom functionalization. This greener approach consisted of deliberate consideration of some green chemistry principles. Firstly, our materials are fabricated from renewable feedstock; waste wood from the milling of tropical hardwoods. Secondly, both the fabrication of pristine AC as well as its subsequent functionalization (at ambient temperature), was done at temperatures which are energy efficient. Typically, phosphoric activations are done at temperatures in the range 400-800 °C(Diao et al., 2002).

4.5.3 Adsorption Results

4.5.3.1 BET surface area, pore volume and pore size distribution analysis

Selected oxidized ACs, produced under the least and most harsh conditions, were used to remove Al^{3+}, Mn^{2+} and Pb^{2+} from model solutions with initial concentration of 10 ppm at pH 3. Interestingly, GH-OX_{10M15} was most successful at removing Al^{3+} Pb^{2+} and Mn^{2+} in single ion systems (**Figure 4.3**(a)). This material had neither the largest surface area nor highest degree of oxidation i.e. total increase in oxygen atomic %. Its effectiveness at removing the target ions was likely due to the confluence of optimized surface area and surface oxygen sites. Moreover, when surface-area-normalized removal efficiencies for all three metals were compared with plots of the amount of each oxygen species present (**Figure 4.3**(a)), oxygen species specific adsorption appeared to occur. Furthermore, consideration of Pearson correlation between normalized removal efficiency and oxygen species (**Figure 4.4**(a-c)) showed that Pb^{2+} adsorption was most

strongly correlated (r = 0.942) with C-OH and C-O-C functions. With respect to Al^{3+}, adsorption was most strongly influenced by C=O species with r = 0.968. The strongest correlation between manganese and surface sites was an inverse correlation with O-C=O functions (r = -0.930). This suggests that Mn^{2+} coordination sites were linked to the presence of acid moieties but were unavailable for binding with the metal due to protonation at acidic pH. These results suggest that metal ion uptake by flash-oxidized ACs is dependent on the proportions of oxygen species present and not necessarily on the total surface oxygen content. The need to tailor oxidation regimes to maximize the production of particular oxygen species should therefore be considered in metal ion adsorption applications.

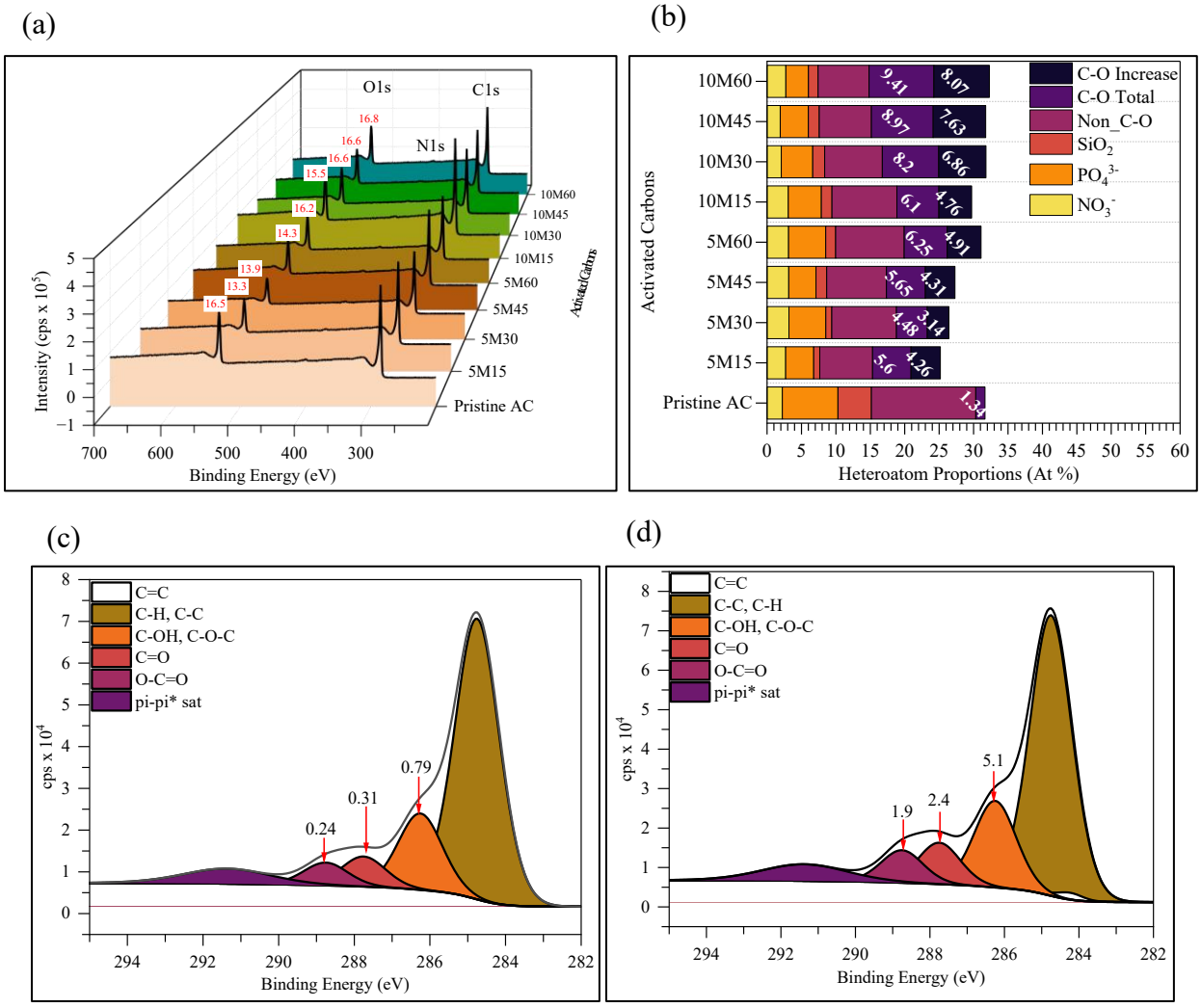

(e)

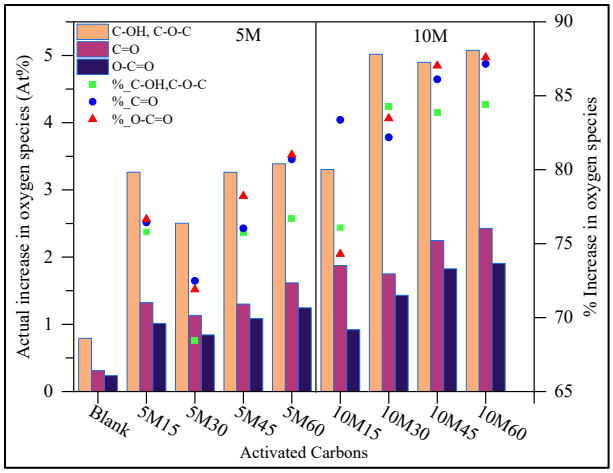

Figure 4.2 a – XPS wide scans showing total oxygen increases, b – plot of real changes in O-heteroatoms and carbon-bound oxygen, c and d – high resolution scans of C1s peak showing changes in oxygen functionality between pristine AC and GH-OX_{10M60} and e – actual and percentage increases in different oxygen species.

(a) (b)

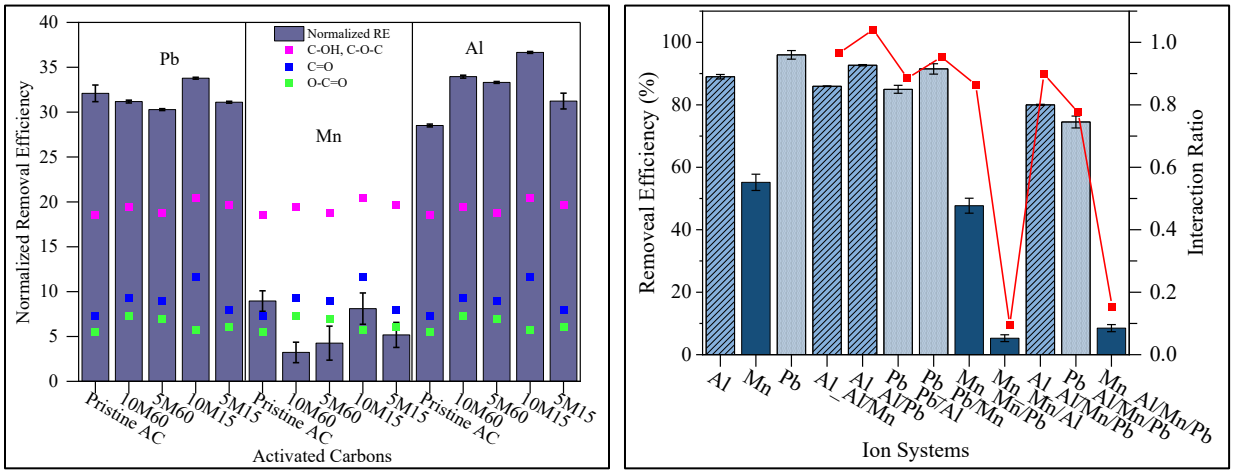

Figure 4.3 a – Removal efficiency for Al^{3+}, Mn^{2+} and Pb^{2+} adsorption normalized to specific surface area with superimposed plots of actual amounts of each oxygen species and b- removal efficiencies and interaction ratios for GH-OX_{10M60} with metal ions in single, binary and ternary-ion model systems.

4.5.3.2 Metal Adsorption Interactions

In binary and ternary ion systems, with the exception of the Al/Pb system, antagonistic adsorption interactions occurred (**Figure 4.3**(b)). These effects were most profound in systems containing Al^{3+} and Mn^{2+} ions where the presence of Al^{3+} drastically reduced the adsorption of Mn^{2+}. This effect may be attributed to the larger charge density of the trivalent Al^{3+} compared with the divalent Mn^{2+} ion. A larger charge density would make Al^{3+} adsorption at anionic surface sites more favorable and simultaneously reduce Mn^{2+} adsorption. A similar effect was seen for the antagonistic impact of Al^{3+} on Mn^{2+} adsorption in biological systems. (Blair and Taylor, 1997). Moderate to poor adsorption of Mn^{2+} in single ions system may be explained in terms of the reduced tendency of Mn^{2+} to form outer sphere complexes via electrostatic interactions since functions such as -COOH are protonated.

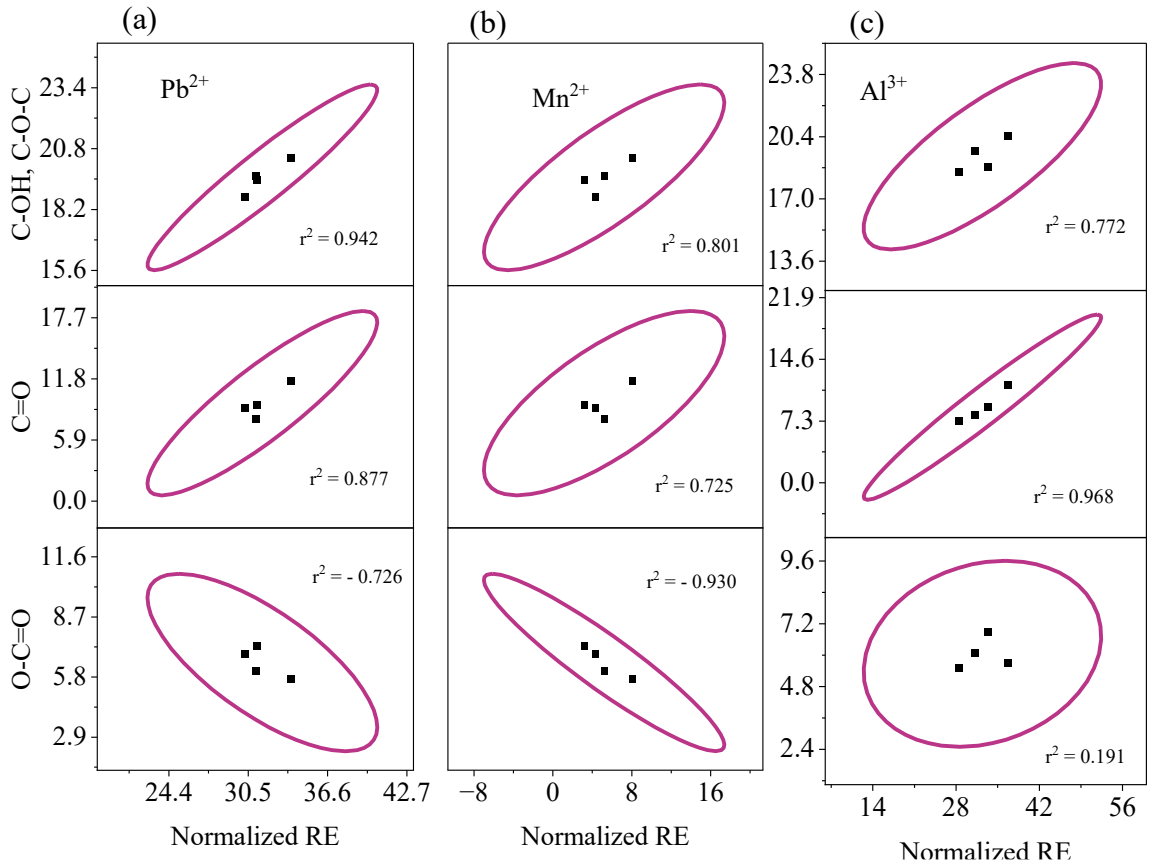

Figure 4.4 a – Scatter matrix plots with confidence ellipses for Pearson correlation coefficient for, a – Pb^{2+}, b – Mn^{2+} and c – Al^{3+} adsorption by various oxygen species.

4.5.3.3 Metal Ion Adsorption Isotherm Modelling

Adsorption data of metal ions on GH-OX_{10M60} at pH 3 at 303 K were fitted to non-linear Langmuir, Freundlich, Sips and Redlich-Peterson adsorption models (**Figure 4.5**(a-c)). Appendix i, **Table 0.2** shows the model parameters, and some statistical evaluations of the model fit. The Akaike Information Criterion (AIC) was used to compare model fits of the 2-parameter model (Langmuir and Freundlich) and the 3-parameter model (Sips and Redlich-Peterson).

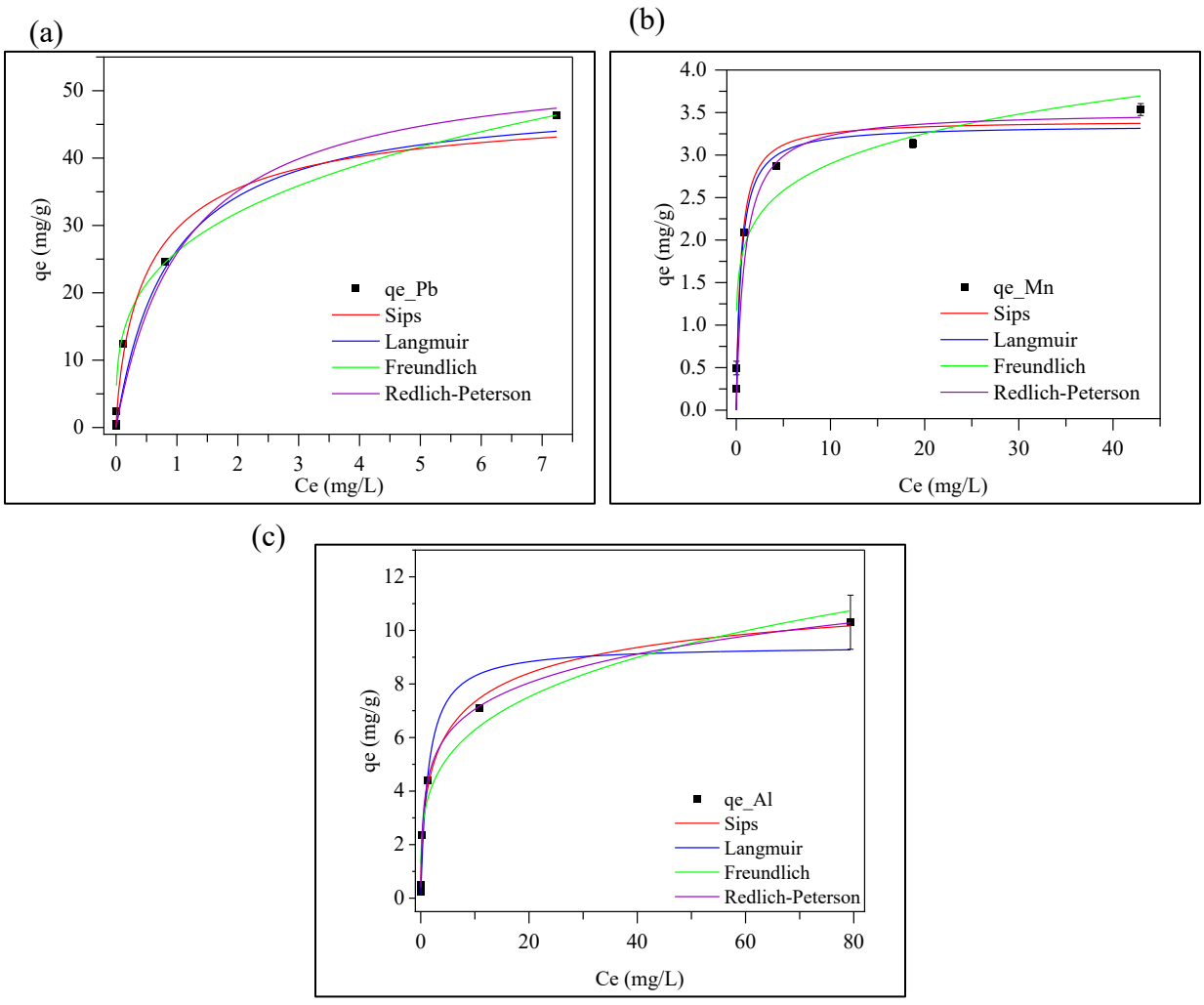

Figure 4.5 Langmuir, Freundlich, Sips and Redlich-Peterson adsorption model isotherms for adsorption of a – Pb^{2+}, b – Mn^{2+} and c – Al^{3+} on GH-OX_{10M60} at 303 K at pH 3.

For the two parameter models, the Langmuir model fitted the data best for Mn^{2+}. Notwithstanding the known heterogeneous nature of activated carbon surfaces, good Langmuir model fit may result from the low adsorbate loading resulting from the unfavorable interactions between Mn^{2+} ions and the adsorbent surface. The Freundlich model fitted the data best for Al^{3+} and Pb^{2+} implying that adsorption sites on GH-OX_{10M60} were heterogeneous and that multi-layer adsorption occurred. With respect to the three parameter models, the Sips model fitted the data best for Mn^{2+} and Pb^{2+} while Al^{3+} adsorption data were fitted best to the Redlich-Peterson model (**Table 0.2**). Langmuir derived maximum adsorption capacities for Al^{3+}, Mn^{2+} and Pb^{2+} were 9.44 ± 0.82, 3.35 ± 0.20 and 49.50 ± 4.95 respectively and were in good agreement with results from previous studies (Appendix i, **Table 0.3**).

4.6 Conclusion

We have demonstrated that strong increases of more than 8 atomic % oxygen can be produced by facile, ambient-temperature flash oxidation of wood based activated carbons and that more than 85 % of the specific surface area of the material is preserved in the process. Furthermore, our functionalized materials have demonstrable adsorption efficacy for Al^{3+} and Pb^{2+} ions in challenging acidic environments with increased absorption of 22 % and 5 % for Al^{3+} and Pb^{2+} when compared to pristine AC. These results are significant in that they provide new insights into oxidative transformations in the less than 60 min time interval; a largely overlooked experimental space. We provide new insights into the oxygen species specific interactions which facilitated the removal of Al^{3+} and Pb^{2+} and retarded Mn^{2+} removal. This work provides an alternative oxygen functionalization tool which is likely to resolve some of the challenges relating to surface area loss resulting from oxygen functionalization, particularly involving nitric acid oxidation. Moreover, the brevity of the procedure and the fact that it can be done at ambient temperature is promising in the context of greener fabrication efforts.

Chapter 5

Preface

Title: Versatile Waste wood-Chitosan ACs for 2,4-D and Paraquat Adsorption: Isotherm Modelling and Thermodynamic Evaluation

Authors: Hamant E. France, Oliver.L.K Strong, Tyler M. Roy, Andrew J. Vreugdenhil

Published in: Chemosphere, Volume 370, 2025, 144008, ISSN 0045-6535, https://doi.org/10.1016/j.chemosphere.2024.144008.Chemosphere

Contributions Hamant E. France: Writing – original draft, Visualization, Validation, Investigation, Formal analysis, Data curation, Conceptualization. Oliver L.K. Strong: Writing – review & editing, Validation, Data curation. Tyler M. Roy: Writing – review & editing, Methodology, Data curation. Andrew J. Vreugdenhil: Writing – review & editing, Writing – original draft, Supervision, Resources, Funding acquisition, Data curation, Conceptualization.

5.1 Graphical Abstract

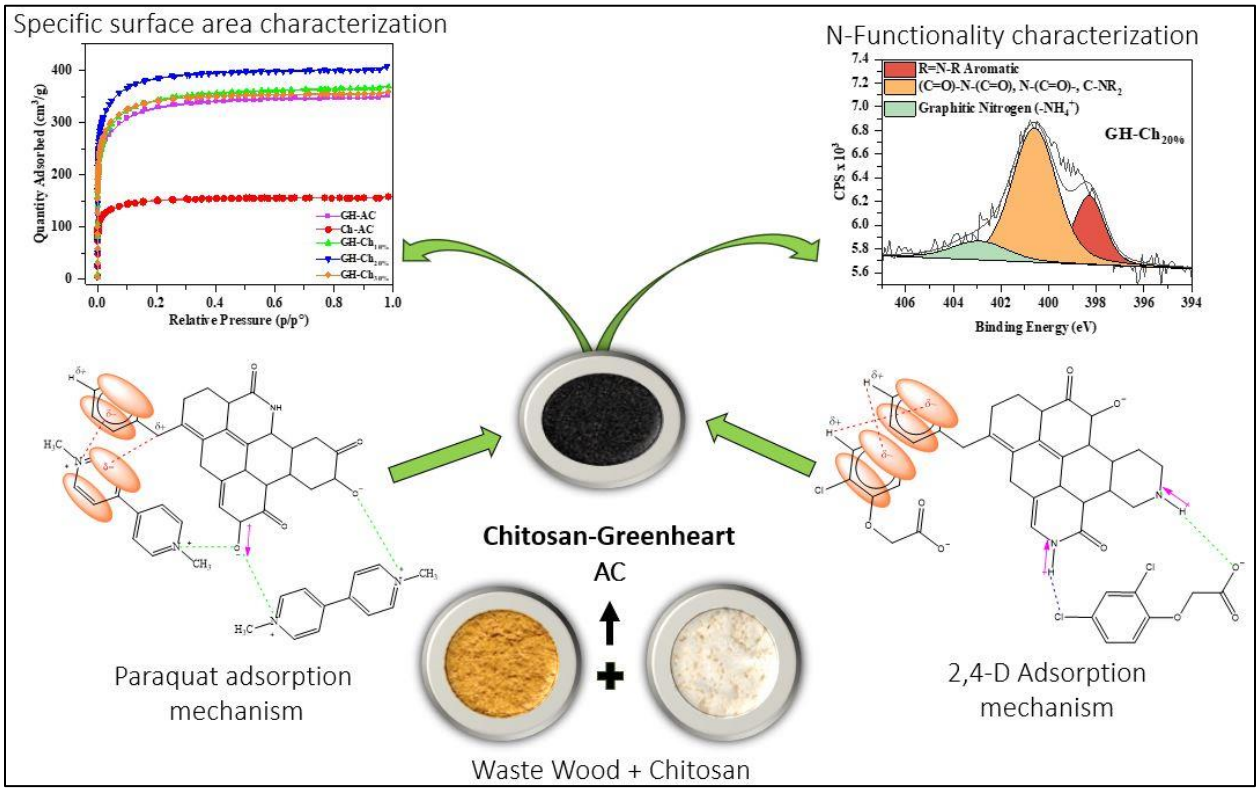

5.2 Abstract

2,4-dichlorophenoxy acetic acid (2,4-D) and 1,1-dimethyl-4,4-bipiridinium chloride (paraquat) are among the most widely used herbicides and are known to be toxic. Fabrication of green adsorbents which are capable of removing both herbicides remains a challenge. Here, we fabricate a novel adsorbent from tropical waste wood and use a facile, chitosan-mediated N-heteroatom functionalization technique to augment surface nitrogen and improve specific surface area. The addition of 20 wt% chitosan to the waste wood feedstock prior to activation, increased specific surface area by 300 m^2/g (~25%) and nitrogen content by 7-fold. This functionalized material removed 69% of 2,4-D and 82% of paraquat at initial concentrations of 4 ppm and 40 ppm from model solutions at pH 7. It also removed 39% 2,4-D and 93% paraquat from binary mixtures demonstrating its versatility. 2,4-D adsorption increased with chitosan addition suggesting synergistic effects between protonated amine functions and the anionic herbicide form. Paraquat adsorption was negatively correlated with chitosan addition, implying antagonistic interaction between protonated amine functions and quaternary nitrogen atoms on herbicide molecules. Adsorption of both herbicides was spontaneous, entropically favored and exothermic with $\Delta G°$: -19.3 kJ/mol and -28.8 kJ/mol; $\Delta S°$: 7.42 and 28.6 J/Kmol and $\Delta H°$: -17.0 kJ/mol and -20.1 kJ/mol for 2,4-D and paraquat respectively. Chitosan addition therefore provides a facile and green alternative for N-heteroatom functionalization, and these nitrogen-doped materials are promising candidates for the removal of multiple herbicides from aqueous systems.

Keywords: waste valorization, N-heteroatom functionalization, chitosan addition, 2,4-D, paraquat, tropical hardwood waste.

5.3 Introduction

Between 1990 and 2021, there was a 191% increase in pesticide use in the Americas (Shattuck et al., 2023). This corresponded to per hectare, per capita and per kg of agricultural production usage rates of 3.01 kg/ha, 1.23 kg/cap and 1.49 kg/1000$ respectively. Moreover, global pesticide use continues to increase (Shattuck et al., 2023) . Herbicide use, in particular, accounts for nearly 50% of all pesticide usage globally. The herbicides 2,4-dichlorophenoxy acetic acid (2,4-D) and 1,1'-dimethyl-4,4'-bipyridinium chloride (paraquat) are among the most widely used (Atwood et al., 2017; Franco et al., 2022; Pellenz et al., 2022).

Extensive herbicide use leads to their accumulation in the aquatic environment where they exert concentration-dependent pernicious effects (Alharbi et al., 2018; Blachnio et al., 2023; Li et al., 2023). It has been reported that 2,4-D and paraquat have been detected in natural waters at 4 mg/L and 40 mg/L respectively (Da Silva et al., 2022; Tsai et al., 2004). Of the technologies employed to remove herbicides from aquatic media, adsorption by low-cost adsorbents derived from sustainable sources such as waste wood and chitosan are particularly attractive due to factors such as ease of application, sustainable precursor sources and versatility.

Large amounts of waste wood continually enter the waste stream (Zimmer et al., 2018). Furthermore, the annual waste wood output in the form of sawdust for countries such as Chile, Austria and Finland is approximately 3 million cubic meters (Mwango and Kambole, 2019). While, published estimates for Guyana are not readily available, a conservative estimate for 2022 of 44,000 m^3 of sawdust is posited. This amount of waste wood, while but a fraction of that generated by larger nations, still poses health risks to persons living near sawmills given the classification of sawdust as a Group 1 carcinogen by the IARC (Mofidi et al., 2022; Vallières et

al., 2015). However, it is well established that sawdust can be efficiently valorized to highly functional activated carbons (Chandrasekar et al., 2022; Pimentel et al., 2024; Quimbaya-Ñañez et al., 2024). The conversion of sawdust to activated carbons which are then used in environmental remediation applications simultaneously eliminates a known hazard and creates effective environmental remediation materials.

Another important waste stream which has been successfully valorized to high value materials is the shells of crustaceans such as crabs and shrimp (Tolesa et al., 2019). It has been reported that approximately 3.4 million tons of shrimp are harvested annually with up to 60% by mass being by-products (Gillett, 2008; Zhang et al., 2024). Guyana, the worlds lead producer of Atlantic Seabob shrimp, produced 17,000 tons of shrimp from 2015–2020 leading to the generation of 9,400 tons of waste (Duong et al., 2023). It is known that shrimp shells are a key source of chitin, the second most abundant polysaccharide on earth and chitin is valorized to chitosan by the deacylation of chitinous wastes (Lin et al., 2024). Chitosan is rich in nitrogenous functions and is potentially a green dopant for incorporation this heteroatom into adsorbent materials.

Heteroatom functionalization is known to aid adsorbate removal. Functionalization techniques include N-doping to improve organic molecule adsorption, metal ion impregnation to improve oxyanion adsorption and various oxidations (Daud and Houshamnd, 2010; Haydar et al., 2003; Jaramillo et al., 2010; Mishra et al., 2021; O. K. Strong et al., 2023). N-functionalization is typically done as a pre- or post-activation treatment, and has been done using urea, ammonia, melamine, or various nitrogenous species (Bégin et al., 2023; Pellenz et al., 2022). While current doping techniques may yield strong increases in atomic % nitrogen, they typically require harsh treatment conditions using either very high temperatures, aggressive chemical treatments or both. Chitosan addition therefore provides an attractive green dopant for material functionalization.

Furthermore, since chitin is the second most abundant biopolymer, using this material as a dopant is inherently sustainable.

In this study, we fabricate activated carbons by two-staged phosphoric acid activation of a novel precursor, *Chlorocardium rodiei* (greenheart). We use facile pre-activation chitosan addition to improve texture and augment N-heteroatom functionality. We deployed these functionalized materials to remove the chlorinated herbicides 2,4-dichlorophenoxyacetic acid (2,4-D) and 1,1′-dimethyl-4,4′-bipyridinium dichloride (paraquat) from model solutions. To the best of our knowledge, no study has been published on the use of chitosan functionalized activated carbons in the removal of these herbicides. Moreover, the use of a single adsorbent which can efficiently remove both herbicides is rarely reported.

We probed the textural characteristics of the resulting ACs by gas adsorption with BET modeling while XPS, pzc and batch adsorption experiments provided information on the chemical characteristics of AC surfaces and their adsorption behaviour. We modeled adsorbate uptake by non-linear Langmuir, Freundlich and Sips adsorption models and evaluated some thermodynamic parameters and isosteric heat of adsorption for the adsorption process. These were used to infer possible chemical interactions between the functionalized materials and herbicide molecules.

5.4 Experimental (Please refer to Chapter 2 *Sections - 2.1.1.1, 2.1.2, 2.1.2.1, 2.1.5, 2.2.6, 2.2.9, 2.2.10 and 2.2.12*)

5.5 Results and Discussion

5.5.1 Texture and Surface Chemistry of Chitosan Augmented ACs

Table 5.1 shows the texture and surface chemistry of ACs produced by activation of greenheart/chitosan mixtures with various weight ratios. Generally, chitosan/greenheart ACs had greater specific surface areas than both the pristine chitosan and pristine greenheart ACs. The 20% addition of chitosan yielded AC with the largest specific surface area (**Table 5.1** and **Figure 5.1**(a)). This AC's surface area was more than 300 m^2/g greater than that of pristine greenheart AC and more than double that of the pristine chitosan AC. An increase (~ 20%) was also seen in the total pore volume of the optimized AC (**Figure 5.1**(b)). Enhanced texture may be due to two factors. Firstly, chitosan experiences significant decomposition in the temperature range 180 ℃ – 340 ℃ (Szymańska and Winnicka, 2015). The evolution of volatiles during thermal degradation of chitosan may mediate additional pore development and increase surface area by gasification. Secondly, improved texture may be the result of the summation of optimized texture of the two components of the mixture under the activation conditions. These results suggest that chitosan addition has an enhancing effect on the specific surface area of greenheart AC. Moreover, they demonstrate that the addition of optimized proportions of a biopolymer dopant to lignocellulosic materials is a green alternative for improving material texture. Chitosan doping also influenced nitrogen functionality and led to a more than 7-fold increase in nitrogen atomic % in GH-$Ch_{30\%}$ compared to GH-AC (**Figure 5.1**(c)). Nitrogen speciation was predominantly in the form of amines, amides, imides, imines and graphitic nitrogen (NH_4^+) (**Figure 5.2**(a) and **Figure 5.2**(b)). C1s high resolution scans provided further evidence for changes in C-N functionality (**Figure 5.2**(c-e)). Of these functions, amines and amides facilitated hydrogen bonding interactions with

herbicide species and were therefore the most useful nitrogen containing groups for adsorption (Appendix ii **Figure 0.1**(a) and **Figure 0.1**(b)). N-doping with chitosan achieved increases in nitrogen atomic % comparable with other techniques reported elsewhere (**Table 5.2**). Additionally, facile pre-activation chitosan doping typically required a dopant ratio comparable with other techniques (Liu et al., 2019; Wang et al., 2016; Zou et al., 2018) but was a greener approach in that less harsh fabrication conditions were employed as well as the use of a sustainable biopolymer; chitosan. Our use of a lower activation temperature (400 °C) than that typically used for chemical activations was selected for two reasons. Firstly, a lower activation temperature consumes less energy during activation and enhances the green nature of the process. And secondly, activation at a lower temperature leads to the preservation of more nitrogen groups in the functionalized material. Activation at higher temperature would cause more nitrogen loss by burnoff. Furthermore, since prior oxidation of AC before nitrogen functionalization was not a requirement with this technique, fewer overall chemical inputs were required. These results demonstrate that an easily applicable means of N-heteroatom increase is afforded by chitosan addition to a lignocellulosic feedstock. Moreover, this technique is promising because it is both cleaner and greener than typical N-functionalization.

Table 5.1 Texture and surface chemistry of chitosan augmented ACs produced by mixing various proportions of chitosan ranging from 10–30% and greenheart waste wood and activated with H_3PO_4 for 30 min at 400 ℃.

Activated Carbons	S_{BET} (m^2/g)	V_t (cm^3/g)	V_{mic} (cm^3/g)	V_{me} (cm^3/g)	Atomic Weight %	
					Oxygen	Nitrogen
Ch-AC_{400}	661 ± 77	0.29 ± 0.04	0.17 ± 0.01	0.12 ± 0.03	15.27 ± 0.74	5.77 ± 0.73
GH-AC_{400}	1261 ± 46	0.56 ± 0.03	0.29 ± 0.01	0.27 ± 0.01	18.14 ± 0.33	0.31 ± 0.24
GH-Ch-$AC_{10\%}$	1244 ± 124	0.53 ± 0.05	0.28 ± 0.02	0.24 ± 0.03	17.19 ± 0.74	1.10 ± 0.42
GH-Ch-$AC_{20\%}$	1565 ± 63	0.67 ± 0.03	0.41 ± 0.02	0.26 ± 0.02	15.64 ± 0.40	1.59 ± 0.15
GH-Ch-$AC_{30\%}$	1341 ± 24	0.56 ± 0.01	0.36 ± 0.03	0.21 ± 0.02	15.21 ± 0.43	2.31 ± 0.16

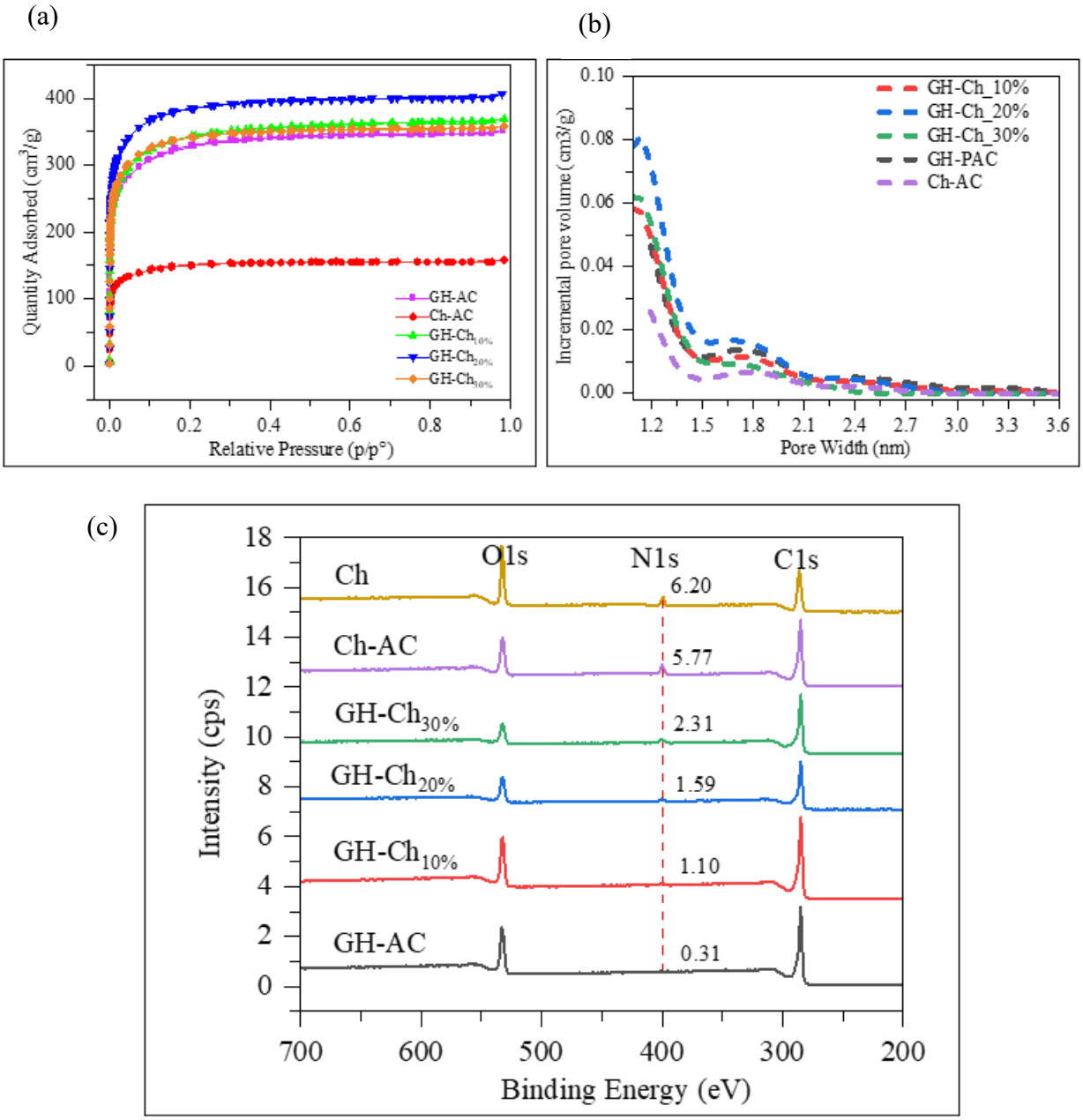

Figure 5.1 a - BET adsorption isotherms and b – pore size distribution for ACs and c - comparison of XPS wide scans of pristine and functionalized ACs.

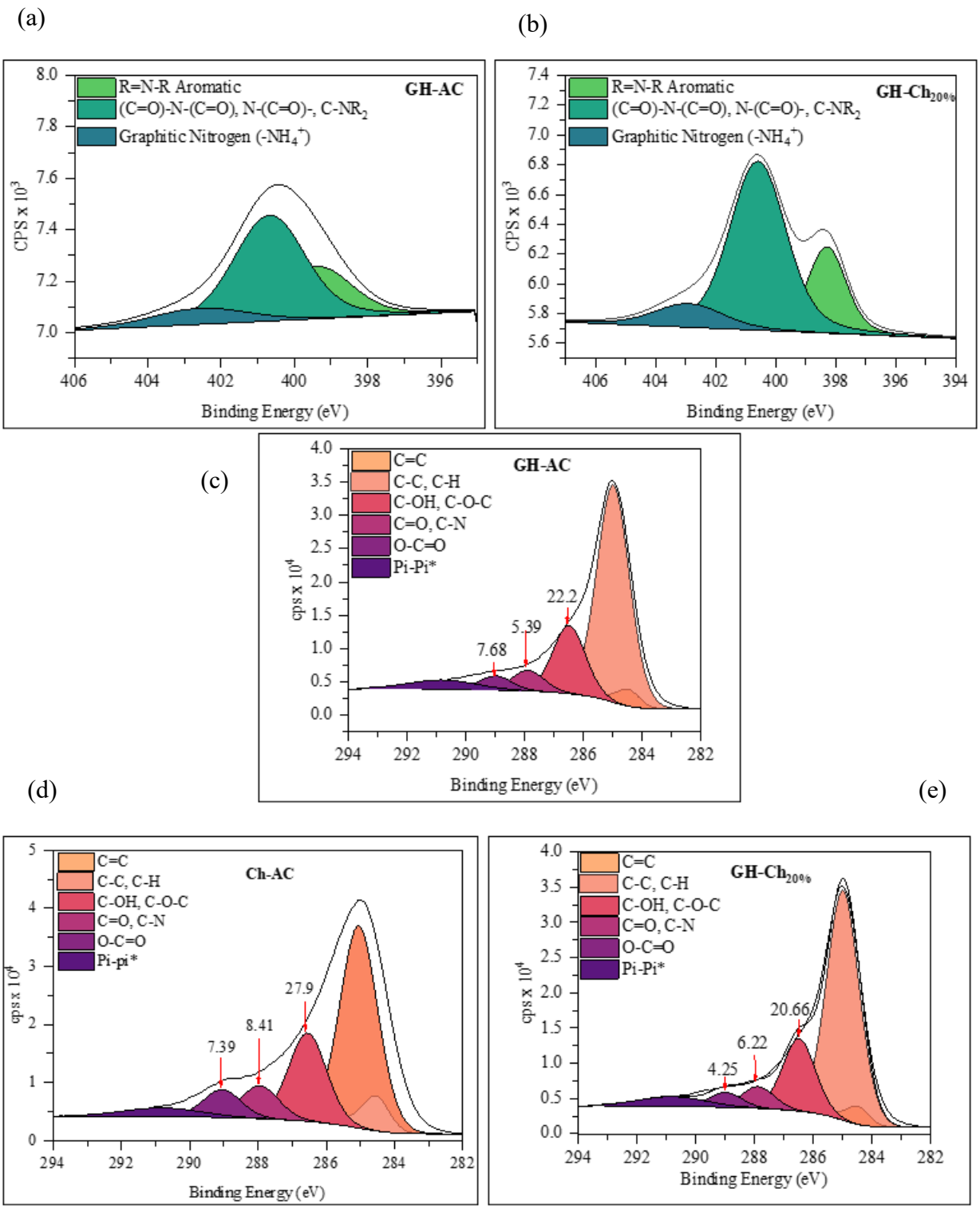

Figure 5.2 Nitrogen functionality from N1s scans for a - GH-AC and b -GH-Ch$_{20\%}$ AC and C-N functionality from C1s scans for c - GH-AC, d – Ch-AC and e – GH-Ch$_{20\%}$.

Table 5.2 Comparison of production parameters and atomic weight % of nitrogen in chitosan doped *Chlorocardium rodiei* and selected ACs from other nitrogenating techniques.

Precursor	Nitrogenating Agent	Treatment/Conditions	Doping Ratio* (g)	N Atomic %	Reference
Camellia oleifera shells	NH_3	l HNO_3 and 30% H_2O_2 at 90 °C for 2 h, 500 °C – 900 °C for 90 min	-	8.03	(Zhai et al., 2016)
Commercial AC	Polyethylenimine	10 min reflux with polyethylenimine, 3h @ 900 °C under Ar	-	2.1	(Zhang et al., 2019)
Peanut shell	Melamine	850 °C, 1h, Ar.	1:5	3.2–8.9	(Sylla et al., 2020)
Wood hydrochar	Melamine	800 °C, 1h	2:1	1.75	(Liu et al., 2019)
Lignin	Urea	400 °C, 1h and 800°C 1h	1:2	1.30	(Wang et al., 2016)
Bagasse	Urea	800 °C, 2h	1:1	2.63	(Zou et al., 2018)
Coal	Melamine	700 °C, 20 min	1:1	3.67	(Li et al., 2024)
Coal	Melamine	Microwave heating, 20 min	1:1	9.35	(Li et al., 2024)
Chitosan	**-**	**400 °C, 30 min**	**-**	**5.77**	**This study**
***Chlorocardium rodiei* Sawdust**	**Chitosan**	**400 °C, 30 min**	**3:1**	**2.31**	**This study**

* Dopant Ratio - mass of precursor to mass of dopant

5.5.2 Adsorption Results

5.5.2.1 2,4-D and paraquat adsorption on Composite ACs

Adsorption equilibrium was attained after 240 min and 120 min for 2,4-D and paraquat respectively. Adsorption experiments to determine the impact of specific surface area on the adsorption of 2,4-D showed no correlation between surface area and removal efficiencies. (Appendix ii, **Figure 0.2**(a)). Although GH-$Ch_{20\%}$ had a 300 m^2/g larger surface area than GH-AC, it adsorbed 14% less 2,4-D. In addition, GH-$Ch_{20\%}$ and Ch-AC removed similar amounts of 2,4-D even though the surface area of Ch-AC was more than 900 m^2/g less. Paraquat adsorption demonstrated better correlation with surface area (Appendix ii, **Figure 0.2**(b)). These results suggest that herbicide adsorption can be highly specific and can be mediated by factors such as surface functions and/or favorable surface charge in addition to surface area.

The impact of chitosan contribution on adsorption was investigated through Langmuir adsorption isotherm modelling. **Table 0.4 (**Appendix i) shows the maximum adsorption capacities and statistical evaluation of model fit for the chitosan functionalized adsorbents. Interestingly, 2,4-D adsorption showed a positive correlation with increases in chitosan contributions (N-heteroatoms) while paraquat adsorption was negatively correlated. These inverse trends in paraquat and 2,4-D adsorption can be explained in terms of the prevailing charge states of acidic and basic functions on the adsorbent surface and herbicide speciation at pH 7.

GH-Ch20% was selected for further adsorption experiments as it exhibited the best combination of nitrogen content and surface area and also generally had the median adsorption capacity of the functionalized materials. This composite was used to remove 2,4-D and paraquat from model

solutions at 4 ppm and 40 ppm respectively in the pH range of 4–8. At pH 4, a 97% removal efficiency was attained for 2,4-D. Removal efficiency decreased gradually and showed a minimum of 41% at pH 8 (Figure 5.3(a)). Paraquat removal efficiency showed an inverse trend when compared with 2,4-D with greater adsorption at pH 8 (88%) and minimum adsorption (44%) at pH 4 (Figure 5.3(d)). Variations in removal efficiency were likely due to the combined effects of adsorbate speciation at various pH and adsorbent surface charge.

GH-$Ch_{20\%}$ had a pH_{pzc} of 2.5. The acidic group of 2,4-D has a pKa of 2.81 (Rambabu et al., 2023) and this herbicide exists in its deprotonated form above pH 2.81. At pH 4 acidic sites on the AC (pKa ~ 4.76) surface as well as amine functions furnished by chitosan would be protonated. The existence of negative formal charges on 2,4-D species at this pH along with the presence of the highly electronegative chlorine and nitrogen heteroatoms most likely facilitated the majority of adsorption by ion-dipole interactions and hydrogen bonding (Appendix ii, **Figure 0.1**(a)). At higher pH the extent of deprotonation of both AC surface functions and adsorbate species increased, resulting in progressively incompatible columbic interactions between the anionic herbicide form and the negatively charged material surface. Similar pH dependence of 2,4-D adsorption on a date palm leaf AC, with a pH at pzc of 3.5, has been reported (Rambabu et al., 2023). Our results demonstrate that chitosan-doped greenheart ACs are best suited to 2,4-D adsorption at low pH although some adsorption does occur across the pH range investigated. Furthermore, they suggest that chitosan functionalized adsorbents may facilitate ion-dipole driven adsorption particularly at low pH in the presence of anionic adsorbate species.

Increased adsorption of 2,4-D (Appendix i, **Table 0.4**) at pH 7 was observed as the proportion of chitosan added to the composite increased. The Langmuir maximum adsorption capacity increased from 129.5 mg/g with the addition of 10 wt.% chitosan to 165.8 mg/g when 20 wt.% of

the dopant was added (28% increase), before beginning to level off at 168.2 mg/g with a 30 wt.% addition. This increase can be attributed to the generation of more positive surface sites on the functionalized composites. More cationic sites were available because the primary amine functions of chitosan are protonated at pH 7 (Clayden et al., 2012). Hence favorable interactions with the deprotonated 2,4-D species were promoted.

Adsorption of paraquat was most likely influenced primarily by both the formal charge and the aromaticity of the bipyridinium moieties. Increasing pH facilitated deprotonation of acidic AC surface sites (producing negative sites). Favorable electrostatic interactions were therefore created between these anionic sites and the cationic bipyridinium moieties. This led to greater adsorption efficiency at higher pH.

At pH 7, increasing proportions of chitosan-furnished amine functionality again produced more cationic sites. Here, however, this caused unfavorable electrostatic interaction between these sites and the quaternary nitrogen on paraquat and was responsible for the reduced adsorption of paraquat observed as the percentage of chitosan increased in the composites. The maximum adsorption capacity for paraquat dropped precipitously from 251.3 ± 5.01 mg/g for GH-$Ch_{10\%}$ to 101.6 ± 3.81 mg/g for GH-$CH_{20\%}$ (Appendix i, **Table 0.4**). Additional evidence for this antagonistic effect is seen in the fact that Ch-AC only adsorbed approximately 7% of paraquat at pH 7 (Appendix ii, **Figure 0.2**). These results imply that chitosan functionalized activated carbons should be used in conjunction with an understanding of the pH of the particular adsorption system and the resultant speciation of the adsorbate as both synergistic or antagonistic effects may result.

The versatility of functionalized composites with 20% chitosan in removing both herbicides was evaluated using a binary 2,4-D-paraquat mixture with initial concentrations of 4 ppm 2,4-D and 40 ppm paraquat. In HPLC analysis, paraquat had a retention time of 2 min while the retention time for 2,4-D was 10 min. The removal efficiencies of 2,4-D and paraquat were 39% and 93% respectively. Reduced 2,4-D adsorption in the binary system may be attributed to its slower adsorption kinetics when compared to paraquat. Paraquat's faster kinetics would ensure that favorable adsorption sites would first be occupied by this species. Further, the presence of these paraquat ions on the material surface may also sterically impede 2,4-D adsorption.

Adsorption modelling and thermodynamic evaluation was carried out at pH 7. This pH was selected as the performance of our adsorbate materials under common drinking water conditions (pH 6.5-10) is of paramount interest even if these conditions are not optimal for the adsorption of 2,4-D.

Various adsorption isotherm models have been advanced to explain adsorbate-adsorbent interactions. Of these, the Langmuir, Freundlich and Sips models are among the most ubiquitously employed. The Langmuir model assumes monolayer adsorbate surface coverage on an adsorbent surface with energetically homogeneous adsorption sites. The Freundlich model, an empirical model, assumes multilayer adsorption on a heterogeneous adsorbent surface, while the Sips model combines an empirical description of both models. It therefore has the ability to provide good descriptions of adsorption processes where the Langmuir and Freundlich models fail.

Adsorption data of 2,4-D and paraquat on GH-Ch20% at pH 7 at 303 K were fitted to non-linear Langmuir, Freundlich and Sips adsorption models (Figure 5.3(c) and Figure 5.3(f)). Table 5.3 shows the model parameters, and some statistical evaluations of the model fit for each model.. Good model fit was generally seen for all three models, but the Langmuir model provided the best fit as seen from adjusted-R^2 and reduced-χ^2 values and predicted maximum adsorption capacities of 166 mg/g and 102 mg/g for 2,4-D and paraquat. Although activated carbons are generally held to have heterogeneous surface sites, the Langmuir model has often been found to provide a good description of adsorption involving activated carbons (Worch, 2012). This is likely because the distribution of enthalpies for adsorbate-adsorbent interaction may have a narrow variance allowing for surface-site adsorption enthalpies to be considered almost homogeneous (Roy et al., 2025). Langmuir model derived maximum adsorption capacity of the chitosan functionalized adsorbent was in good agreement with other carbonaceous adsorbents (Appendix i, **Table 0.5)**.

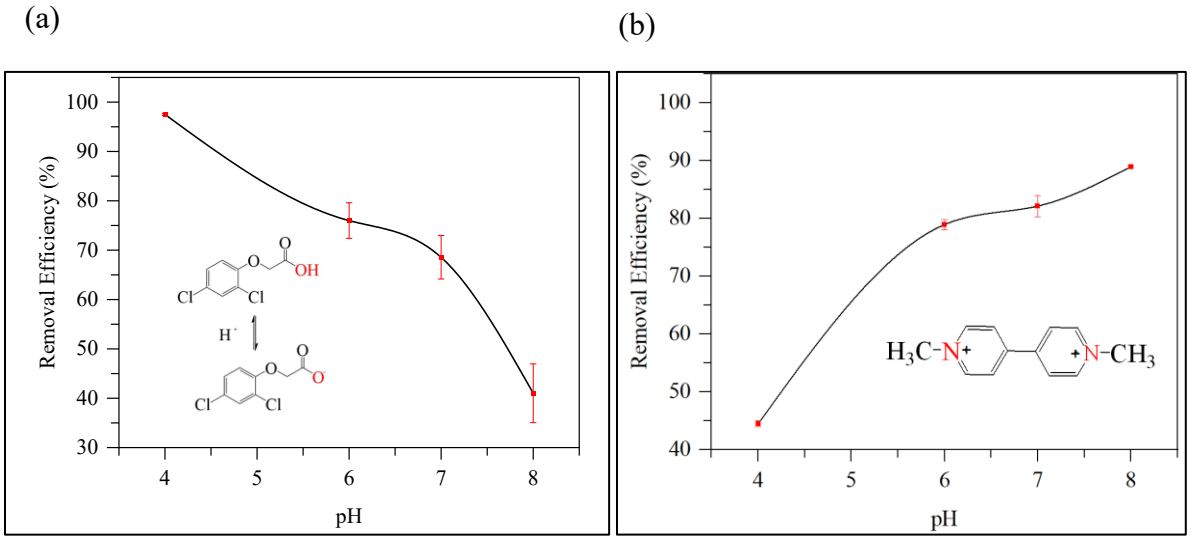

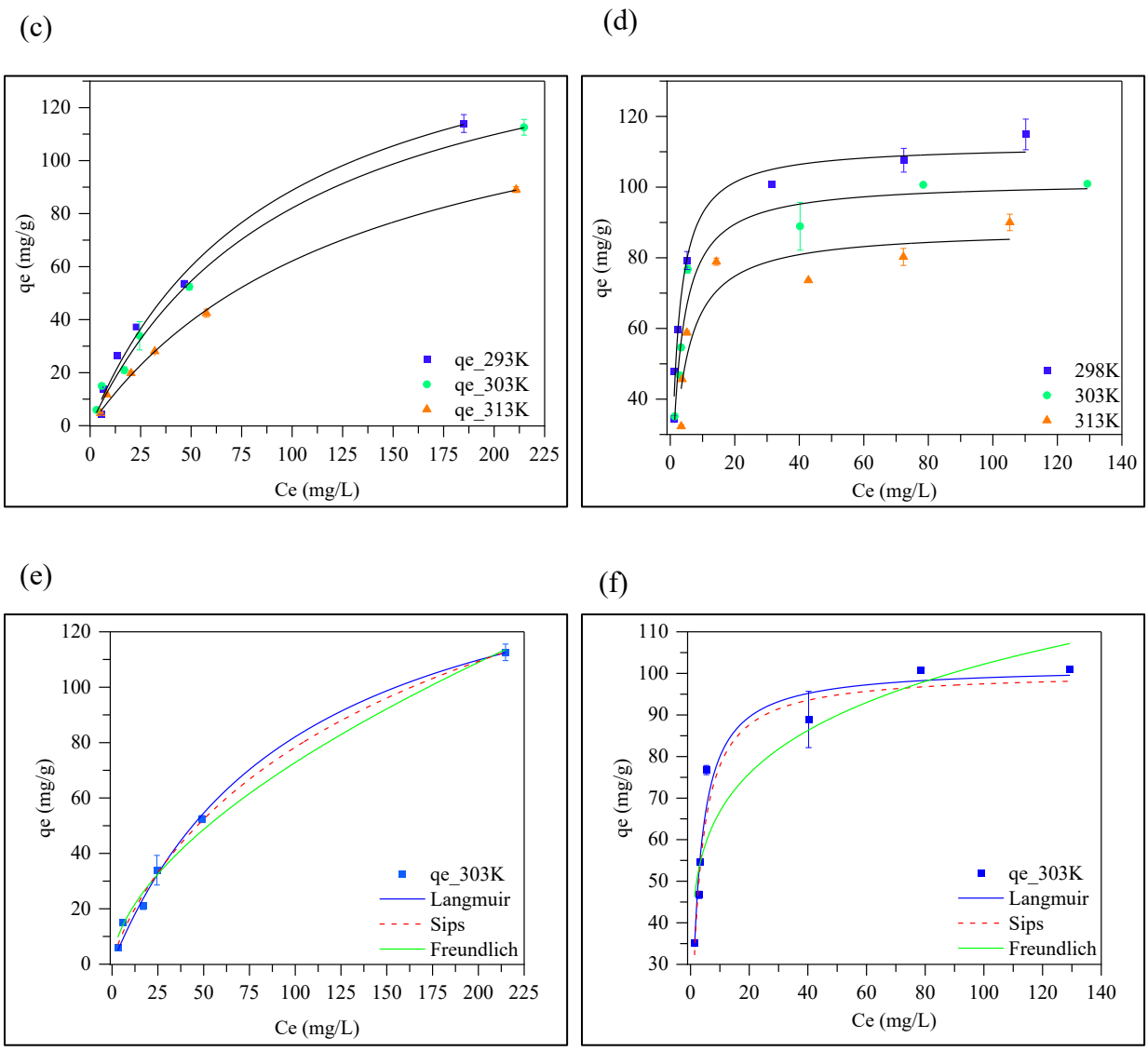

Figure 5.3 pH dependence, temperature dependence and Langmuir, Freundlich and Sips isotherm models for adsorption of a, c, e – 2,4-D and b, d, f - paraquat on GH-Ch$_{20\%}$ at pH 7.

Table 5.3 Model parameters and statistical evaluation of model fit for Langmuir, Freundlich and Sips adsorption isotherms at 303 K at pH 7.

Model	Herbicides and Model Fit					
	2,4-D	Adj R^2	Red χ^2	Paraquat	Adj R^2	Red χ^2
Langmuir						
Q_0 *(mg/g)*	165.8 ± 7.92	0.999	4.62	101.6 ± 3.81	0.952	34.1
K_L *(L/mg)*	0.0098 ± 0.001			0.37 ± 0.06		
Freundlich						
K_F *(L/mg)*	5.00 ± 0.83	0.992	15.8	43.6 ± 5.46	0.855	102
N	1.72 ± 0.10			5.40 ± 0.97		
Sips						
Q_0*(mg/g)*	230.7 ± 98.4	0.995	11.6	100.3 ± 6.95	0.953	49.5
K_s	0.012 ± 0.00			0.34 ± 0.11		
n_s	0.81 ± 0.15			1 ± 0.3		

5.5.2.2 *Evaluation of some thermodynamic parameters for 2,4-D and paraquat adsorption.*

Van't Hoff Plots, (Appendix ii, Figure 0.4(a) and Figure 0.4(b)) in conjunction with equations 2.7 – 2.9, were used to determine thermodynamic parameters. The Gibbs energy for the adsorption of 2,4-D on GH-Ch20% at 303 K was calculated to be -19.3 kJ/mol and confirmed the spontaneous nature of 2,4-D adsorption on the chitosan functionalized adsorbent. This value is in very good agreement with 2,4-D adsorption on a commercial AC (-22.56 kJ/mol at 303 K) (Ghatbandhe et al., 2013), on AC derived from carbon slurry from fertilizer production (-21.08 kJ/mol at 300 K) (Gupta et al., 2006) and was larger than that obtained by adsorption on an algal magnetic nanocomposite AC (-4.715 kJ/mol at 303 K) (Vinayagam et al., 2023). Gibbs free energy increased with increasing temperature (Table 5.4).

Figure 5.3(b) shows that adsorption decreased with increasing temperature for 2,4-D adsorption implying the exothermic nature of adsorption. Further, 2,4-D adsorption was enthalpically and entropically favorable with enthalpy and entropy values of -17.0 kJ/mol and 7.42 J/Kmol (Table 5.4). Evaluation of the isosteric heat of adsorption showed adsorption enthalpies increasing from -21.5 kJ/mol at 0.1 mg/g loading to -23.4 kJ/mol at 50 mg/g loading (Appendix ii, Figure 0.4(c) and **Figure 0.4**(d)). Increases in isosteric heat with surface coverage are consistent with materials with energetically heterogeneous adsorbent sites (Gimeno et al., 2003). Moreover, attractive lateral interactions may lead to such increases (Duong, 1998). In general, these values are in good agreement with adsorption enthalpy (-17.0 kJ/mol) obtained from the Langmuir model parameters. Isosteric adsorption enthalpy estimated in the Henry's Law adsorption region, that is, the region of low adsorbate loading, yields a more accurate estimate. Here, lateral interactions between adsorbate molecules adsorbed on the adsorbent surface are minimal. Infinitesimal adsorbate loadings imply that molecules are less subject to steric hindrance from other surface bound molecules (Liu and LeVan, 2009). Potential intramolecular interactions between GH-$Ch_{20\%}$ and 2,4-D are supplied in **Figure 0.1**(a) (Appendix ii). Justification for this mechanism is derived primarily from two sources. Firstly, XPS data (**Figure 5.2**(b)) confirms the presence of amine and amide functionalities on the AC surface. Secondly, the enthalpy of adsorption was determined to be less than 80 kJ/mol indicating that the predominant intermolecular interactions were physisorption.

Paraquat adsorption was also spontaneous ($\Delta G° = -28.8$ kJ/mol), entropically favored ($\Delta S° =$ 28.6 JK/mol) and exothermic ($\Delta H° = -20.1$ kJ/mol) (**Table 5.4**). The Gibbs free energy for adsorption of paraquat on chitosan doped greenheart AC was comparable with that for paraquat adsorption on carbonated Jujube seeds, decorated hexagonal mesoporous silica and GO-SiO_2 and

an order of magnitude higher than adsorption on decorated magnetite nanoparticles (Appendix i, **Table 0.6**).

Table 5.4 Thermodynamic parameters and model fit for adsorption of 2,4-D and paraquat on GH-$Ch_{20\%}$ AC.

Herbicide	T (K)	ΔG° (kJ/mol)	ΔH° (kJ/mol)	ΔS° (J/Kmol)	R^2
2,4-D	293	-19.2	-17.0	7.42	0.981
	303	-19.3			
	313	-19.4			
Paraquat	293	-28.5	-20.1	28.6	0.998
	303	-28.8			
	313	-29.1			

Enthalpy and entropy values were typically on the same order of magnitude as that for paraquat adsorption on selected adsorbents. Here also, the isosteric heat of adsorption estimated at near zero surface coverage (-22.7 kJ/mol) (Appendix ii, **Figure 0.4**(d)) is in good agreement with that derived from Langmuir model parameters (-21.1 kJ/mol). Since the adsorption enthalpy value was well below 80 kJ/mol, a physisorption mechanism of adsorption is also implied. Possible interactions between chitosan-greenheart AC and paraquat are supplied in Appendix ii, **Figure 0.1**(b). These results imply that chitosan doped greenheart AC is an efficient adsorbent for anionic herbicides such as 2,4-D and also remove modest amounts of paraquat at pH 7. Moreover, the adsorption performance of this material is comparable with other adsorbents but has the advantage of being a greener material with a facile fabrication procedure.

5.6 Conclusion

In this work we demonstrate the green, nitrogen heteroatom functionalization of a waste wood-derived activated carbon by a facile fabrication procedure. We show that as much as a 7-fold increase in nitrogen atomic % is attainable by pre-activation chitosan doping of a lignocellulosic precursor followed by low temperature activation under an inert atmosphere in the presence of phosphoric acid. These results are significant in that they provide a nitrogen heteroatom augmentation procedure which does not require harsh fabrication conditions or potentially harmful dopants. Furthermore, since chitosan doping also resulted in an ~ 25% increase in specific surface area of the functionalized material, this procedure provides a promising means of simultaneously increasing texture and N-heteroatom functionalization. Furthermore, with removal efficiencies of 69% and 82% for the herbicides 2,4-D and paraquat in single species systems and 39% and 93% in binary systems at pH 7, these chitosan functionalized materials have demonstrable versatility and efficacy in the drinking water pH range. Isotherm modelling analysis revealed that the adsorption of both paraquat and 2,4-D was adequately described by the Langmuir model with predicted maximum adsorption capacities of 102 mg/g and 166 mg/g respectively for composites with 20 wt% chitosan. Thermodynamic evaluation suggested that the adsorption of herbicides was spontaneous, entropically favored and exothermic. Moreover, XPS data in conjunction with thermodynamic evaluation suggested that the predominant interactions between herbicide molecules and the functionalized materials were hydrogen bonding, ion-dipole and pi-pi interactions. The herbicides where therefore physisorbed on the chitosan-functionalized adsorbent. These green adsorbents, fabricated from sustainable biomaterials, are promising environmental remediation materials.

Chapter 6

Preface

Title:	Co-valorization of shrimp and wood waste by fabrication of high-value adsorbents: Fabrication, characterization and herbicide adsorption studies
Authors:	Hamant E. France, Julia Pohling, O.L.K Strong, Tyler M. Roy, Andrew J. Vreugdenhil and Yuana Yesika
Reference:	This chapter is currently with an editor. The published version of this manuscript will appear with minor modifications from the chapter presented here.
Contributions:	Hamant E. France: Writing – original draft, Visualization, Validation, Investigation, Formal analysis, Data curation, Conceptualization. Oliver L.K. Strong: Writing – review & editing, Validation, Data curation. Tyler M. Roy: Writing – review & editing, Methodology, Data curation. Andrew J. Vreugdenhil: Writing – review & editing, Writing – original draft, Supervision, Resources, Funding acquisition, Data curation, Conceptualization, Julia Pohling: review and editing, Investigation, Methodology, Yuana Yesika: Investigation, Methodology.

6.1 Graphical Abstract

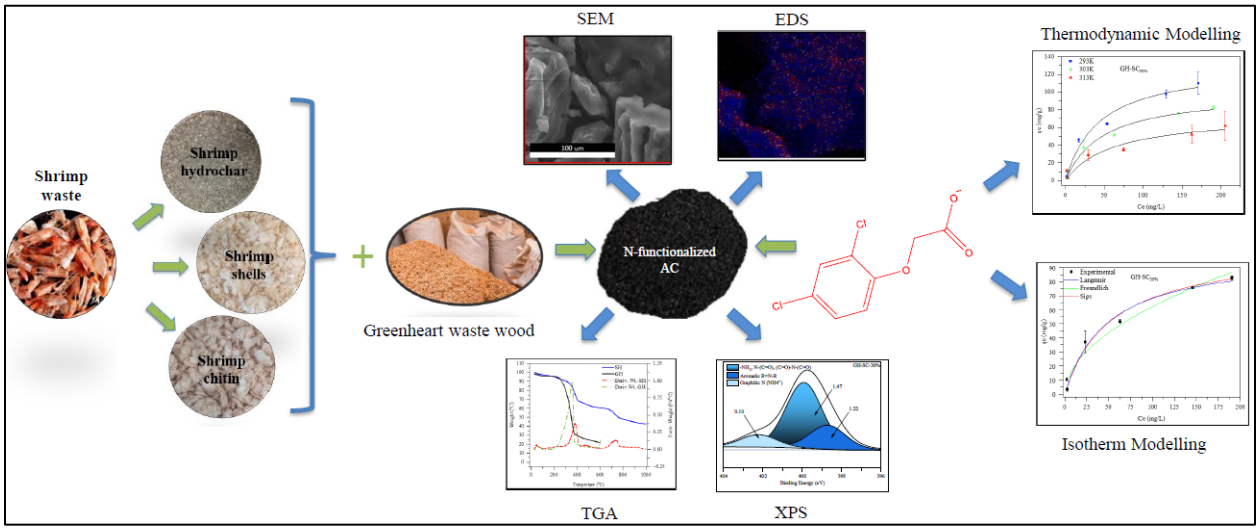

6.2 Abstract

This study investigates the fabrication of nitrogen-enriched adsorbents by the co-valorization of a shrimp hydrochar, shrimp chitin, and shrimp shells with a waste wood feedstock, greenheart, by a facile and environmentally benign phosphoric acid activation process. These nitrogen-rich materials were characterized and subsequently deployed to remove 2,4-dichlorophenoxy acetic acid from model solutions at 50 ppm concentration at pH 7. Shrimp shell and shrimp hydrochar composites were typically mesoporous but shrimp chitin composites were microporous. Specific surface area ranged from 1224 m^2/g to 1974 m^2/g. Surface nitrogen peaked at 2.94 atomic % with amine, amide and imide function predominating. The largest specific surface area and greatest nitrogen content of composites was more than 56% and 5 times greater than the pristine greenheart adsorbent. The nitrogen functionality was uniformly distributed on the composite surface imply that there was homogeneous combination of the co-valorized feedstocks. The shrimp-chitin-greenheart composite was most efficient at removing 2,4-D with a maximum adsorption capacity of 101 mg/g. Maximum adsorption of composites was most strongly correlated with amine groups (0.86), total nitrogen (0.88), total surface nitrogen density (0.90) and specific surface area (0.87). Adsorption of 2,4-D on all composites was best described by the Freundlich isotherm model implying the heterogeneous nature of adsorption sites. Adsorption was spontaneous and entropically favored and adsorption enthalpies ranged from -12 kJ/mol to -17 kJ/mole indicating that physisorption interactions dominated the adsorption process. These composites, with demonstrated efficacy in removing 2,4-D, are promising environmental remediation materials.

Keywords: *waste valorization, shrimp chitin, shrimp hydrochar, shrimp shells, 2,4-D, greenheart, tropical hardwood waste.*

6.3 Introduction

Lignocellulosic waste generated from the milling of lumber and shrimp waste (SW) generated from the commercial harvesting of shrimp are two of the most globally ubiquitous waste streams (FAO, 2024.; Gillett, 2008; Zimmer et al., 2018). In 2018, 12.2 million tons of waste wood went to landfill (US EPA, 2020) while approximately 2 million tons of shrimp waste were produced (Gillett, 2008). Efforts to divert these waste streams from landfill continues to generate significant interest among researchers (da Silva Alves et al., 2021). One key technique currently employed to manage and upcycle these wastes involves their valorization to high surface adsorbents such as activated carbons (Shahib et al., 2023). Adsorbents fabricated from lignocellulosic and shrimp wastes are rich in heteroatoms such as oxygen, sulfur and nitrogen and it is known that heteroatoms play a key role in the adsorption performance of adsorbents (Tan et al., 2023; Yang et al., 2025).

Typically, the incorporation of nitrogen heteroatoms into adsorbent materials is done utilizing potentially harmful agents such as melamine and ammonia (Pellenz et al., 2022; Wang et al., 2012). Furthermore, energy intensive and protracted fabrication steps typically accompany the use of these nitrogenating agents. However, employing shrimp waste as a nitrogenating agent is both a desirable waste management strategy and allows for the incorporation of N-heteroatoms into adsorbent materials in a facile, energy efficient and therefore greener process. Moreover, it has been demonstrated that N-heteroatom inclusion imparts versatility to carbonaceous adsorbents both with respect to them being able to function in diverse pH environments and in removing various adsorbate species such as multiple organic herbicides (France et al., 2025).

The organo-chlorine herbicide 2,4-dichlorophenoxy acetic acid is among the most widely used pesticides and is known to be toxic (Alharbi et al., 2018; Blachnio et al., 2023; Li et al., 2023). Furthermore, The International Agency for Research on Cancer (IARC) has designated it to be "possibly carcinogenic" (group 2B) (APVMA, 2019). The extensive use of this herbicide in agricultural belts results in accumulation in the aquatic environment. It has been reported that less than 15% of the applied pesticide reaches target organisms (Singh et al., 2023). The presence of 2,4-D in the environment may be greatest at point sources such as drainage or irrigation canals where spray cans are washed after use. At these sites 2,4-D levels ranging from 3.3 ppm – 312 ppm have been documented (Islam et al., 2018). Developing technologies which are able to efficiently remove this herbicide continues to attract on-going attention.

Fabricating low-cost adsorbents, sourced from multiple-sustainable biowaste streams, is particularly attractive given that this approach simultaneously incorporates elements of the circular economy, diverts multiple copious waste streams form landfill and creates sustainable environmental remediation materials.

Here, we fabricate activated carbons by a two-staged phosphoric acid activation of a lignocellulosic precursor, *Chlorocardium rodiei* (greenheart) and use a facile pre-activation shrimp waste addition to improve texture and increase nitrogen functionality. These functionalized materials were then used to remove the chlorinated herbicides 2,4-dichlorophenoxyacetic acid (2,4-D) from model solutions at pH 7. To the best of our knowledge, no study has been published on the N-functionalization of *Chlorocardium rodiei* by shrimp shells, shrimp hydrochar and shrimp chitin and the use of these composites in the removal of 2,-

D. Moreover, extensive isothermal and thermodynamic evaluation of the adsorption performance of adsorbents derived from co-valorized lignocellulosic and shrimp waste is seldom reported.

We probed the textural characteristics of the ACs by gas adsorption, DFT PSD, TGA and SEM-EDS, while XPS, pHpzc measurements and batch adsorption experiments provided information on the chemical characteristics of AC surfaces and their adsorption behaviour.

6.4 Experimental (Please refer to Chapter 2 *Sections - 2.1.1.1, 2.1.2, 2.1.2.1, 2.1.5, 2.1.6, 2.2.5, 2.2.6, 2.2.9 and 2.2.13*)

6.5 Results and Discussion

6.5.1 Texture of shrimp waste augmented composite ACs

Table 6.1 shows the texture, yield and surface chemistry summary of composites produced by activation of GH/SW mixtures with various weight ratios. Composites typically had greater specific surface areas than both pristine shrimp waste and pristine greenheart ACs. Interestingly, optimized specific surface areas were obtained by the addition of differing weight ratios of SW (**Figure 6.1**(a)). Surface areas of optimized composites were between 36%–56% larger than that of pristine greenheart AC and as much as 38 times larger than pristine SW ACs. Increases in specific surface area may be the result of additional porosity derived from gasification due to the evolution of volatiles during thermal degradation of shrimp wastes (France et al., 2025). **Figure 6.1**(b) and **Table 6.1** confirm that the composites had greater total pore volumes than the pristine adsorbent. Shrimp shell and shrimp hydrochar composites were typically mesoporous but shrimp chitin composites were microporous. Additional evidence for the mesoporous texture of shrimp shell and shrimp hydrochar composites was seen on BET adsorption isotherms (**Figure 6.1**(a)), which had Type IV isotherms with H4 hysteresis (Thommes et al., 2015b). Hysteresis in adsorption isotherms is known to be the result of capillary condensation of the adsorptive in mesopores.

Figure 6.1(c) shows TGAs of the shrimp waste precursors while **Figure 6.1**(d–f) shows TGA and DTG thermograms of the various shrimp wastes overlayed with the thermogram of greenheart waste wood. **Figure 6.1**(c) reveals that the general range of temperatures in which the major decomposition events for all shrimp wastes occurs is between 350–450 °C. This is significant because this range coincides with major decomposition range of greenheart feedstock. The overlap of these two decomposition ranges may provide addition evidence for the increased

porosity and by extension surface area realized by secondary gasification processes. These results suggest that the addition of shrimp waste to lignocellulosic feedstock prior to activation has an ameliorating effect on the texture of the derived activated carbons. Moreover, they clearly show that using biopolymer dopants is an attractive green approach to enhancing the texture of lignocellulosic-derived activated carbons composites.

(a)

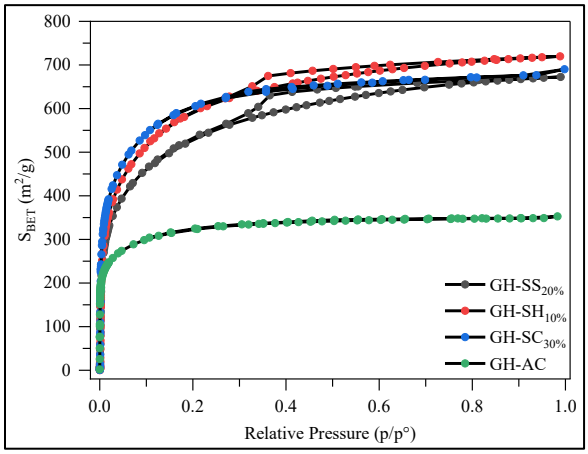

(b)

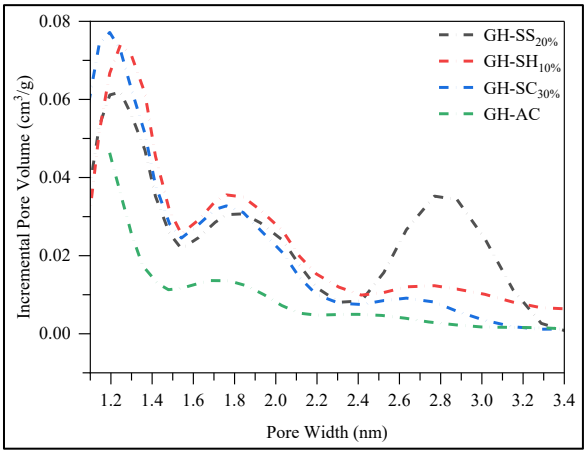

(c)

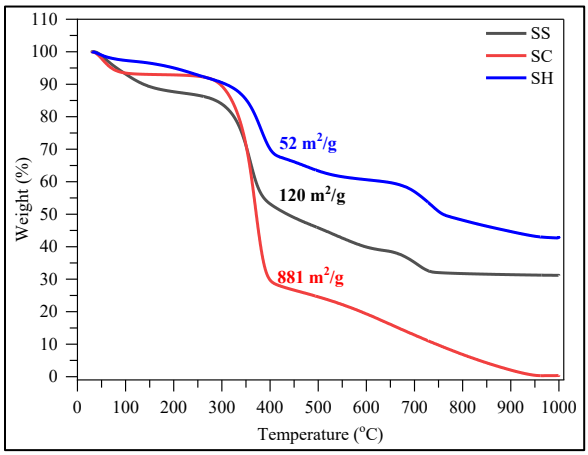

(d)

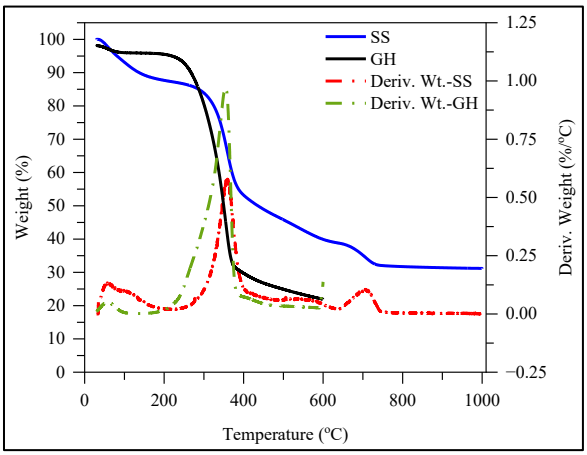

(e) (f)

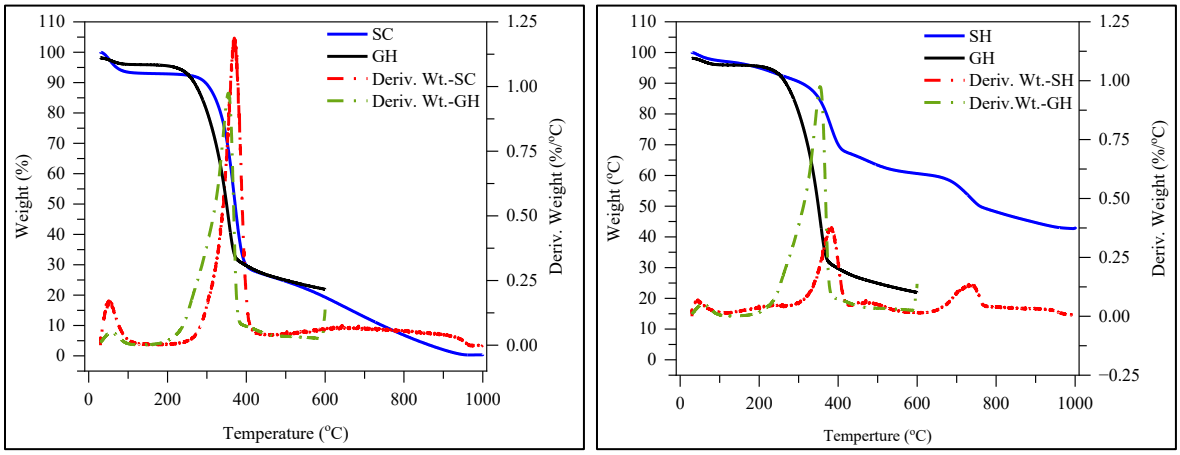

Figure 6.1 a – BET adsorption isotherms, b – DFT pore size distribution of surface area optimized GH-SW-ACs and c – TGA of shrimp waste precursors and d – f TGA and DTG thermograms of surface area optimized GH-SW-ACs with superimposed thermogram of pristine GH-AC.

6.5.2 pH_{pzc} and XPS analysis of surface chemistry of shrimp waste augmented composite ACs

Figure 0.3 (Appendix ii) shows the pH at point of zero charge of optimized composites. These values were marginally higher than those for pristine GH-AC (1.98). increased pH_{pzc} may be attributed to the presence of basic amine functions, supplied by shrimp wastes, on the material surfaces. Strong increases were seen in the surface nitrogen content of the composites. **Table 6.1** shows that total surface nitrogen increased by 2.5–5 times when compared with the pristine GH-AC. Further consideration of the types of nitrogen speciation in the optimized composites (**Figure 6.3**(a-e)) shows the presence of amine, amide and imide functions with amine group

functions predominating. GH-$SC_{30\%}$ had the largest increase in amine group nitrogen; a 3.5 – fold increase. Shrimp waste N-doping compared favorably with other techniques used to improve nitrogen functionality in ACs (Appendix i, **Table 0.7**). Moreover, comparable increases in nitrogen content were achieved by lower ratios of dopant and under vastly milder treatment regimes. This approach to nitrogen functionalization of adsorbent materials is therefore promising given that fact that a sustainable biopolymer waste stream is being valorized, fewer chemical inputs are required and milder fabrication conditions utilized. These results clearly demonstrate that an easily applicable means of N-heteroatom increase is afforded by shrimp waste functionalization of lignocellulosic feedstock.

6.5.3 SEM-EDS analysis of surface chemistry of shrimp waste augmented composite ACs

SEM and EDS images (**Figure 6.2(**a-d)) show the absence of localized N-agglomerates. Moreover, the images show that nitrogen functionality in GH-SW-ACs was generally uniformly distributed on the materials implying that more-or-less homogeneous hybrid material were fabricated. This is significant given the advantage of producing composites with adsorption sites that are well distributed on the material surface. Good spatial distribution of adsorption sites is likely to reduce the variability in adsorption performance of the composites.

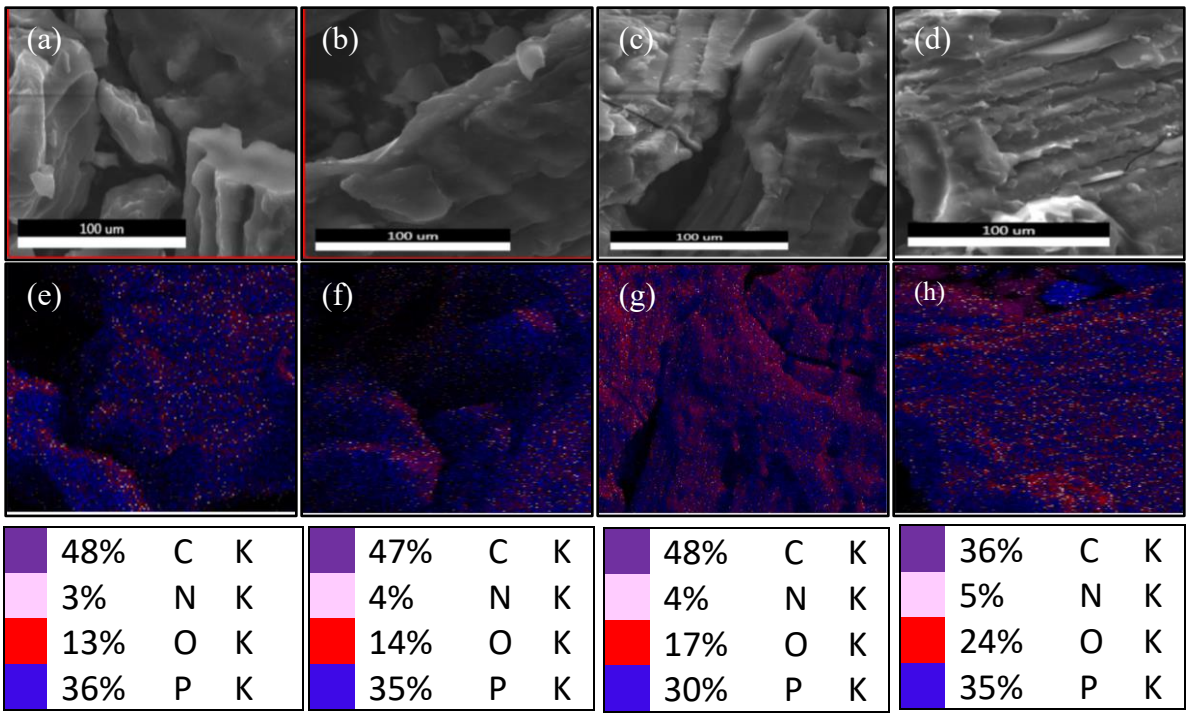

Figure 6.2 a – d SEM images showing surface morphology and e – h EDS showing distribution of selected elements for pristine and SW-functionalized ACs.

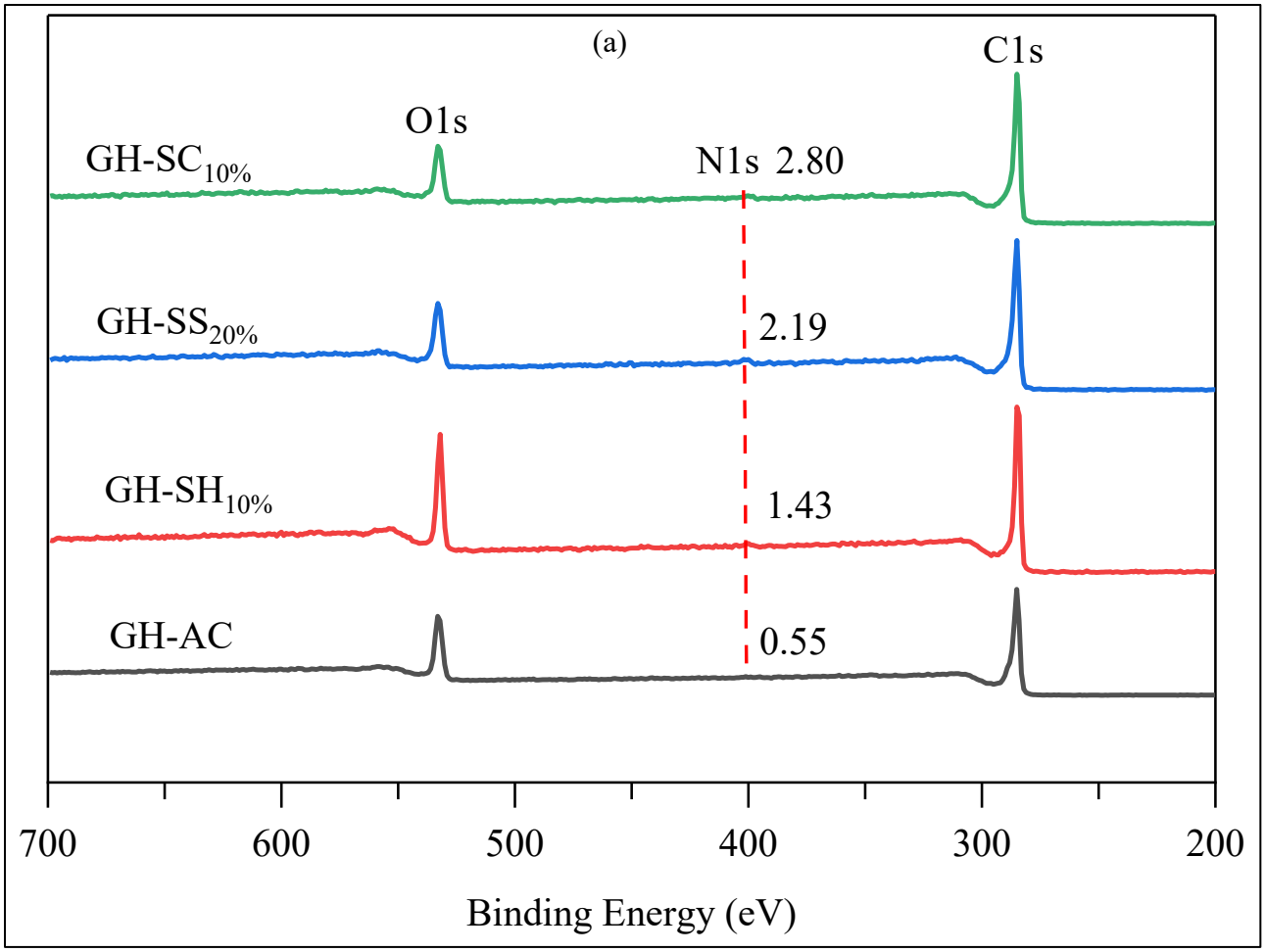
(a)
C1s
O1s
N1s 2.80
GH-SC10%
GH-SS20%
2.19
GH-SH10%
1.43
GH-AC
0.55
700
600
500
400
300
200
Binding Energy (eV)

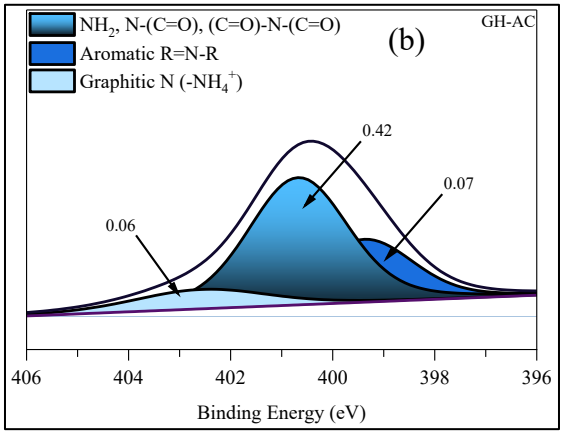
NH2, N-(C=O), (C=O)-N-(C=O)
Aromatic R=N-R
Graphitic N (-NH4+)
(b)
GH-AC
0.42
0.07
0.06
406
404
402
400
398
396
Binding Energy (eV)

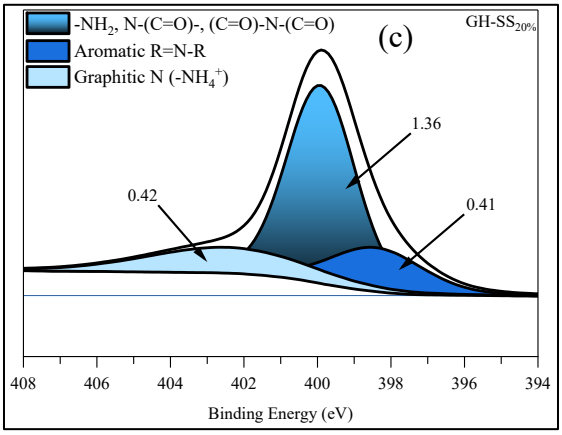
-NH2, N-(C=O)-, (C=O)-N-(C=O)
Aromatic R=N-R
Graphitic N (-NH4+)
(c)
GH-SS20%
1.36
0.42
0.41
408
406
404
402
400
398
396
394
Binding Energy (eV)

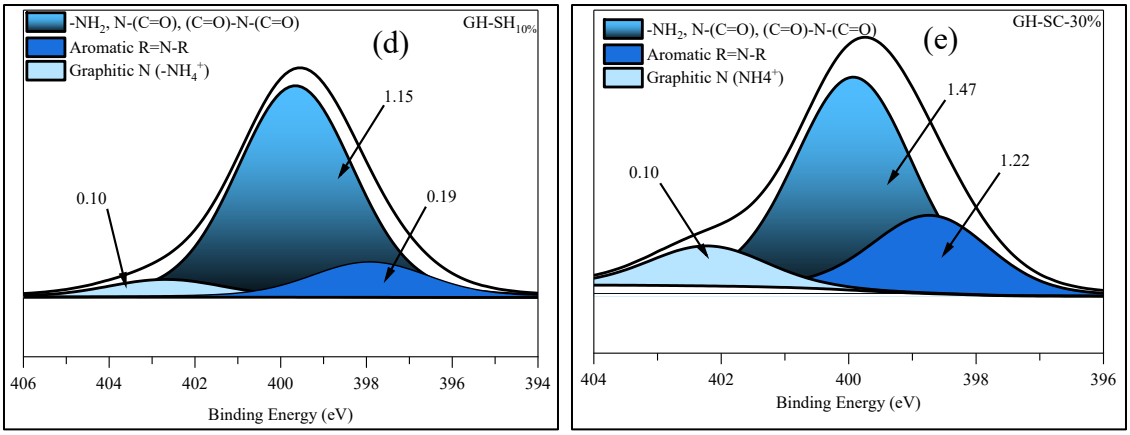

Figure 6.3 XPS survey scans showing changes in total atomic % N for surface area optimized GH-SW ACs and comparison of high resolution N1s scans showing N-functionality in b – pristine GH-AC, c – GH-$SS_{20\%}$, d – GH-$SH_{10\%}$, and e – GH-$SC_{30\%}$.

Table 6.1 Texture, surface chemistry and yield of composite ACs from shrimp shell, shrimp hydrochar, shrimp chitin and greenheart waste wood.

Activated Carbons	S_{BET} (m^2/g)	ΔS_{BET} (m^2/g)	V_t (cm^3/g)	V_{mic} (cm^3/g)	V_{me} (cm^3/g)	Yield (%)	Atomic %		
							C	O	N
GH-AC	1261 ± 46	-	0.56 ± 0.03	0.29 ± 0.01	0.27 ± 0.01	37.7 ± 0.9	84.11	13.09	0.55
GH-SS-AC_{10}	1617 ± 168	356	0.72 ± 0.08	0.26 ± 0.05	0.47 ± 0.03	40.4 ± 0.1	82.65	14.27	1.81
GH-SS-AC_{20}	1719 ± 21	458	0.86 ± 0.00	0.24 ± 0.00	0.62 ± 0.00	41.0 ± 1.6	80.45	15.80	2.19
GH-SS-AC_{30}	1230 ± 147	-31	0.60 ± 0.09	0.24 ± 0.15	0.36 ± 0.07	39.1 ± 1.2	79.06	15.79	2.94
SS-AC_{100}	120 ± 30	-	0.09 ± 0.02	0.02 ± 0.00	0.06 ± 0.04	45.6 ± 0.3	56.71	26.3	6.57
GH-SH-AC_{10}	1974 ± 56	713	0.94 ± 0.02	0.37 ± 0.00	0.57 ± 0.02	39.2 ± 0.6	69.91	19.16	1.43
GH-SH-AC_{20}	1651 ± 168	390	0.78 ± 0.11	0.27 ± 0.06	0.51 ± 0.17	37.5 ± 0.5	77.20	17.29	2.61
GH-SH-AC_{30}	1224 ± 24	-37	0.57 ± 0.01	0.25 ± 0.01	0.32 ± 0.00	42.1 ± 1.0	77.26	17.44	2.87
SH-AC_{100}	52 ± 25	-	0.04 ± 0.02	0.01 ± 0.01	0.04 ± 0.01	42.1 ± 1.4	59.83	26.24	3.74
GH-SC-AC_{10}	1262 ± 126	1	0.57 ± 0.05	0.31 ± 0.02	0.26 ± 0.03	44.4 ± 0.6	82.27	14.67	1.42
GH-SC-AC_{20}	1340 ± 47	79	0.59 ± 0.06	0.33 ± 0.07	0.26 ± 0.12	44.0 ± 1.3	79.95	15.81	2.23
GH-SC-AC_{30}	1931 ± 114	670	0.85 ± 0.04	0.37 ± 0.01	0.48 ± 0.04	42.1 ± 0.3	80.76	15.08	2.80
SC-AC_{100}	881 ± 102	-	0.41 ± 0.06	0.21 ± 0.02	0.19 ± 0.04	44.8 ± 0.1	75.85	16.52	4.97

6.6 Adsorption Results

6.6.1 Comparison of Langmuir model maximum adsorption capacities

Adsorption equilibrium was attained in approximately 4 h for all composites (**Figure 6.4**(e)). The impact of the contributions of shrimp-waste-supplied chemical functions to the adsorption performance of surface-area-optimized composites was investigated through Langmuir adsorption isotherm modelling. **Table 6.2** shows the maximum adsorption capacities with corresponding statistical evaluation of model fit for the composites (GH-$SH_{10\%}$, GH-$SS_{20\%}$ GH-$SC_{30\%}$) and pristine GH-AC. Maximum adsorption capacities of GH-$SH_{10\%}$, GH-$SS_{20\%}$ were greater than that of pristine GH-AC but within the margins of the standard deviations. Q_{max} for GH-$SC_{30\%}$ was, however, 34 mg/g larger than that of the pristine material. **Table 0.8** (Appendix ii) shows that the maximum adsorption capacities of shrimp waste functionalized greenheart AC was greater than for 2,4-D adsorption on a date palm activated carbon (50 mg/g) but generally lower than those for adsorption on date stone AC (238 mg/g) and greeheart/chitosan composite AC (166 mg/g).

Pearson correlation between Q_{max} and several physicochemical properties of optimized composites (**Figure 6.4**(f)) indicated that adsorption capacities were most strongly correlated with total surface nitrogen density (0.90), total nitrogen (0.88), amine group nitrogen (0.86) and specific surface area (0.87). This suggests that adsorption of 2,4-D was strongly influenced by nitrogen adsorption sites. It is known that protonated amine sites promote favorable electrostatic interactions with deprotonated 2,4-D molecules at pH with promote these chemical states (France et al., 2025). Poor correlation was generally seen between maximum adsorption capacities and micropore and mesopore volume, implying that adsorbate molecules were accommodated by pores of all sizes.

Experiments in this work were carried out at pH 7 since the performance of our composite materials under drinking-water-like pH was of interest. Since this pH was above the pH at point of zero charge of all materials, their net surface charge would be negative and would typically offer unfavorable adsorption interaction with deprotonated 2,4-D molecules. However, the inclusion of shrimp waste supplied amine functions would lend additional positive sites for adsorption since these amine functions would be protonated at pH 7. This is likely the key driving force for the generally better adsorption performance seen for N-functionalized adsorbents when compared to the pristine material. Furthermore, comparison of the adsorption performance among the composite materials (**Table 6.2**) showed that GH-$SC_{30\%}$, which had the largest proportion of amine-group functions (**Figure 6.3**(c-e)), performed best.

6.6.2 Isotherm modelling analysis

Several isotherm models are often used to further investigate the types of adsorption interactions which take place between adsorbate species and adsorbent surfaces. Models such as the Langmuir, Freundlich and Sips models enjoy ubiquitous use in literature. The Langmuir model assumes that adsorption sites have near homogeneous enthalpies of adsorption, that lateral interactions between adsorbed species are non-existent and that monolayer adsorption coverage takes place. The Freundlich model espouses multilayer adsorbate coverage on surface sites with heterogenous adsorption enthalpies. The Sips model combines mathematical descriptions of both the Langmuir and Freundlich models and is typically able to provide good model fits to adsorption systems which may be poorly described by either of its component models.
In this work, adsorption of 2,4-D on SW-functionalized adsorbents was best described by the Freundlich model (**Table 6.2**) and **Figure 6.4**(a-c), except for GH-$SH_{10\%}$ where the Sips model

statistically fit the adsorption data best. Adjusted R^2 values were higher and reduced χ^2 values were lower for model fits with the Freundlich model. This implied that the adsorption sites on GH-SW composites were heterogeneous in nature.

(a)

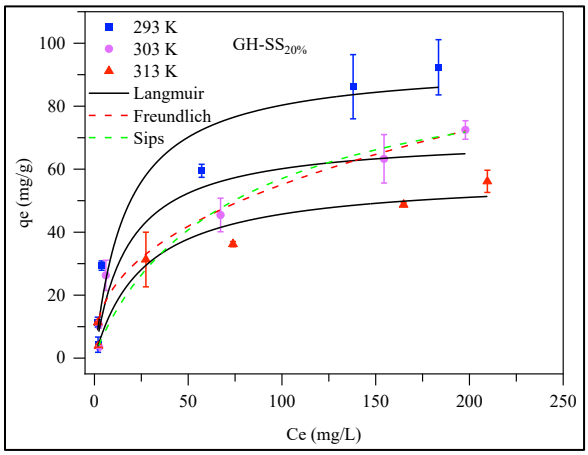

(b)

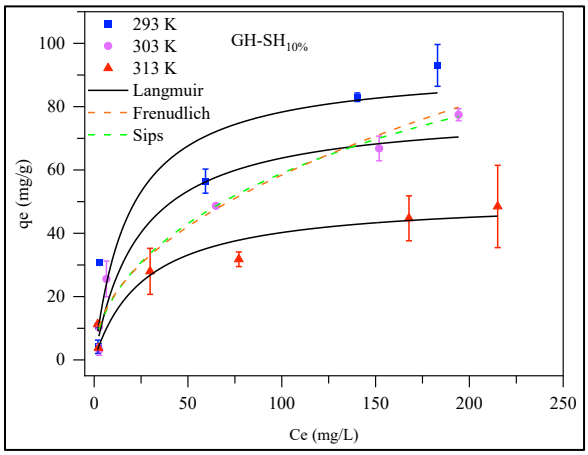

(c)

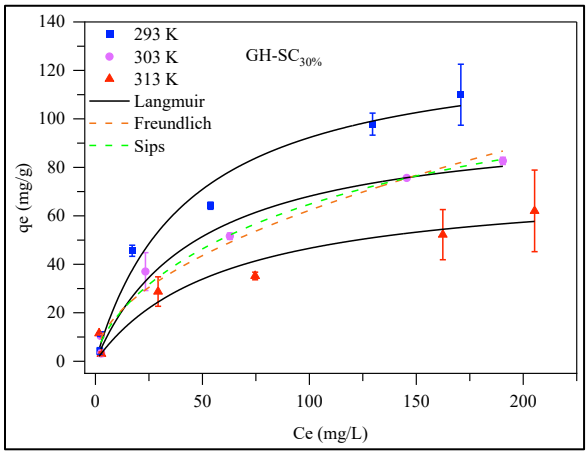

(d)

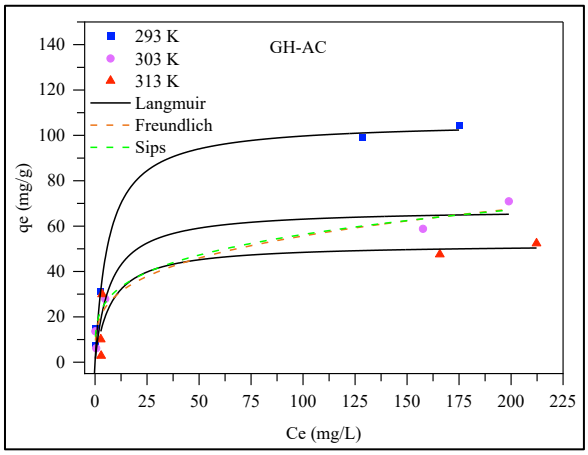

(e) (f)

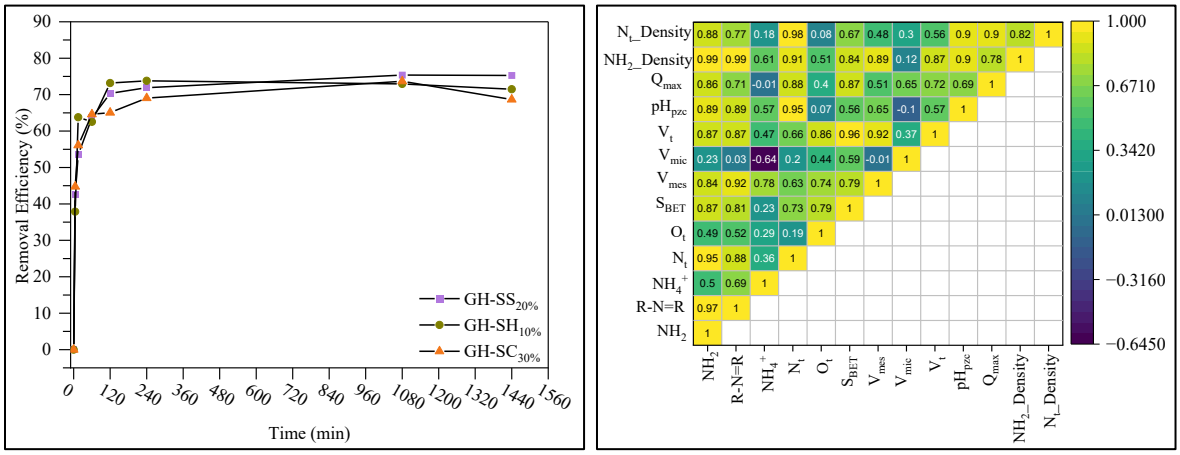

Figure 6.4 a – f Temperature dependence of adsorption of 2,4-D on surface area optimized GH-SW-ACs and pristine GH-AC at 303 K at pH 7 with superimposed Langmuir, Freundlich and Sips adsorption model isotherms, e – kinetics plots of SW ACs and f - Pearson matrix for correlation between Q_{max} and selected physicochemical properties.

Table 6.2 Model parameters and statistical evaluation of model fit for Langmuir, Freundlich and Sips adsorption isotherms at 303 K at pH 7.

Parameters	GH-AC	GH-$SS_{20\%}$	GH-$SH_{10\%}$	GH-$SC_{30\%}$
	Langmuir			
Q_0 *(mg/g)*	67.2 ± 6.61	70.6 ± 7.73	79.2 ± 9.08	101 ± 8.58
K_L *(L/mg)*	0.156 ± 0.084	0.0573 ± 0.031	0.0412 ± 0.021	0.021 ± 0.005
Adj R^2	0.913	0.915	0.935	0.980
Red χ^2	69.8	66.9	59.9	21.3
	Freundlich			
K_F *(L/mg)*	15.5 ± 3.70	8.23 ± 2.66	7.71 ± 2.43	5.82 ± 1.47
N	3.40 ± 0.628	2.45 ± 0.398	2.29 ± 0.342	1.943 ± 0.193
Adj R^2	0.953	0.950	0.960	0.994
Red χ^2	37.7	39.4	37.2	9.96
	Sips			
Q_0*(mg/g)*	69.1 ± 14.3	99.0 ± 74.6	147 ±68.4	105 ± 25.9
K_s	0.134 ± 0.148	0.012 ± 0.039	0.002 ± .002	0.019 ± 0.01
n_s	1.00 ± 1.01	0.882 ± 0.623	0.519 ± 0.071	1 ± 0.32
Adj R^2	0.864	0.878	0.987	0.972
Red χ^2	108	17.1	7.15	29.8

6.6.3 Evaluation of some thermodynamic parameters for 2,4-D adsorption on GH-SW-ACs

Table 6.3 shows the Gibbs energy for the adsorption of 2,4-D on pristine GH-AC as well as optimized composites. For all adsorbents, Gibbs free energy increased with increasing temperature, implying increasing spontaneity of the adsorbate-adsorbent interaction with temperature.

Table 6.3 Standard state thermodynamic parameters for adsorption of 2,4-D on pristine GH-AC and GH-SW-ACs.

T	$GH\text{-}SS_{20\%}$			$GH\text{-}SH_{10\%}$			$GH\text{-}SC_{30\%}$			GH-AC		
(k)	ΔG° (kJ/mol)	ΔH° (kJ/mol)	ΔS° (J/Kmol)	ΔG° (kJ/mol)	ΔH° (kJ/mol)	ΔS° (J/Kmol)	ΔG° (kJ/mol)	ΔH° (kJ/mol)	ΔS° (J/Kmol)	ΔG° (kJ/mol)	ΔH° (kJ/mol)	ΔS° (J/Kmol)
293	-23.24	-16.75	22.14	-22.78	-14.12	29.54	-20.86	-12.61	28.16	-27.51	-12.10	45.70
303	-23.46			-23.08			-21.14			-27.97		
313	-23.68			-23.37			-21.43			-28.43		

Gibbs energy values were in good agreement with 2,4-D adsorption on a commercial AC (-22.56 kJ/mol at 303 K) (Ghatbandhe et al., 2013), on AC derived from carbon slurry from fertilizer production (-21.08 kJ/mol at 300 K) (Gupta et al., 2006) and chitosan functionalized greenheart composite (-19.3 kJ/mol) (France et al., 2025). Adsorption was also entropically favored and exothermic with ΔH values of -16.8 kJ/mol, -14.1 kJ/mol and -12.6 kJ/mol for 2,4-D adsorption on GH-$SS_{20\%}$, GH-$SH_{10\%}$ and GH-$SC_{30\%}$ respectively. **Table 0.9** (Appendix i) further shows considerable variations in ΔG°, ΔH° and ΔS° values for 2,4-D adsorption on various adsorbents. This is to be expected given the highly variable nature of the surface functional and textural properties of the materials and their consequent adsorption chemistries.

Adsorption enthalpy values suggest that physisorption interactions predominate the adsorption process. Moreover, the subtle changes in adsorption enthalpies suggest that the various processing parameters impacted surface functionalities differently and lead to differences in the types of physisorption interaction that took place between each type of shrimp waste composite and 2,4-D molecules.

6.7 Conclusion

In this work we demonstrate that wood and shrimp wastes can be efficiently co-valorized to nitrogen-rich, high-surface-area adsorbents which can remove the toxic herbicide 2,4-D from aquatic matrices at pH 7. The works significance is manifested in its demonstration of the concept of the circular economy by diverting these low-value waste streams from landfill and using them to fabricate green environmental remediation materials . Furthermore, the facile fabrication procedure used here, and the minimal chemical inputs involved, adds to the green nature of the approach. We show that up to a 5-fold increase in surface nitrogen and a 56% increase in specific surface area are attainable by pre-activation shrimp waste addition to tropical waste wood feedstock followed by low temperature activation under an inert atmosphere in the presence of phosphoric acid. Optimized materials derived from this process had greater Langmuir maximum adsorption capacities than pristine greenheart AC, demonstrating the enhanced adsorption performance of the functionalization materials. Furthermore, strong correlation between maximum adsorption capacities and shrimp-waste supplied N-functionality points to the impact of these functions in facilitating adsorbate-adsorbent interactions. Isotherm modelling further indicated the Freundlich model fitted the data best implying that the composites had energetically heterogeneous adsorption sites. Thermodynamic evaluation showed that the adsorption of 2,4-D was spontaneous, entropically favored and exothermic with Gibbs energy increasing with temperature. The range of adsorption enthalpies for all composites was between -12 kJ/mol and -17 kJ/mol suggesting that herbicide molecules were physisorbed on the shrimp-waste-functionalized adsorbent. These biopolymer-derived adsorbents are promising green materials for environmental remediation applications.

Chapter 7 Conclusions and Contributions to Science

7.1 General Conclusions

In this work we have valorized tropical waste wood feedstock (greenheart) by fabricating high-surface area adsorbents; demonstrating that the tropical hardwood feedstock is indeed conducive to phosphoric acid activation. We show that both pristine and functionalized adsorbents are efficient at removing cationic metal and organic pollutants from aquatic matrices. These results are significant in that they demonstrate that a copious waste stream can be diverted from landfill and upcycled to versatile, tunable, green adsorbents. Further, the fact that few chemical inputs are used, sustainable biopolymer dopants are employed, moderate temperatures are used and that the process is facile, augurs well for potential commercialization and scale up. This is particularly important given the fact that numerous newly fabricated adsorbents are too costly for viable scale up.

We have further shown that this adsorbent has tunable surface functionality and lends itself to facile base treatment, O-functionalization by ambient-temperature flash oxidation and N-functionalization by pre-activation addition of variously processed shrimp wastes. Herein, several major findings of this study were realized. Firstly, ambient temperature flash-oxidation increased surface oxygen 8-fold in just 60 min, indicating that protracted oxidations are not necessary. Moreover, the fact that our procedure preserved more than 85% of the material's surface area and does little to alter porosity addresses a persistent worry relating to surface area loss and pore collapse from oxidations. Secondly, N-functionalization with shrimp-waste derived dopants led to comparable increases in surface nitrogen using milder conditions and less toxic reagents than is typically reported. Here again, our use of sustainable biopolymers is progressive

in the context of green chemistry applications. And thirdly it was demonstrated that surface area increases in functionalized ACs, when compared to pristine AC, are achievable with the application of certain weight ratios of shrimp waste dopants as well as under some oxidation conditions. This provides new insights into textural amendments from both functionalization procedures. While additional work is required to elucidate the exact mechanisms of textural increases with shrimp waste doping of greenheart AC, it is proffered that secondary gasification reactions may be responsible.

Adsorption performance was enhanced by all treatments in this work. Base-wash treatments improved the removal of aluminum, manganese and iron from pit-lake waters by providing more negative surface sites for removal of cationic metal species. Flash oxidation enhanced the removal of aluminum and lead. Manganese removal was challenging in general but was also increased when functionalized AC was used. Interestingly, metal adsorption by oxygen functionalized AC was more closely correlated with specific oxygen containing functional groups than with the total oxygen content. This suggests that a different mechanism of interaction may mediate the removal of each metal ion. Nitrogen functionalization had varied impacts on 2,4-D and paraquat removal. 2,4-D removal increased with N-functionalization implying that under experimental pH conditions, more amine-supplied cationic sites were furnished for interaction with the deprotonated 2,4-D acid moiety. Conversely, N-functionalization lead to more antagonistic interactions between protonated amines and cationic moieties of the paraquat molecule. These findings underscore the importance of a thorough understanding of adsorbate speciation under experimental conditions and the need to clearly assess modification strategies as both enhanced and retarded adsorption may result.

Isotherm modelling showed that Langmuir, Freundlich and Sips models provided good fits for the adsorption data. Thus, it may be concluded that adsorption sites on ACs though variable, possess a narrow range of adsorption enthalpies. Evaluation of standard state thermodynamic parameters led to the conclusion that organic herbicides interacted with functionalized ACs by physisorption; with adsorption enthalpies < 50 kJ/mol. This finding was corroborated with isosteric heat calculations which showed minimal increases in adsorption enthalpy as surface coverage increased. Another significant finding generated from thermodynamic evaluation was regarding adsorption entropies. These were large and indicated the presence of numerous and/or diverse surface sites capable of interacting with herbicide molecules. This is advantageous and may be responsible for the demonstrated versatility of the adsorbents.

7.2 Future Work

1. ***Investigate the mechanism of surface area augmentation due to pre-activation shrimp waste doping of lignocellulosic feedstock***. While clear enhancements in surface area were seen when various weight ratios of shrimp wastes were added to greenheart waste wood prior to activation, the mechanism by which these enhancements occurred is unclear. We proffer that secondary gasification reaction may be responsible but concede that a detailed study is warranted. This is so because understanding this mechanism is the first step in utilizing this technique to obtain controlled increases in surface area. Furthermore, it would be of interest to obtain a clearer understanding of the impact played by dopant weight ratios, dopant type or activation temperature on these enhancements.

2. ***Evaluation of the adsorption performance of N-functionalized ACs in real world aquatic matrices containing paraquat and 2,4-D so that potential synergistic or antagonistic interactions may be understood***. It is well known that real-world matrices present additional challenges in adsorption applications. Factors such as impact of additional species should be studies. In particular, the impact of the presence of humic substances and inorganic cations on the adsorption performance of the composites should be evaluated.

3. ***Investigating the adsorption performance of pristine and functionalized greenheart ACs in oil sand process affected water (OSPW) treatment to evaluate how surface functionality and texture impacts the adsorption performance of these adsorbents in a complex aquatic matrix.*** It is known that OSPW is comprised of a wide range of naphthenic acids with large variations in structure. Moreover, recalcitrant species which are not easily removed by standard activated carbons, have been identified. Leveraging the textural and surface chemistry properties of our composites to tackle the removal of such species is likely to be a fruitful undertaking.

7.3 Contributions to science

7.3.1 ***Publications***

The following papers were published in collaboration with the named authors:-

1. **Hamant E. France[1]**, Oliver.L.K Strong[2], Kevin M. Scotland[2], Tyler M. Roy[2], Andrew J. Vreugdenhil[2], (2024) "***Pit-Lake remediation by chemically activated Chlorocardium rodiei: Simultaneous metal ion removal from acidic waters***", *Sustainable Chemistry for the Environment.* *https://doi.org/10.1016/j.scenv.2024.100103*

2. Oliver K.L. Strong[1], **Hamant E. France[2]**, Kevin Scotland[1], Kelly Wright[1], Andrew J. Vreugdenhil[1],* (2023)"***Selenite adsorption and reduction via Iron(II) impregnated activated carbon produced from the phosphoric acid activation of landfill waste wood",*** *Archives of Environmental Contamination and Toxicology.* *https://doi.org/10.1007/s00244-023-01032-y*

3. **Hamant E. France[1]**, Oliver.L.K Strong[2], Tyler M. Roy[2], Andrew J. Vreugdenhil[2], (2025), "***Versatile Chlorocardium rodiei-chitosan adsorbent for 2,4-D and paraquat adsorption: Isotherm modelling and thermodynamic evaluation".*** *https://doi.org/10.1016/j.chemosphere.2024.144008*

4. **Hamant E. France[1],** O.L.K. Strong[2], Andrew J. Vreugdenhil[2]**,** (2025) **"*Fabrication and ambient temperature flash O-functionalization of chlorocardium rodiei-based carbon for toxic metal adsorption*".** https://doi.org/10.1016/j.cartre.2025.100536

7.3.2 ***Publications Under Review***

5. **Hamant E. France[1]** , Bunnel Bernard[2], O.L.K Strong[2], Tyler M. Roy[2], Andrew J. Vreugdenhil[2], (2025), "***Evaluation of the Impact of Flash O-Functionalization on Physicochemical Properties of Lignocellulosic AC: An RSM Study.***"

6. **Hamant E. France[1]** , Julia Pohlina[2], O.L.K Strong[2], Tyler M. Roy[2], Andrew J. Vreugdenhil[2], Yuana Yesika[3], (2025), ***"Co-valorization of Shrimp Shell and Tropical Wood Waste by Fabrication of High-Surface, Nitrogen-Rich ACs: Characterization and Herbicide Adsorption Studies."***

7. Tyler M. Roy[1] , Oliver L. K. Strong[1] **, Hamant E. France[1]** , Paul R. Pede[2] , Andrew J. Vreugdenhil[1], (2025) ***"The Adsorption Thermodynamics of Model Naphthenic Acids onto Porous Adsorbents: Validating Adsorption Mechanisms."***

7.3.3 ***Conferences***

Below is a list of conferences and fora I attended, and presentations made in contribution to the fields of material and environmental science:-

1. Canadian Chemistry Conference & Exhibition – CCCE(CSC) – Ottawa, Ontario, June 2025 – Oral presentation on ***Co-valorization of Tropical Hardwood and Shrimp Wastes by Fabrication of High-Surface, Nitrogen-Rich ACs: Production and 2,4-D Adsorption Studies*** **- Hamant E. France[1]** and Andrew J. Vreugdenhil[2]

2. Environmental and Life Sciences Graduate Conference (ENLS) Peterborough, Ontario, May 2025 - Oral presentation on ***Aquatic Environmental Remediation Applications of Tunable Waste wood-derived Adsorbents*****, Hamant E. France[1]** and Andrew J. Vreugdenhil[2].

3. International Institute of Environmental Studies (IIES) Johannesburg, South Africa, April 2025 - Oral presentation on ***Chitosan-waste wood Nitrogen-Doped ACs for 2,4-D and Paraquat Removal –*** **Hamant E. France[1]** and Andrew J. Vreugdenhil[2].

4. American Chemical Society (ACS Spring) – San Diego, California, March 2025 – Poster presentation on ***Versatile Chlorocardium rodiei-chitosan adsorbent for 2,4-D and paraquat adsorption: Isotherm modelling and thermodynamic evaluation –*** **Hamant E. France[1]** and Andrew J. Vreugdenhil[2].

5. Symons Seminary Series Gala, Trent University, Peterborough, Ontario, April 2025, Oral presentation on ***Environmental Remediation Applications of Tropical Waste Streams*** – **Hamant E. France[1]** and Andrew J. Vreugdenhil[2].

6. Symons Seminary Series, Trent University, Peterborough, Ontario, January 2025, Oral presentation on ***Environmental Remediation Applications of Tropical Waste Streams*** – **Hamant E. France[1]** and Andrew J. Vreugdenhil[2].

7. Canadian Chemical Engineering Conference – CSChE – Toronto, Ontario, October 2024 **-** Poster presentation on ***Facile Fabrication of High Surface, Nitrogen-rich Activated Carbons from Chitosan and Waste wood –*** **Hamant E. France[1]** and Andrew J. Vreugdenhil[2].

8. Canadian Chemistry Conference & Exhibition – CCCE(CSC) – Winnipeg, Manitoba, June 2024 - Oral presentation on ***Heteroatom and Textural Improvement of Tropical Hardwood Derived Activated Carbons: Chitosan Addition and Flash Oxidation -*** Hamant E. France[1] and **Andrew J. Vreugdenhil[2]**.

9. Canadian Chemistry Conference & Exhibition - CCCE (CSC) – Vancouver, British Colombia, June 2023 - Poster presentation on ***Investigating Adsorption Interactions Between Chemically Activated Carbons and Selected Cations and Methylene Blue -*** **Hamant E. France[1]** and Andrew J. Vreugdenhil[2].

10. International Institute of Environmental Studies (IIES) – Ho Chi Minh, Vietnam, October 2022 – Oral presentation on ***Chemically Activated Tropical Hardwood waste for Environmental Remediation Materials: Production and Multi-Cation Removal –*** **Hamant E. France[1]** and Andrew J. Vreugdenhil[2].

11. ICES and 7th Annual IIES Science & Policy Workshop Graduate Student Forum - Phu Quoc Island Vietnam, October 2022 – Oral presentation on ***"Pit-Lake Remediation by Greenheart waste wood Activated Carbons"*** - **Hamant E. France[1]** and Andrew J. Vreugdenhil[2].

12. Canadian Chemistry Conference & Exhibition - CCCE (CSC) – Calgary, Alberta, June 2022 – Poster presentation on ***Chemically Activated Tropical Hardwood waste: Production and Characterization*** - **Hamant E. France[1]** and Andrew J. Vreugdenhil[2].

7.3.1 ***Acknowledgment***

The authors would like to acknowledge the financial support of CGX, Frontera Energy, Trent University, and the University of Guyana through the Sustainable Guyana Program. We would also like to acknowledge support from CASD/MI and Dr. Kelly Hawboldt at Memorial University.

References

A. Akl, M., 2013. Removal of Iron and Manganese in Water Samples Using Activated Carbon Derived from Local Agro-Residues. Journal of Chemical Engineering & Process Technology 04. https://doi.org/10.4172/2157-7048.1000154

Abdulhamid, Q.M., Al-Tikrity, E.T.B., Fadhil, A.B., Foot, P.J.S., 2023. Thermal cracking of Al-Dora asphalt for the simultaneous production of light fuel and activated carbon for desulfurization process. J Anal Appl Pyrolysis 173. https://doi.org/10.1016/j.jaap.2023.106072

Advancing Sustainable Materials Management: 2018 Fact Sheet Assessing Trends in Materials Generation and Management in the United States, 2020.

Alharbi, O.M.L., Basheer, A.A., Khattab, R.A., Ali, I., 2018. Health and environmental effects of persistent organic pollutants. J Mol Liq. https://doi.org/10.1016/j.molliq.2018.05.029

Alluhaybi, A.A., Alharbi, A., Alshammari, K.F., El-Desouky, M.G., 2023. Efficient Adsorption and Removal of the Herbicide 2,4-Dichlorophenylacetic Acid from Aqueous Solutions Using MIL-88(Fe)-NH2. ACS Omega 8, 40775–40784. https://doi.org/10.1021/acsomega.3c05818

Al-Muhtaseb, S.A., El-Naas, M.H., Abdallah, S., 2008. Removal of aluminum from aqueous solutions by adsorption on date-pit and BDH activated carbons. J Hazard Mater 158, 300–307. https://doi.org/10.1016/j.jhazmat.2008.01.080

Ang, T.N., Young, B.R., Burrell, R., Taylor, M., Aroua, M.K., Baroutian, S., 2021. Oxidative hydrothermal surface modification of activated carbon for sevoflurane removal. Chemosphere 264. https://doi.org/10.1016/j.chemosphere.2020.128535

Ania, C.O., Parra, J.B., Pis, J.J., 2002. Effect of texture and surface chemistry on adsorptive capacities of activated carbons for phenolic compounds removal.

Anirudhan, T.S., Sreekumari, S.S., 2011. Adsorptive removal of heavy metal ions from industrial effluents using activated carbon derived from waste coconut buttons. Journal of Environmental Sciences 23, 1989–1998. https://doi.org/10.1016/S1001-0742(10)60515-3

APVMA, 2019. 2,4-D (2,4-dichlorophenoxyacetic acid).

Atwood, D., Paisley-Jones, C., Ocspp, Opp, 2017. US EPA - Pesticides Industry Sales and Usage 2008 - 2012.

Australian and New Zealand Environment and Conservation Council., Agriculture and Resource Management Council of Australia and New Zealand., 2000. Australian and New Zealand guidelines for fresh and marine water quality 2000. Australian and New Zealand Environment and Conservation Council.

Bégin, S.J., Scotland, K.M., Pede, P.R., Vreugdenhil, A.J., 2023. Polyacrylamide Grafted Activated Carbon by Surface-Initiated AGET ATRP for the Flocculation of MFT. Macromol Chem Phys 224. https://doi.org/10.1002/macp.202300223

Bergna, D., Hu, T., Prokkola, H., Romar, H., Lassi, U., 2020. Effect of Some Process Parameters on the Main Properties of Activated Carbon Produced from Peat in a Lab-Scale Process. Waste Biomass Valorization 11, 2837–2848. https://doi.org/10.1007/s12649-019-00584-2

Bhatnagar, A., Hogland, W., Marques, M., Sillanpää, M., 2013. An overview of the modification methods of activated carbon for its water treatment applications. Chemical Engineering Journal. https://doi.org/10.1016/j.cej.2012.12.038

Binh, Q.A., Nguyen, H.H., 2020. Investigation the isotherm and kinetics of adsorption mechanism of herbicide 2,4-dichlorophenoxyacetic acid (2,4-D) on corn cob biochar. Bioresour Technol Rep 11. https://doi.org/10.1016/j.biteb.2020.100520
Blachnio, M., Kusmierek, K., Swiatkowski, A., Derylo-Marczewska, A., 2023. Adsorption of Phenoxyacetic Herbicides from Water on Carbonaceous and Non-Carbonaceous Adsorbents. Molecules. https://doi.org/10.3390/molecules28145404
Blair, L.M., Taylor, G.J., 1997. Environmental and Experimental Botany The nature of interaction between aluminum and manganese on growth and metal accumulation in Triticum aestivum, Environmental and Experimental Botany.
Brigante, M., Avena, M., 2014. Synthesis, characterization and application of a hexagonal mesoporous silica for pesticide removal from aqueous solution. Microporous and Mesoporous Materials 191, 1–9. https://doi.org/10.1016/j.micromeso.2014.02.035
Carabineiro, S.A.C., Thavorn-Amornsri, T., Pereira, M.F.R., Figueiredo, J.L., 2011. Adsorption of ciprofloxacin on surface-modified carbon materials. Water Res 45, 4583–4591. https://doi.org/10.1016/j.watres.2011.06.008
Carneiro Brandão Pereira, T., Batista dos Santos, K., Lautert-Dutra, W., de Souza Teodoro, L., de Almeida, V.O., Weiler, J., Homrich Schneider, I.A., Reis Bogo, M., 2020. Acid mine drainage (AMD) treatment by neutralization: Evaluation of physical-chemical performance and ecotoxicological effects on zebrafish (Danio rerio) development. Chemosphere 253. https://doi.org/10.1016/j.chemosphere.2020.126665
Castendyk, D.N., Eary, L.E., Balistrieri, L.S., 2015. Modeling and management of pit lake water chemistry 1: Theory. Applied Geochemistry. https://doi.org/10.1016/j.apgeochem.2014.09.004
Castro, J.M., Moore, J.N., 2000. Cases and solutions 1254, Environmental Geology. Springer-Verlag.
Cecen, F., 2011. Water and Wastewater Treatment: Historical Perspective of Activated Carbon Adsorption and its Integration with Biological Processes.
Chandrasekar, R., Rajendran, H.K., Priyan V, V., Narayanasamy, S., 2022. Valorization of sawdust by mineral acid assisted hydrothermal carbonization for the adsorptive removal of bisphenol A: A greener approach. Chemosphere 303. https://doi.org/10.1016/j.chemosphere.2022.135171
Clayden, J., Greeves, N., Warren, S., 2012. Organic Chemistry Organic Chemistry-online support.
da Silva Alves, D.C., Healy, B., Pinto, L.A. de A., Cadaval, T.R.S., Breslin, C.B., 2021. Recent developments in Chitosan-based adsorbents for the removal of pollutants from aqueous environments. Molecules. https://doi.org/10.3390/molecules26030594
Da Silva, A.P., Morais, E.R., Oliveira, E.C., Ghisi, N. de C., 2022. Does exposure to environmental 2,4-dichlorophenoxyacetic acid concentrations increase mortality rate in animals? A meta-analytic review. Environmental Pollution. https://doi.org/10.1016/j.envpol.2022.119179
Daud, W.M.A.W., Houshamnd, A.H., 2010. Textural characteristics, surface chemistry and oxidation of activated carbon. Journal of Natural Gas Chemistry. https://doi.org/10.1016/S1003-9953(09)60066-9
de Celis, J., Amadeo, N.E., Cukierman, A.L., 2009. In situ modification of activated carbons developed from a native invasive wood on removal of trace toxic metals from wastewater. J Hazard Mater 161, 217–223. https://doi.org/10.1016/j.jhazmat.2008.03.075
Dehghani, Z., Sedghi-Asl, M., Ghaedi, M., Sabzehmeidani, M.M., Adhami, E., 2021. Ultrasound-assisted adsorption of paraquat herbicide from aqueous solution by graphene

oxide/ mesoporous silica. J Environ Chem Eng 9. https://doi.org/10.1016/j.jece.2021.105043
Diao, Y., Walawender, W.P., Fan, L.T., 2002. Activated carbons prepared from phosphoric acid activation of grain sorghum.
Díaz-Díez, M.A., Gómez-Serrano, V., Fernández González, C., Cuerda-Correa, E.M., Macías-García, A., 2004. Porous texture of activated carbons prepared by phosphoric acid activation of woods, in: Applied Surface Science. Elsevier, pp. 309–313. https://doi.org/10.1016/j.apsusc.2004.05.228
Du, T., Bogush, A., Mašek, O., Purton, S., Campos, L.C., 2022. Algae, biochar and bacteria for acid mine drainage (AMD) remediation: A review. Chemosphere. https://doi.org/10.1016/j.chemosphere.2022.135284
Duan, C., Ma, T., Wang, J., Zhou, Y., 2020. Removal of heavy metals from aqueous solution using carbon-based adsorbents: A review. Journal of Water Process Engineering. https://doi.org/10.1016/j.jwpe.2020.101339
Duong, D.Do., 1998. Adsorption analysis : equilibria and kinetics. Imperial College Press.
Duong, G., Rankin, M., Ahmed, G., Rice, J., Nguyen, H., Esnard, T., Mcfee, D., 2023. The seabob value chain in Guyana.
Fadhil, A.B., Saeed, H.N., Saeed, L.I., 2021. Polyethylene terephthalate waste-derived activated carbon for adsorptive desulfurization of dibenzothiophene from model gasoline: Kinetics and isotherms evaluation. Asia-Pacific Journal of Chemical Engineering 16. https://doi.org/10.1002/apj.2594
Fan, Q., Song, C., Fu, P., 2024. Advances in the improvement of the quality and efficiency of biomass-derived porous carbon: A comprehensive review on synthesis strategies and heteroatom doping effects. J Clean Prod. https://doi.org/10.1016/j.jclepro.2024.142169
FAO, 2017. World fertilizer trends and outlook to 2020.
Fashola, M.O., Ngole-Jeme, V.M., Babalola, O.O., 2016. Heavy metal pollution from gold mines: Environmental effects and bacterial strategies for resistance. Int J Environ Res Public Health. https://doi.org/10.3390/ijerph13111047
France, H.E., Strong, O.L.K., Roy, T.M., Vreugdenhil, A.J., 2025. Versatile waste wood-chitosan composites for 2,4-D and paraquat adsorption: Isotherm modelling and thermodynamic evaluation. Chemosphere 370, 144008. https://doi.org/10.1016/j.chemosphere.2024.144008
France, H.E., Strong, O.L.K., Scotland, K.M., Roy, T.M., Vreugdenhil, A.J., 2024. Pit-lake remediation by chemically activated Chlorocardium rodiei: Simultaneous metal ion removal from acidic waters. Sustainable Chemistry for the Environment 6, 100103. https://doi.org/10.1016/j.scenv.2024.100103
Franco, D.S.P., Georgin, J., Lima, E.C., Silva, L.F.O., 2022. Advances made in removing paraquat herbicide by adsorption technology: A review. Journal of Water Process Engineering. https://doi.org/10.1016/j.jwpe.2022.102988
Gao, Y., Yue, Q., Gao, B., Sun, Y., Wang, W., Li, Q., Wang, Y., 2013. Preparation of high surface area-activated carbon from lignin of papermaking black liquor by KOH activation for Ni(II) adsorption. Chemical Engineering Journal 217, 345–353. https://doi.org/10.1016/j.cej.2012.09.038
Ghasemi, H., Afshang, M., Gilvari, T., Aghabarari, B., Mozaffari, S., 2023. Rapid and effective removal of heavy metal ions from aqueous solution using nanostructured clay particles. Results in Surfaces and Interfaces 10. https://doi.org/10.1016/j.rsurfi.2023.100097

Ghatbandhe, A.S., Jahagirdar, H.G., Yenkie, M.K.N., Deosarkar, S.D., 2013. Evaluation of thermodynamic parameters of 2, 4-dichlorophenoxyacetic acid (2, 4-D) adsorption. J Chem. https://doi.org/10.1155/2013/519304

Gillett, R.D.., 2008. Global study of shrimp fisheries. Food and Agriculture Organization of the United Nations.

Gimeno, O., Plucinski, P., Kolaczkowski, S.T., Rivas, F.J., Alvarez, P.M., 2003. Removal of the herbicide MCPA by commercial activated carbons: Equilibrium, kinetics, and reversibility. Ind Eng Chem Res 42, 1076–1086. https://doi.org/10.1021/ie020424x

Goher, M.E., Hassan, A.M., Abdel-Moniem, I.A., Fahmy, A.H., Abdo, M.H., El-sayed, S.M., 2015. Removal of aluminum, iron and manganese ions from industrial wastes using granular activated carbon and Amberlite IR-120H. Egypt J Aquat Res 41, 155–164. https://doi.org/10.1016/j.ejar.2015.04.002

Gómez-Serrano, V., Cuerda-Correa, E.M., Fernández-González, M.C., Alexandre-Franco, M.F., Macías-García, A., 2005. Preparation of activated carbons from chestnut wood by phosphoric acid-chemical activation. Study of microporosity and fractal dimension. Mater Lett 59, 846–853. https://doi.org/10.1016/j.matlet.2004.10.064

Gupta, V.K., Ali, I., Suhas, Saini, V.K., 2006. Adsorption of 2,4-D and carbofuran pesticides using fertilizer and steel industry wastes. J Colloid Interface Sci 299, 556–563. https://doi.org/10.1016/j.jcis.2006.02.017

Hameed, B.H., Salman, J.M., Ahmad, A.L., 2009. Adsorption isotherm and kinetic modeling of 2,4-D pesticide on activated carbon derived from date stones. J Hazard Mater 163, 121–126. https://doi.org/10.1016/j.jhazmat.2008.06.069

Haydar, ´ S, Ferro-Garcıa, M.A., Rivera-Utrilla, J., Joly, J.P., 2003. A dsorption of p-nitrophenol on an activated carbon with different oxidations, Carbon.

He, P., Zhang, Y., Zhang, X., Chen, H., 2021. Diverse zeolites derived from a circulating fluidized bed fly ash based geopolymer for the adsorption of lead ions from wastewater. J Clean Prod 312. https://doi.org/10.1016/j.jclepro.2021.127769

Hinwood, A.L., Heyworth, J., Tanner, H., McCullough, C., 2012. Recreational Use of Acidic Pit Lakes—Human Health Considerations for Post Closure Planning. J Water Resour Prot 04, 1061–1070. https://doi.org/10.4236/jwarp.2012.412122

Huang, C.F., Tu, C.W., Lee, R.H., Yang, C.H., Hung, W.C., Andrew Lin, K.Y., 2019. Study of various diameter and functionality of TEMPO-oxidized cellulose nanofibers on paraquat adsorptions. Polym Degrad Stab 161, 206–212. https://doi.org/10.1016/j.polymdegradstab.2019.01.023

Hussein, A.A., Fadhil, A.B., 2021. Kinetics and isothermal evaluations of adsorptive desulfurization of dibenzothiophene over mixed bio-wastes derived activated carbon. Energy Sources, Part A: Recovery, Utilization and Environmental Effects. https://doi.org/10.1080/15567036.2021.1895372

Hwang, H., Sahin, O., Choi, J.W., 2017. Manufacturing a super-active carbon using fast pyrolysis char from biomass and correlation study on structural features and phenol adsorption. RSC Adv 7, 42192–42202. https://doi.org/10.1039/c7ra06910c

Hynes, L., Montiel, G., Jones, A., Riel, D., Abdulaziz, M., Viva, F., Bonetta, D., Vreugdenhil, A., Trevani, L., 2020. Melamine adsorption on carbon materials: Impact of carbon texture and surface chemistry. Mater Adv 1, 262–270. https://doi.org/10.1039/d0ma00097c

Islam, F., Wang, J., Farooq, M.A., Khan, M.S.S., Xu, L., Zhu, J., Zhao, M., Muños, S., Li, Q.X., Zhou, W., 2018. Potential impact of the herbicide 2,4-dichlorophenoxyacetic acid on human and ecosystems. Environ Int. https://doi.org/10.1016/j.envint.2017.10.020

Jaramillo, J., Álvarez, P.M., Gómez-Serrano, V., 2010. Oxidation of activated carbon by dry and wet methods surface chemistry and textural modifications. Fuel Processing Technology 91, 1768–1775. https://doi.org/10.1016/j.fuproc.2010.07.018

Juurlink, D.N., 2016. Activated charcoal for acute overdose: A reappraisal. Br J Clin Pharmacol 81, 482–487. https://doi.org/10.1111/bcp.12793

Kazmi, M.Z.H., Karmakar, A., Michaelis, V.K., Williams, F.J., 2019. Separation of cellulose/hemicellulose from lignin in white pine sawdust using boron trihalide reagents. Tetrahedron 75, 1465–1470. https://doi.org/10.1016/j.tet.2019.02.009

Khalid, R.Y., Fadhil, A.B., 2024. Adsorptive removal of dibenzothiophene from model fuel over activated carbon developed by KOH activation of pinecone: Equilibrium and kinetic studies. Asia-Pacific Journal of Chemical Engineering 19. https://doi.org/10.1002/apj.2976

Kirchherr, J., Yang, N.H.N., Schulze-Spüntrup, F., Heerink, M.J., Hartley, K., 2023. Conceptualizing the Circular Economy (Revisited): An Analysis of 221 Definitions. Resour Conserv Recycl. https://doi.org/10.1016/j.resconrec.2023.107001

Kocherbitov, V., Arnebrant, T., 2010. Hydration of lysozyme: The protein-protein interface and the enthalpy-entropy compensation. Langmuir 26, 3918–3922. https://doi.org/10.1021/la903210e

Kostenko, L.S., Tomashchuk, I.I., Kovalchuk, T. V., Zaporozhets, O.A., 2019. Bentonites with grafted aminogroups: Synthesis, protolytic properties and assessing Cu(II), Cd(II) and Pb(II) adsorption capacity. Appl Clay Sci 172, 49–56. https://doi.org/10.1016/j.clay.2019.02.009

Kouchakinejad, R., Shariati, S., Abolhasani, J., Kalhor, E.G., Vardini, M.T., 2022. Core-shells of magnetite nanoparticles decorated by SBA-3-SO3H mesoporous silica for magnetic solid phase adsorption of paraquat herbicide from aqueous solutions. Colloids Surf A Physicochem Eng Asp 643. https://doi.org/10.1016/j.colsurfa.2022.128709

Kumar, A., Jena, H.M., 2016. Preparation and characterization of high surface area activated carbon from Fox nut (Euryale ferox) shell by chemical activation with H3PO4. Results Phys 6, 651–658. https://doi.org/10.1016/j.rinp.2016.09.012

Li, H., Qi, H., Yin, M., Chen, Y., Deng, Q., Wang, S., 2021. Carbon tubes from biomass with prominent adsorption performance for paraquat. Chemosphere 262. https://doi.org/10.1016/j.chemosphere.2020.127797

Li, J., Zhou, W., Huang, Y., Zhao, Y., Li, X., Xue, N., Qu, Z., Tang, Z., Xie, L., Meng, X., Gao, J., Sun, F., Wang, P., Pi, X., Zhao, G., Qin, Y., 2024. Rapid, simple and sustainable preparation of N-rich activated carbons with high performance for gas adsorption, via microwave heating. Sep Purif Technol 330. https://doi.org/10.1016/j.seppur.2023.125464

Li, S., Han, K., Li, J., Li, M., Lu, C., 2017. Preparation and characterization of super activated carbon produced from gulfweed by KOH activation. Microporous and Mesoporous Materials 243, 291–300. https://doi.org/10.1016/j.micromeso.2017.02.052

Li, Y., Guo, R., Liang, X., Yao, B., Yan, S., Guo, Y., Han, Y., Cui, J., 2023. Pollution characteristics, ecological and health risks of herbicides in a drinking water source and its inflowing rivers in North China. Environmental Pollution 334. https://doi.org/10.1016/j.envpol.2023.122130

Ligero, A., Solís, R.R., Blázquez, G., Muñoz-Batista, M.J., Pérez, A., Calero, M., 2024. On the cutting-edge of non-recyclable plastic waste valorization: From pyrolysis char to nitrogen-enriched activated carbon for landfill biogas upgrading. J Environ Chem Eng 12. https://doi.org/10.1016/j.jece.2024.112265

Lim, W.C., Srinivasakannan, C., Balasubramanian, N., 2010. Activation of palm shells by phosphoric acid impregnation for high yielding activated carbon. J Anal Appl Pyrolysis 88, 181–186. https://doi.org/10.1016/j.jaap.2010.04.004
Lin, X., Chan, K., Kingkhambang, K., Hayashi, H., Zinchenko, A., 2024. Hydrothermal preparation of pharmaceuticals adsorbents from chitin and chitosan: Optimization and mechanism. Bioresour Technol 414. https://doi.org/10.1016/j.biortech.2024.131583
Liu, F., Gao, Y., Zhang, C., Huang, H., Yan, C., Chu, X., Xu, Z., Wang, Z., Zhang, H., Xiao, X., Yang, W., 2019. Highly microporous carbon with nitrogen-doping derived from natural biowaste for high-performance flexible solid-state supercapacitor. J Colloid Interface Sci 548, 322–332. https://doi.org/10.1016/j.jcis.2019.04.005
Liu, J., LeVan, M.D., 2009. Isosteric heats of adsorption in the Henry's law region for carbon single wall cylindrical nanopores and spherical nanocavities. Carbon N Y 47, 3415–3423. https://doi.org/10.1016/j.carbon.2009.07.054
Lobo-Recio, M.Á., Rodrigues, C., Custódio Jeremias, T., Lapolli, F.R., Padilla, I., López-Delgado, A., 2021. Highly efficient removal of aluminum, iron, and manganese ions using Linde type-A zeolite obtained from hazardous waste. Chemosphere 267. https://doi.org/10.1016/j.chemosphere.2020.128919
Lota, G., Krawczyk, P., Lota, K., Sierczyńska, A., Kolanowski, Ł., Baraniak, M., Buchwald, T., 2016. The application of activated carbon modified by ozone treatment for energy storage. Journal of Solid State Electrochemistry 20, 2857–2864. https://doi.org/10.1007/s10008-016-3293-5
Lu, X., Shao, Y., Gao, N., Ding, L., 2015. Equilibrium, thermodynamic, and kinetic studies of the adsorption of 2,4-dichlorophenoxyacetic acid from aqueous solution by MIEX resin. J Chem Eng Data 60, 1259–1269. https://doi.org/10.1021/je500902p
Lupul, I., Yperman, J., Carleer, R., Gryglewicz, G., 2015. Tailoring of porous texture of hemp stem-based activated carbon produced by phosphoric acid activation in steam atmosphere. Journal of Porous Materials 22, 283–289. https://doi.org/10.1007/s10934-014-9894-4
Mahmood, U., Alkorbi, A.S., Hussain, T., Nazir, A., Qadir, M.B., Khaliq, Z., Faheem, S., Jalalah, M., 2024. Adsorption of lead ions from wastewater using electrospun zeolite/MWCNT nanofibers: kinetics, thermodynamics and modeling study. RSC Adv 14, 5959–5974. https://doi.org/10.1039/d3ra07720a
Marrakchi, F., Ahmed, M.J., Khanday, W.A., Asif, M., Hameed, B.H., 2017. Mesoporous-activated carbon prepared from chitosan flakes via single-step sodium hydroxide activation for the adsorption of methylene blue. Int J Biol Macromol 98, 233–239. https://doi.org/10.1016/j.ijbiomac.2017.01.119
Marrakchi, F., Khanday, W.A., Asif, M., Hameed, B.H., 2016. Cross-linked chitosan/sepiolite composite for the adsorption of methylene blue and reactive orange 16. Int J Biol Macromol 93, 1231–1239. https://doi.org/10.1016/j.ijbiomac.2016.09.069
Marsh, Harry., Rodríguez-Reinoso, F., 2006a. Activated carbon. Elsevier.
Marsh, Harry., Rodríguez-Reinoso, F., 2006b. Activated carbon. Elsevier.
McCullough, C.D., Schultze, M., Vandenberg, J., 2020. Realizing beneficial end uses from abandoned pit lakes. Minerals. https://doi.org/10.3390/min10020133
Menon, V., Rao, M., 2012. Trends in bioconversion of lignocellulose: Biofuels, platform chemicals & biorefinery concept. Prog Energy Combust Sci. https://doi.org/10.1016/j.pecs.2012.02.002
Mishra, R., Prasad, P.R., Panda, P., Barman, S., 2021. Highly Porous Activated N-Doped Carbon as an Ideal Electrode Material for Capacitive Energy Storage and Physisorption of H2,

CO2, and CH4. Energy and Fuels 35, 14177–14187. https://doi.org/10.1021/acs.energyfuels.1c02051
Mofidi, A., Tompa, E., Kalcevich, C., McLeod, C., Lebeau, M., Song, C., Kim, J., Demers, P.A., 2022. Occupational Exposure to Wood Dust and the Burden of Nasopharynx and Sinonasal Cancer in Canada. Int J Environ Res Public Health 19. https://doi.org/10.3390/ijerph19031144
Mopoung, S., Moonsri, P., Palas, W., Khumpai, S., 2015. Characterization and Properties of Activated Carbon Prepared from Tamarind Seeds by KOH Activation for Fe(III) Adsorption from Aqueous Solution. https://doi.org/10.1155/2015/415961
Moreno-Castilla, ´ C, Lopez-Ramon, M. V, Carrasco-Marın, F., 2000. Changes in surface chemistry of activated carbons by wet oxidation, Carbon.
Moreno-Castilla, C., Ferro-García, M.A., Joly, J.P., Carrasco-Marín, F., Rivera-Utrilla, J., 1995. Activated Carbon Surface Modifications by Nitric Acid, Hydrogen Peroxide, and Ammonium Peroxydisulfate Treatments, Langmuir.
Mwango, A., Kambole, C., 2019. Engineering Characteristics and Potential Increased Utilisation of Sawdust Composites in Construction—A Review. Journal of Building Construction and Planning Research 07, 59–88. https://doi.org/10.4236/jbcpr.2019.73005
Núñez-Gómez, D., Alves, A.A. de A., Lapolli, F.R., Lobo-Recio, M.A., 2017a. Aplication of the statistical experimental design to optimize mine-impacted water (MIW) remediation using shrimp-shell. Chemosphere 167, 322–329. https://doi.org/10.1016/j.chemosphere.2016.09.094
Núñez-Gómez, D., Alves, A.A. de A., Lapolli, F.R., Lobo-Recio, M.A., 2017b. Aplication of the statistical experimental design to optimize mine-impacted water (MIW) remediation using shrimp-shell. Chemosphere 167, 322–329. https://doi.org/10.1016/j.chemosphere.2016.09.094
Olivares-Marín, M., Fernández-González, C., Macías-García, A., Gómez-Serrano, V., 2006. Preparation of activated carbons from cherry stones by activation with potassium hydroxide. Appl Surf Sci 252, 5980–5983. https://doi.org/10.1016/j.apsusc.2005.11.018
Patawat, C., Silakate, K., Chuan-Udom, S., Supanchaiyamat, N., Hunt, A.J., Ngernyen, Y., 2020. Preparation of activated carbon fromDipterocarpus alatusfruit and its application for methylene blue adsorption. RSC Adv 10, 21082–21091. https://doi.org/10.1039/d0ra03427d
Pellenz, L., da Silva, L.J.S., Mazur, L.P., de Figueiredo, G.M., Borba, F.H., Ulson de Souza, A.A., Guelli Ulson de Souza, S.M.A., da Silva, A., 2022. Functionalization of graphene with nitrogen-based groups for water purification via adsorption: A review. Journal of Water Process Engineering. https://doi.org/10.1016/j.jwpe.2022.102873
Perdomo, O.P., de Francisco, L.E.R., Aceituno, J., Galvan, Y.A., Brehm, N., Yacou, C., Gaspard, S., Manduca-Artiles, M., Garriga, A.M., Jauregui-Haza, U., 2023. Adsorption of 2,4-dichlorophenoxyacetic acid (2,4D) on sargassum activated carbon. Afinidad 80, 142–150. https://doi.org/10.55815/417977
Pimentel, C.H., Freire, M.S., Gómez-Díaz, D., González-Álvarez, J., 2024. Continuous Adsorption of Acid Wood Dyes onto an Activated Carbon Prepared from Pine Sawdust. Applied Sciences 14, 841. https://doi.org/10.3390/app14020841
Pohling, J., Dave, D., Liu, Y., Murphy, W., Trenholm, S., 2022. Two-step demineralization of shrimp (: Pandalus Borealis) shells using citric acid: An environmentally friendly, safe and cost-effective alternative to the traditional approach. Green Chemistry 24, 1141–1151. https://doi.org/10.1039/d1gc03140f

Poletto, M., Zattera, A.J., Forte, M.M.C., Santana, R.M.C., 2012. Thermal decomposition of wood: Influence of wood components and cellulose crystallite size. Bioresour Technol 109, 148–153. https://doi.org/10.1016/j.biortech.2011.11.122

Qasem, N.A.A., Mohammed, R.H., Lawal, D.U., 2021. Removal of heavy metal ions from wastewater: a comprehensive and critical review. NPJ Clean Water. https://doi.org/10.1038/s41545-021-00127-0

Quimbaya-Ñañez, C., Serna-Galvis, E.A., Silva-Agredo, J., Huerta, L., Torres-Palma, R.A., Ávila-Torres, Y., 2024. Mn-based material derived from industrial sawdust for the elimination of ciprofloxacin: Loss of antibiotic activity and toxicity via carbocatalysis assisted by ultrasound. J Environ Chem Eng 12, 112015. https://doi.org/10.1016/j.jece.2024.112015

Radenković, M., Petrović, J., Pap, S., Kalijadis, A., Momčilović, M., Krstulović, N., Živković, S., 2024. Waste biomass derived highly-porous carbon material for toxic metal removal: Optimisation, mechanisms and environmental implications. Chemosphere 347. https://doi.org/10.1016/j.chemosphere.2023.140684

Radkevich, V.Z., Senko, T.L., Wilson, K., Grishenko, L.M., Zaderko, A.N., Diyuk, V.Y., 2008. The influence of surface functionalization of activated carbon on palladium dispersion and catalytic activity in hydrogen oxidation. Appl Catal A Gen 335, 241–251. https://doi.org/10.1016/j.apcata.2007.11.029

Rahmana Putra, N., Veza, I., Irianto, I., 2024. Harnessing wood waste for sustainable biofuel: A bibliometric analysis and review of valorisation strategies. Waste Management Bulletin. https://doi.org/10.1016/j.wmb.2024.11.006

Rambabu, K., AlYammahi, J., Bharath, G., Thanigaivelan, A., Sivarajasekar, N., Banat, F., 2021. Nano-activated carbon derived from date palm coir waste for efficient sequestration of noxious 2,4-dichlorophenoxyacetic acid herbicide. Chemosphere 282. https://doi.org/10.1016/j.chemosphere.2021.131103

Rambabu, K., Bharath, G., Avornyo, A., Thanigaivelan, A., Hai, A., Banat, F., 2023. Valorization of date palm leaves for adsorptive remediation of 2,4-dichlorophenoxyacetic acid herbicide polluted agricultural runoff. Environmental Pollution 316. https://doi.org/10.1016/j.envpol.2022.120612

Rao, G.P., Lu, C., Su, F., 2007. Sorption of divalent metal ions from aqueous solution by carbon nanotubes: A review. Sep Purif Technol 58, 224–231. https://doi.org/10.1016/j.seppur.2006.12.006

Rashda, Aryee, A.A., Kailu, D., Kiran, S., Li, Z., Han, R., 2024. Adsorption of 2,4-dichlorophenoxyacetic acid and 4-chlorophenol using bio-based activated carbon: Thermodynamics, kinetics and cytotoxicity evaluation. Environmental Functional Materials 3, 46–58. https://doi.org/10.1016/j.efmat.2024.09.002

Roy, T.M., Nazari, E., Strong, O.K.L., Pede, P.R., Vreugdenhil, A.J., 2025. The effect of adsorbent textural and functional properties on model naphthenic acid adsorption. J Environ Sci (China) 148, 27–37. https://doi.org/10.1016/j.jes.2024.01.003

Rutherford, D.W., Wershaw, R.L., Rostad, C.E., Kelly, C.N., 2012. Effect of formation conditions on biochars: Compositional and structural properties of cellulose, lignin, and pine biochars. Biomass Bioenergy 46, 693–701. https://doi.org/10.1016/j.biombioe.2012.06.026

Ryczkowski, J., Pasieczna, S., Figueiredo, J.L., Pereira, M.F.R., Borowiecki, T., 2004. Characterization of activated carbons by FT-IR/PAS and TPD, in: Journal De Physique. IV : JP. pp. 57–63. https://doi.org/10.1051/jp4:2004117009

Sebio-Puñal, T., Naya, S., López-Beceiro, J., Tarrío-Saavedra, J., Artiaga, R., 2012. Thermogravimetric analysis of wood, holocellulose, and lignin from five wood species, in: Journal of Thermal Analysis and Calorimetry. pp. 1163–1167. https://doi.org/10.1007/s10973-011-2133-1

Seo, S.-K., Roh, J.-S., Kim, E.-S., Chi, S.-H., Kim, S.-H., Lee, S.-W., 2009. Thermal Emissivity of a Nuclear Graphite as a Function of Its Oxidation Degree (2) - Effect of Surface Structural Changes -. Carbon letters 10, 300–304. https://doi.org/10.5714/cl.2009.10.4.300

Shahib, I.I., Ifthikar, J., Wang, S., Elkhlifi, Z., Wang, J., Chen, Z., 2023. Nitrogen-rich carbon composite fabricated from waste shrimp shells for highly efficient oxo-vanadate adsorption-coupled reduction. Chemosphere 340. https://doi.org/10.1016/j.chemosphere.2023.139915

Sharma, G.K., Jena, R.K., Ray, P., Yadav, K.K., Moharana, P.C., Cabral-Pinto, M.M.S., Bordoloi, G., 2021. Evaluating the geochemistry of groundwater contamination with iron and manganese and probabilistic human health risk assessment in endemic areas of the world's largest River Island, India. Environ Toxicol Pharmacol 87. https://doi.org/10.1016/j.etap.2021.103690

Shattuck, A., Werner, M., Mempel, F., Dunivin, Z., Galt, R., 2023. Global pesticide use and trade database (GloPUT): New estimates show pesticide use trends in low-income countries substantially underestimated. Global Environmental Change 81. https://doi.org/10.1016/j.gloenvcha.2023.102693

Siabi, W.K., Owusu-Ansah, E.D.-J., Essandoh, H.M.K., Asiedu, N.Y., 2021. Modelling the adsorption of iron and manganese by activated carbon from teak and shea charcoal for continuous low flow. Water-Energy Nexus 4, 88–94. https://doi.org/10.1016/j.wen.2021.02.001

Singh, N.K., Sanghvi, G., Yadav, M., Padhiyar, H., Christian, J., Singh, V., 2023. Fate of pesticides in agricultural runoff treatment systems: Occurrence, impacts and technological progress. Environ Res. https://doi.org/10.1016/j.envres.2023.117100

Sircar, S., Golden, T.C., Rao, M.B., 1996. ACTIVATED CARBON FOR GAS SEPARATION AND STORAGE, Carbon.

Somyanonthanakun, W., Ahmed, R., Krongtong, V., Thongmee, S., 2023. Studies on the adsorption of Pb(II) from aqueous solutions using sugarcane bagasse-based modified activated carbon with nitric acid: Kinetic, isotherm and desorption. Chemical Physics Impact 6. https://doi.org/10.1016/j.chphi.2023.100181

Song, X., Liu, H., Cheng, L., Qu, Y., 2010. Surface modification of coconut-based activated carbon by liquid-phase oxidation and its effects on lead ion adsorption. Desalination 255, 78–83. https://doi.org/10.1016/j.desal.2010.01.011

Srivastava, V.C., Mall, I.D., Mishra, I.M., 2008. Antagonistic competitive equilibrium modeling for the adsorption of ternary metal ion mixtures from aqueous solution onto bagasse fly ash. Ind Eng Chem Res 47, 3129–3137. https://doi.org/10.1021/ie0709842

Strong, O.K., France, H.E., Scotland, K.M., Wright, K., Vreugdenhil, A.J., 2023. Selenite Adsorption and Reduction via Iron(II) Impregnated Activated Carbon Produced from the Phosphoric Acid Activation of Construction Waste Wood. Arch Environ Contam Toxicol 85. https://doi.org/10.1007/s00244-023-01032-y

Strong, O.K.L., 2019. Abstract Phosphoric Acid Chemically Activated Waste Wood: Production, Modification and Selenium Adsorption.

Strong, O.K.L., France, H.E., Scotland, K., Wright, K., Vreugdenhil, A.J., 2023. Selenite Adsorption and Reduction via Iron(II) Impregnated Activated Carbon Produced from the Phosphoric Acid Activation of Construction Waste Wood. Arch Environ Contam Toxicol. https://doi.org/10.1007/s00244-023-01032-y

Sun, Y., Yue, Q., Gao, B., Huang, L., Xu, X., Li, Q., 2012. Comparative study on characterization and adsorption properties of activated carbons with H 3PO 4 and H 4P 2O 7 activation employing Cyperus alternifolius as precursor. Chemical Engineering Journal 181–182, 790–797. https://doi.org/10.1016/j.cej.2011.11.098

Sylla, N.F., Ndiaye, N.M., Ngom, B.D., Mutuma, B.K., Momodu, D., Chaker, M., Manyala, N., 2020. Ex-situ nitrogen-doped porous carbons as electrode materials for high performance supercapacitor. J Colloid Interface Sci 569, 332–345. https://doi.org/10.1016/j.jcis.2020.02.061

Szymańska, E., Winnicka, K., 2015. Stability of chitosan - A challenge for pharmaceutical and biomedical applications. Mar Drugs. https://doi.org/10.3390/md13041819

Tan, X., Wang, H., Guo, X., Ho, S.H., 2023. Effects of nitrogen doped-biochar on wastewater remediation. Environ Technol Innov 32. https://doi.org/10.1016/j.eti.2023.103413

Thommes, M., Kaneko, K., Neimark, A. V., Olivier, J.P., Rodriguez-Reinoso, F., Rouquerol, J., Sing, K.S.W., 2015a. Physisorption of gases, with special reference to the evaluation of surface area and pore size distribution (IUPAC Technical Report). Pure and Applied Chemistry 87, 1051–1069. https://doi.org/10.1515/pac-2014-1117

Thommes, M., Kaneko, K., Neimark, A. V., Olivier, J.P., Rodriguez-Reinoso, F., Rouquerol, J., Sing, K.S.W., 2015b. Physisorption of gases, with special reference to the evaluation of surface area and pore size distribution (IUPAC Technical Report). Pure and Applied Chemistry 87, 1051–1069. https://doi.org/10.1515/pac-2014-1117

Tolesa, L.D., Gupta, B.S., Lee, M.J., 2019. Chitin and chitosan production from shrimp shells using ammonium-based ionic liquids. Int J Biol Macromol 130, 818–826. https://doi.org/10.1016/j.ijbiomac.2019.03.018

Tsai, W.T., Lai, C.W., Hsien, K.J., 2004. Adsorption kinetics of herbicide paraquat from aqueous solution onto activated bleaching earth. Chemosphere 55, 829–837. https://doi.org/10.1016/j.chemosphere.2003.11.043

Valentín-Reyes, J., García-Reyes, R.B., García-González, A., Soto-Regalado, E., Cerino-Córdova, F., 2019. Adsorption mechanisms of hexavalent chromium from aqueous solutions on modified activated carbons. J Environ Manage 236, 815–822. https://doi.org/10.1016/j.jenvman.2019.02.014

Vallières, E., Pintos, J., Parent, M.E., Siemiatycki, J., 2015. Occupational exposure to wood dust and risk of lung cancer in two population-based case-control studies in Montreal, Canada - No section-. Environ Health 14. https://doi.org/10.1186/1476-069X-14-1

Vieira, T., Becegato, V.A., Paulino, A.T., 2021. Equilibrium Isotherms, Kinetics, and Thermodynamics of the Adsorption of 2,4-Dichlorophenoxyacetic Acid to Chitosan-Based Hydrogels. Water Air Soil Pollut 232. https://doi.org/10.1007/s11270-021-05021-6

Vinayagam, R., Ganga, S., Murugesan, G., Rangasamy, G., Bhole, R., Goveas, L.C., Varadavenkatesan, T., Dave, N., Samanth, A., Radhika Devi, V., Selvaraj, R., 2023. 2,4-Dichlorophenoxyacetic acid (2,4-D) adsorptive removal by algal magnetic activated carbon nanocomposite. Chemosphere 310. https://doi.org/10.1016/j.chemosphere.2022.136883

Wajima, T., Murakami, K., Kato, T., Sugawara, K., 2009. Heavy metal removal from aqueous solution using carbonaceous K2 S-impregnated adsorbent. Journal of Environmental Sciences 21, 1730–1734. https://doi.org/10.1016/S1001-0742(08)62480-8

Wang, H., Maiyalagan, T., Wang, X., 2012. Review on recent progress in nitrogen-doped graphene: Synthesis, characterization, and its potential applications. ACS Catal. https://doi.org/10.1021/cs200652y

Wang, J., Guo, X., 2020. Adsorption kinetic models: Physical meanings, applications, and solving methods. J Hazard Mater. https://doi.org/10.1016/j.jhazmat.2020.122156

Wang, J., Zhuang, S., 2022. Chitosan-based materials: Preparation, modification and application. J Clean Prod. https://doi.org/10.1016/j.jclepro.2022.131825
Wang, K., Xu, M., Gu, Y., Gu, Z., Fan, Q.H., 2016. Symmetric supercapacitors using urea-modified lignin derived N-doped porous carbon as electrode materials in liquid and solid electrolytes. J Power Sources 332, 180–186. https://doi.org/10.1016/j.jpowsour.2016.09.115
Williams, M.S., Oyedotun, T.D.T., Simmons, D.A., 2020a. Assessment of water quality of lakes used for recreational purposes in abandoned mines of Linden, Guyana. Geology, Ecology, and Landscapes 4, 269–281. https://doi.org/10.1080/24749508.2019.1633220
Williams, M.S., Oyedotun, T.D.T., Simmons, D.A., 2020b. Assessment of water quality of lakes used for recreational purposes in abandoned mines of Linden, Guyana. Geology, Ecology, and Landscapes 4, 269–281. https://doi.org/10.1080/24749508.2019.1633220
Xu, F., Zhu, T.T., Rao, Q.Q., Shui, S.W., Li, W.W., He, H.B., Yao, R.S., 2017. Fabrication of mesoporous lignin-based biosorbent from rice straw and its application for heavy-metal-ion removal. J Environ Sci (China) 53, 132–140. https://doi.org/10.1016/j.jes.2016.03.026
Yagmur, E., Tunc, M.S., Banford, A., Aktas, Z., 2013. Preparation of activated carbon from autohydrolysed mixed southern hardwood. J Anal Appl Pyrolysis 104, 470–478. https://doi.org/10.1016/j.jaap.2013.05.025
Yang, H., Yan, R., Chen, H., Lee, D.H., Zheng, C., 2007. Characteristics of hemicellulose, cellulose and lignin pyrolysis. Fuel 86, 1781–1788. https://doi.org/10.1016/j.fuel.2006.12.013
Yang, M., Luo, S., Zeng, P., Wu, Y., 2025. Fabrications and Properties of Heteroatom-Based Co-Doped Biochar for Environmental Application: A Review. Separations 12, 20. https://doi.org/10.3390/separations12020020
Yang, X., Muhammad, T., Yang, J., Yasen, A., Chen, L., 2020. In-situ kinetic and thermodynamic study of 2,4-dichlorophenoxyacetic acid adsorption on molecularly imprinted polymer based solid-phase microextraction coatings. Sens Actuators A Phys 313. https://doi.org/10.1016/j.sna.2020.112190
Yorgun, S., Yildiz, D., 2015. Preparation and characterization of activated carbons from Paulownia wood by chemical activation with H3PO4. J Taiwan Inst Chem Eng 53, 122–131. https://doi.org/10.1016/j.jtice.2015.02.032
Zeng, W., Lu, Y., Zhou, J., Zhang, J., Duan, Y., Dong, C., Wu, W., 2024. Simultaneous removal of Cd(II) and As(V) by ferrihydrite-biochar composite: Enhanced effects of As(V) on Cd(II) adsorption. J Environ Sci (China) 139, 267–280. https://doi.org/10.1016/j.jes.2023.04.020
Zhai, Y., Xu, B., Zhu, Y., Qing, R., Peng, C., Wang, T., Li, C., Zeng, G., 2016. Nitrogen-doped porous carbon from Camellia oleifera shells with enhanced electrochemical performance. Materials Science and Engineering C 61, 449–456. https://doi.org/10.1016/j.msec.2015.12.079
Zhang, S., Shi, X., Wróbel, R., Chen, X., Mijowska, E., 2019. Low-cost nitrogen-doped activated carbon prepared by polyethylenimine (PEI) with a convenient method for supercapacitor application. Electrochim Acta 294, 183–191. https://doi.org/10.1016/j.electacta.2018.10.111
Zhang, Y., Song, X., Zhang, P., Gao, H., Ou, C., Kong, X., 2020. Production of activated carbons from four wastes via one-step activation and their applications in Pb2+ adsorption: Insight of ash content. Chemosphere 245. https://doi.org/10.1016/j.chemosphere.2019.125587
Zhang, Z., Ma, Z., Song, L., Farag, M.A., 2024. Maximizing crustaceans (shrimp, crab, and lobster) by-products value for optimum valorization practices: A comparative review of

their active ingredients, extraction, bioprocesses and applications. J Adv Res. https://doi.org/10.1016/j.jare.2023.11.002
Zimmer, A.T., Weitz, K., Padhye, A., Sifleet, S., Gabriele, H.-S., 2018. Wood Waste Inventory Final Report Project Officer/Technical Lead.
Zou, K., Deng, Y., Chen, J., Qian, Y., Yang, Y., Li, Y., Chen, G., 2018. Hierarchically porous nitrogen-doped carbon derived from the activation of agriculture waste by potassium hydroxide and urea for high-performance supercapacitors. J Power Sources 378, 579–588. https://doi.org/10.1016/j.jpowsour.2017.12.081
Zou, R., Yang, Z., Zhang, J., Lei, R., Zhang, W., Fnu, F., Tsang, D.C.W., Heyne, J., Zhang, X., Ruan, R., Lei, H., 2024. Machine learning application for predicting key properties of activated carbon produced from lignocellulosic biomass waste with chemical activation. Bioresour Technol 399. https://doi.org/10.1016/j.biortech.2024.130624
Zuanazzi, N.R., Ghisi, N. de C., Oliveira, E.C., 2020. Analysis of global trends and gaps for studies about 2,4-D herbicide toxicity: A scientometric review. Chemosphere. https://doi.org/10.1016/j.chemosphere.2019.125016

Appendix i

Table 0.1 Comparison of Langmuir maximum adsorption capacity of Al^{3+}, Mn^{2+} and Pb^{2+} in this work with selected previous studies.

Adsorbent	Temperature (℃)	pH	Q_0 (mg/g)			Reference
			Al^{3+}	Mn^{2+}	Pb^{2+}	
Date Pith AC	22	4	5.8	-	-	(Al-Muhtaseb et al., 2008)
Commercial AC (BDH)	22	4	6.6	-	-	(Al-Muhtaseb et al., 2008)
Phillipsite (zeolite)	25	6.8	-	-	254	(He et al., 2021)
Oxidized Coconut shell AC	-	-	-	-	40	(Song et al., 2010)
Zeolite/MWCNT	-	-	-	-	6	(Mahmood et al., 2024)
Linde type-A Zeolite	25	3.5	15.2	1.4	-	(Lobo-Recio et al., 2021)
GAC	Ambient	5	106	7.63	-	(Goher et al., 2015)
Chlorocardium rodiei AC	30	3	6.0	18	-	(France et al., 2024)
Oxidized Sawdust AC	30	3	9.4	3.4	49	This study

Table 0.2 Model Parameters and statistical evaluation of model fit for Langmuir, Freundlich Redlich-Peterson, and Sips Adsorption Isotherms.

Metal Ions	Model Parameters			Model Fit		
	Langmuir			Adj R^2	Red χ^2	AIC_C
	Q_0 (mg/g)	K_L (L/mg)				
Mn	3.35 ± 0.20	1.97 ± 0.82		0.966	0.082	0.59
Pb	49.50 ± 4.95	1.55 ± 0.59		0.953	13.7	29.97
Al	9.44 ± 0.82	0.73 ± 0.30		0.943	0.896	14.91
	Freundlich					
	K_F (L/mg)	n				
Mn	1.97 ± 0.21	0.17 ± 0.04		0.936	0.123	16.97
Pb	25.5 ± 1.75	3.30 ± 0.42		0.978	6.48	24.72
Al	3.47 ± 0.45	0.26 ± 0.03		0.955	0.711	13.52
	Sips					
	Q_0 (mg/g)	K_s	n_s			
Mn	3.41 ± 0.34	2.14 ± 1.26	1.00 ± 0.78	0.939	0.118	22.92
Pb	49.00 ± 0.00	1.52 ± 0.30	0.80 ± 0.15	0.978	7.76	27.86
Al	12.83 ± 1.85	0.41 ± 0.10	0.51 ± 0.09	0.988	0.181	32.18
	Redlich-Peterson					
	a_{RP}	K_{RP}	g			
Mn	1.14 ± 0.23	4.00 ± 0.00	1.00 ± 0.07	0.938	0.121	23.75
Pb	0.90 ± 0.34	49.00 ± 0.00	1.00 ± 0.20	0.950	16.7	32.48
Al	4.76 ± 0.84	23.45 ± 3.45	0.83 ± 0.01	0.999	0.014	32.48

Table 0.3 Comparison of Langmuir maximum adsorption capacity of Al^{3+}, Mn^{2+} and Pb^{2+} in this work with selected previous studies.

Adsorbent	Temperature (℃)	pH	Q_0 (mg/g)			Reference
			Al^{3+}	Mn^{2+}	Pb^{2+}	
Date Pith AC	22	4	5.8	-	-	(Al-Muhtaseb et al., 2008)
Commercial AC (BDH)	22	4	6.6	-	-	(Al-Muhtaseb et al., 2008)
Phillipsite (zeolite)	25	6.8	-	-	254	(He et al., 2021)
Oxidized Coconut shell AC	-	-	-	-	40	(Song et al., 2010)
Zeolite/MWCNT	-	-	-	-	6	(Mahmood et al., 2024)
Linde type-A Zeolite	25	3.5	15.2	1.4	-	(Lobo-Recio et al., 2021)
GAC	Ambient	5	106	7.63	-	(Goher et al., 2015)
Chlorocardium rodiei AC	30	3	6.0	18	-	(France et al., 2024)
Oxidized Sawdust AC	**30**	**3**	**9.4**	**3.4**	**49**	**This study**

Table 0.4 Langmuir-derived maximum adsorption capacities for adsorption of 2,4-D and paraquat on GH-AC, GH-$Ch_{10\%}$, GH-$Ch_{20\%}$ and GH-$Ch_{30\%}$.

Composite AC	Herbicides and Model Fit					
	2,4-D	Adj R^2	Red χ^2	Paraquat	Adj R^2	Red χ^2
GH-AC	120.4 ± 19.2	0.964	41.7	244.2 ± 5.70	0.999	6.30
GH-$Ch_{10\%}$	129.5 ± 8.50	0.997	91.8	251.3 ± 5.01	0.999	8.90
GH-$Ch_{20\%}$	165.8 ± 7.92	0.999	4.62	101.6 ± 3.81	0.952	34.1
GH-$Ch_{30\%}$	168.2 ± 6.67	0.998	40.0	108.6 ± 11.3	0.986	69.6

Table 0.5 Comparison of Langmuir maximum adsorption capacity for 2,4-D and paraquat on various adsorbents.

Herbicide	Adsorbent	Temperature (K)	pH	Q_0 (mg/g)	Reference
2,4-D	Date stone AC	-	3.6	238	(Hameed et al., 2009)
	Carbonaceous adsorbent	318	7.5	153	(Gupta et al., 2006)
	Date palm coir waste AC	303	2	50.2	(Rambabu et al., 2021)
	Greenheart/chitosan AC	**303**	**7**	**166**	**This Study**
Paraquat	Modified-CNT	-	7	191	(Li et al., 2021)
	Bleaching earth	298	-	40	(Tsai et al., 2004)
	Oxidized cellulose nanofibers	303	7	108	(Huang et al., 2019)
	Greenheart/chitosan AC	**303**	**7**	**102**	**This Study**

Table 0.6 Comparison of thermodynamic parameters and model fit for adsorption of 2,4-D and paraquat at 303 K on GH-$Ch_{20\%}$ AC with other reported works.

Herbicide	Adsorbent	T (K)	ΔG° (kJ/mol)	ΔH° (kJ/mol)	ΔS° (J/Kmol)	Reference
2,4-D	**Chitosan/Wood AC**	**303**	**-19.2**	**-13.0**	**20.7**	**This study**
	Commercial GAC	303	-22.6	5.02	92.3	(Ghatbandhe et al., 2013)
	MOF (MIL-88(Fe)-NH2)	303	-1.01	27.9	97.1	(Alluhaybi et al., 2023)
	Molecular Imprinted Polymer	308	1.50	-16.2	-57.6	(Yang et al., 2020)
	Chitosan-Hydrogel	303	-4.15	4.8	117	(Vieira et al., 2021)
Paraquat	**Chitosan/Wood AC**	**303**	**-28.8**	**-20.1**	**28.6**	**This study**
	Carbonated Jujube Seeds	303	-27.5	35	200	(Franco et al., 2022)
	Decorated magnetite nanoparticles	308	-3.48	-4.70	-0.04	(Kouchakinejad et al., 2022)
	Hexagonal mesoporous silica	298	-29.1	-32.3	-11.5	(Brigante and Avena, 2014)
	GO-SiO_2	298	-29.6	-48.8	-62.4	(Dehghani et al., 2021)

Table 0.7 Comparison of Production Parameters and Atomic weight % of nitrogen in Shrimp Waste doped *Chlorocardium rodiei* and selected ACs from other nitrogenating techniques.

Precursor	Nitrogenating Agent	Treatment/Conditions	Doping Ratio* (g)	N Atomic wt%	Reference
Camellia oleifera shells	NH_3	l HNO_3 and 30% H_2O_2 at 90 °C for 2 h, 500 °C – 900 °C for 90 min	-	8.03	(Zhai et al., 2016)
Commercial AC	Polyethylenimine	10 min reflux with polyethylenimine, 3h @ 900 °C under Ar	-	2.1	(Zhang et al., 2019)
Peanut shell	Melamine	850 °C, 1h, Ar.	1:5	3.2–8.9	(Sylla et al., 2020)
Wood hydrochar	Melamine	800 °C, 1h	2:1	1.75	(Liu et al., 2019)
Lignin	Urea	400 °C, 1h and 800°C 1h	1:2	1.30	(Wang et al., 2016)
Chitosan	-	400 °C, 30 min	-	5.77	(France et al., 2025)
Chlorocardium rodiei Sawdust	Chitosan	400 °C, 30 min	3:1	2.31	(France et al., 2025)
Chlorocardium rodiei Sawdust	Shrimp shells	400 °C, 30 min	5:1	2.19	This work
Chlorocardium rodiei Sawdust	Shrimp hydrochar	400 °C, 30 min	9:1	1.43	This work
Chlorocardium rodiei Sawdust	Shrimp Chitin	400 °C, 30 min	7:3	2.80	This work

Table 0.8 Comparison of Langmuir maximum adsorption capacity for 2,4-D at pH 7 at 303 K on GH-SW ACs with other reported works.

Adsorbent	Temperature (K)	pH	Q_0 (mg/g)	Reference
Date stone AC	-	3.6	238	(Hameed et al., 2009)
Carbonaceous adsorbent	318	7.5	153	(Gupta et al., 2006)
Date palm coir waste AC	303	2	50.2	(Rambabu et al., 2021)
Corn cob biochar	-	2	37	(Binh and Nguyen, 2020)
Sargassum based AC	293	2.5	51	(Perdomo et al., 2023)
Peanut husk AC	303	3	166	(Rashda et al., 2024)
Greenheart-chitosan AC	303	7	166	(France et al., 2025)
Greenheart-shrimp chitin AC	303	7	101	This Study
Greenheart-shrimp hydrochar AC	303	7	79	This Study
Greenheart-shrimp shell AC	303	7	71	This Study
Greenheart AC	303	7	67	This Study

Table 0.9 Comparison of standard state thermodynamic parameters for adsorption of 2,4-D at pH 7 at 303 K on GH-SW ACs with other reported works.

Adsorbent	T (K)	ΔG° (kJ/mol)	ΔH° (kJ/mol)	ΔS° (J/Kmol)	Reference
MOF (MIL-88(Fe)-NH2)	303	-1.01	27.9	97.1	(Alluhaybi et al., 2023)
Peanut husk AC	303	-14.6	106	308	(Rashda et al., 2024)
Molecular Imprinted Polymer	308	1.50	-16.2	-57.6	(Yang et al., 2020)
Chitosan-Hydrogel	303	-4.15	4.8	117	(Vieira et al., 2021)
MIEX Resin	303	1.44	19.85	60.76	(Lu et al., 2015)
Commercial chitosan-greenheart AC	303	-19.04	-12.97	20.71	(France et al., 2025)
Shrimp shell-greenheart AC	303	-23.46	-16.75	22.14	This study
Shrimp hydrochar-greenheart AC	303	-23.08	-14.12	29.54	This study
Shrimp chitin-greenheart AC	303	-21.14	-12.61	28.16	This study
Greenheart AC	303	-27.51	-12.10	45.70	This study

Appendix ii

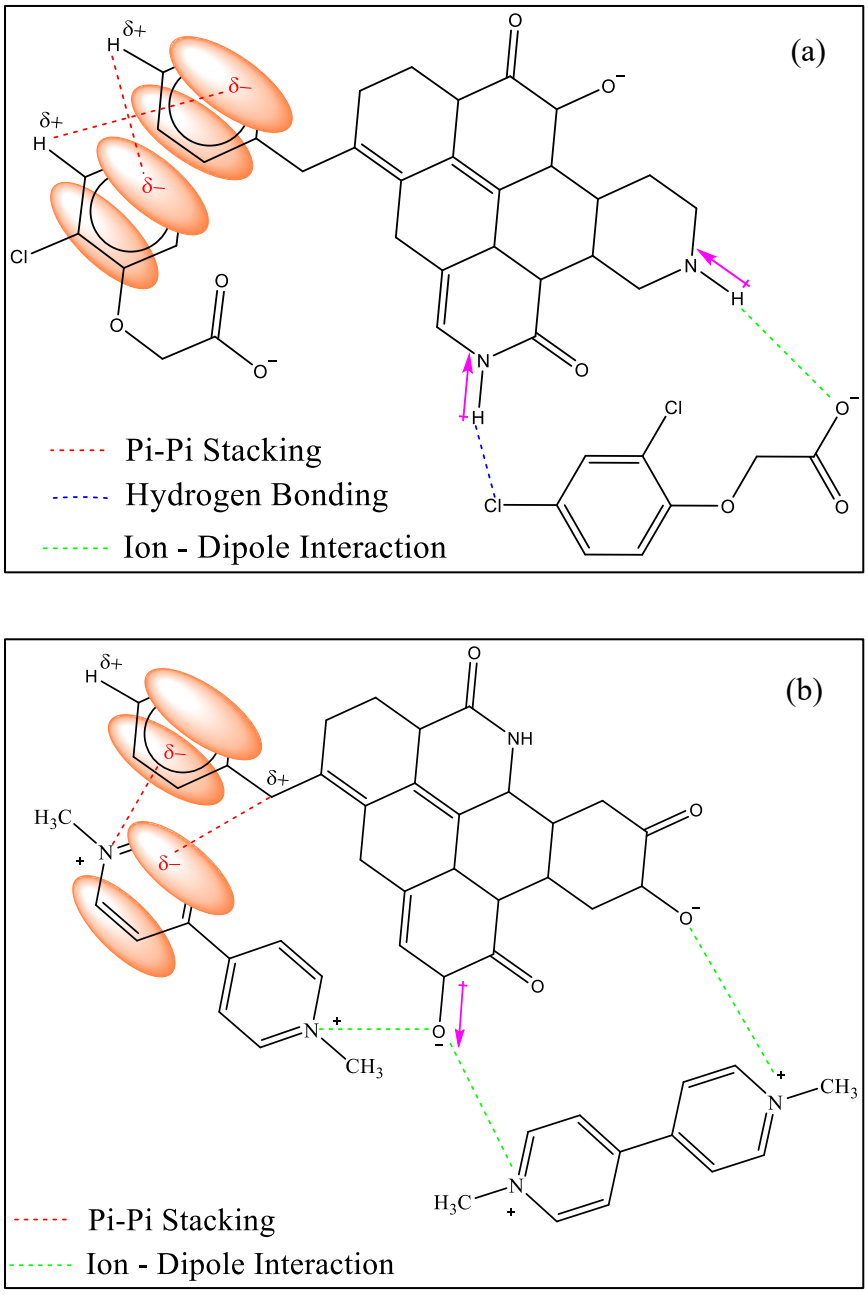

Figure 0.1 Predominant intermolecular interactions between GH-Ch$_{20\%}$ and a - 2,4-D and b – paraquat at pH 7.

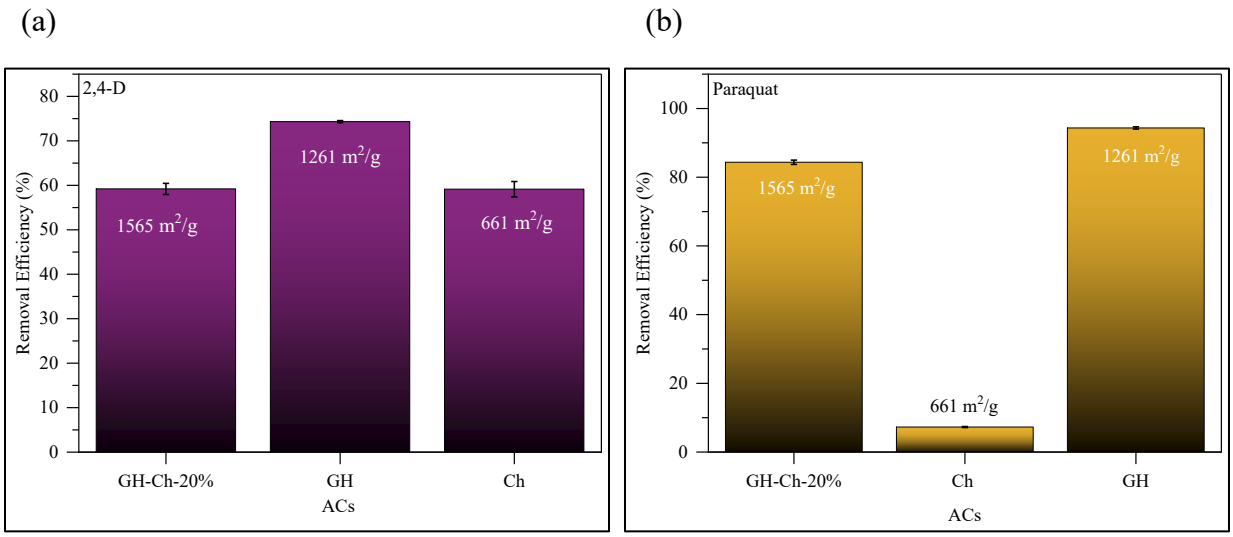

Figure 0.2 Plots of impact of specific surface area of GH-Ch$_{20\%}$, GH-AC and Ch-AC on removal of (a) - 2,4-D and (b) - paraquat.

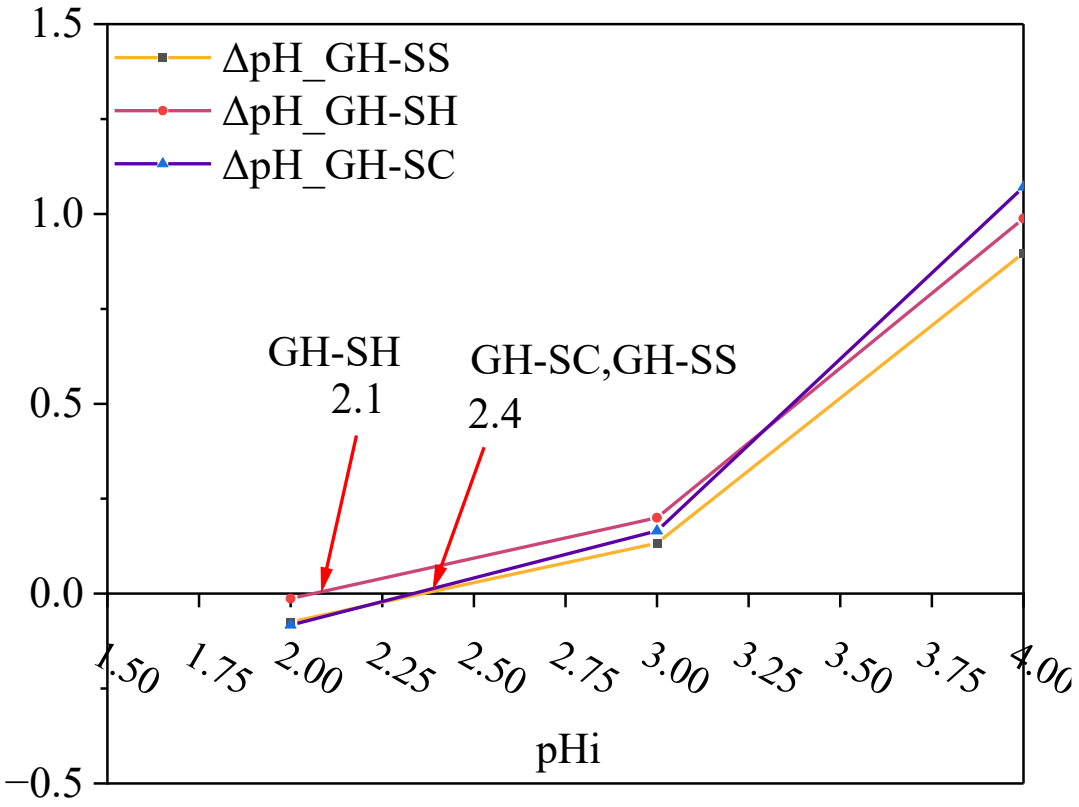

Figure 0.3 pH$_{pzc}$ of GH-SW-ACs

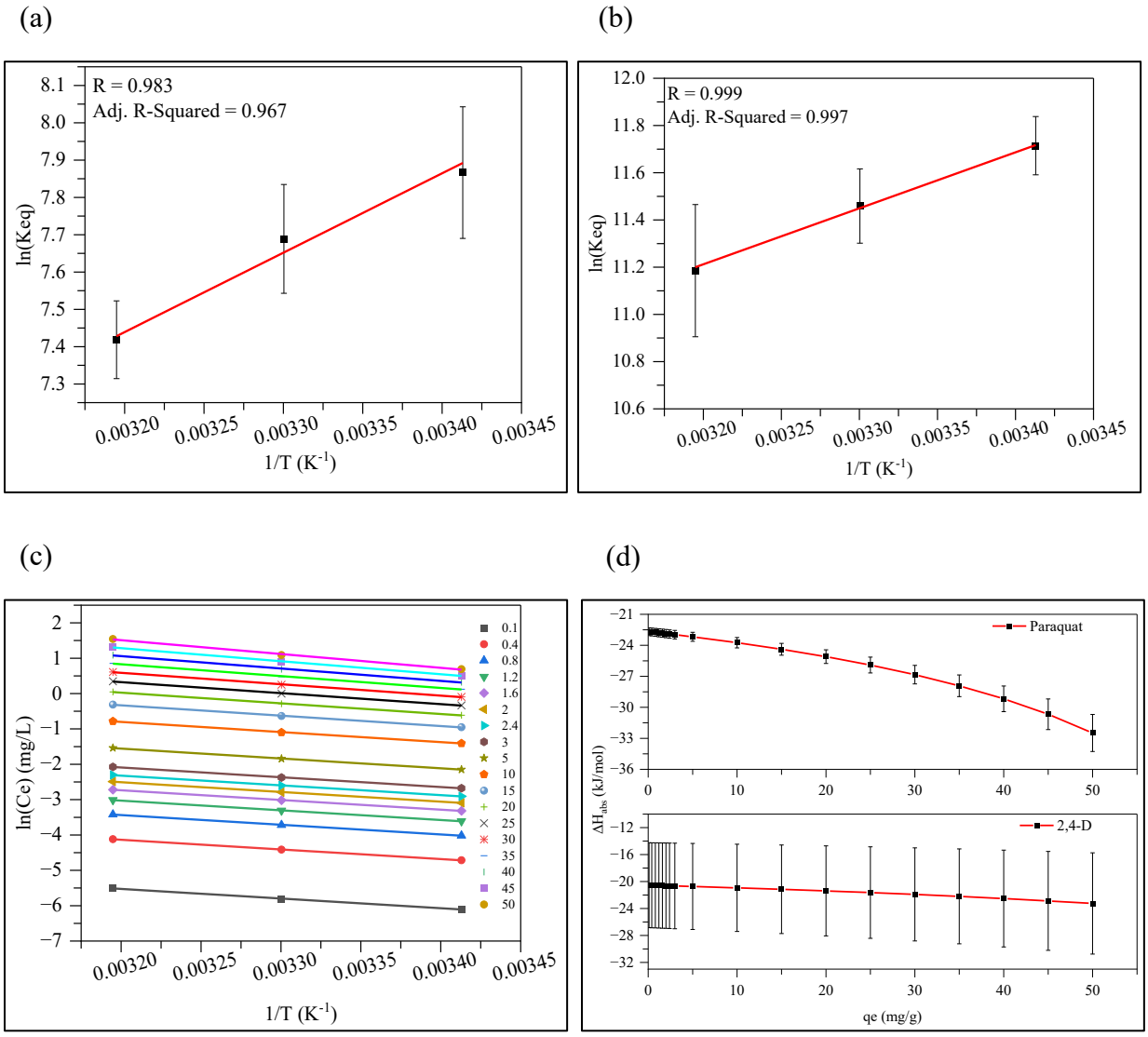

Figure 0.4 Van't Hoff Plots used to determine thermodynamic parameters for a – 2,4-D and b – paraquat and c – isosteric heats and d – surface coverage dependence of isosteric heat of adsorption for 2,4-D and paraquat.